Vanadia Promoted Co-Al_2O_3 Fischer-Tropsch Catalysts

By

Seneliso T. Zwane

B.Sc. Science, B.Sc Eng (Chem.)

Submitted to the University of Cape Town in partial fulfillment of the requirements for the degree of

Master of Science in Chemical Engineering

Department of Chemical Engineering

University of Cape Town

P/B Rondebosch

7701

South Africa

February 2004

Acknowledgments

I would like to thank Prof. Eric van Steen for his encouragement, advise and support throughout this work without which this would not have been possible.

Many thanks to Dr. Michael Claeys whose magic touches in the lab were amazing. Your advice and creative suggestions are appreciated.

I thank the University of Cape Town and the National Research Foundation for their financial support, which made this work possible.

To my home support base, mom, my sisters and brothers… thanks for your patience and belief in me. My friends-there is so many of you guys, thanks for being there for me all the time.

Last but not least, the Catalysis Research Unit students and staff, you guys are awesome. Thank you for acting as my second family, it has been a real pleasure and privilege to work in your midst.

Synopsis

The primary aim of this work was to study systematically V_2O_5 promotion on γ-Al_2O_3 supported cobalt-based Fischer-Tropsch catalysts. The γ-Al_2O_3 support was modified by addition of varying amounts of vanadia and was subsequently loaded with the same Co content (10 wt-%). The modified supports and catalysts were characterised using conventional characterisation methods. The physio-chemical properties of the vanadia promoted supports and catalysts were characterised using Atomic Adsorption Spectroscopy (AAS), zeta-potential measurements, and BET measurements, X-ray Diffraction (XRD), Temperature Programmed Reduction (TPR), Transmission Electron Microscopy (TEM), and CO chemisorption. Catalyst performance in the Fischer-Tropsch synthesis was tested in fixed bed reactor. A catalysts synthesised from plain γ-Al_2O_3 was used as a base catalyst.

Characterization results show that modification of γ-Al_2O_3 support to obtain V_2O_5 loadings beyond 1-monolayer vanadia coverage was difficult when using ion exchange. Ion-exchange equilibrium limitations might have caused the poor vanadia loadings beyond 1-monolayer coverage. The supports net surface charge as measured using zeta potential, was decreased by vanadia content in the supports. CO chemisorption results were complex and could only be modelled using dual site Langmuir model assuming the presence of two different sites absorbing CO on the Co-V-Al catalyst system. This made extraction of physical properties from this method rather difficult.

Fischer Tropsch synthesis reaction was carried out at typical industrial conditions (T=220^{o}C, P=20 bar (a), H_2/CO=2 X_{CO}~60 mol-%) for cobalt catalysts. Vanadia promoted catalysts showed a marked decrease in initial activity. However, the overall deactivation rate was lower with increasing vanadia content. The vanadia content did not affect the chain growth kinetic behavior of the catalyst in the Fischer-Tropsch synthesis hence C_{5+} selectivity in the Fischer-Tropsch synthesis was unperturbed by vanadia content. Increasing the vanadia content in the catalyst resulted in high n-olefin content

and high 1-olefin content. The observed increase in olefin content might be due to the low catalytic activity observed for the catalysts with high vanadia loadings. The most pronounced effect of vanadia promotion on Fischer-Tropsch synthesis was in the oxygenate content in the Fischer-Tropsch product. Catalysts with high vanadia loading yielded high amounts of oxygenate products; mainly alcohols and aldehydes.

Table of Contents

Page

List of Figures

Page

List of Tables

Page

Chapter 1
Introduction

1 INTRODUCTION

Fischer-Tropsch synthesis is the conversion of synthesis gas to aliphatic hydrocarbons over metal catalyst at high pressure and moderate temperatures (Dry, 1981). Industrially applied catalysts are iron and cobalt based. The Fischer-Tropsch reaction can be written as follows (Storch et al., 1951; van der Laan, 1999):

$$(2n+1)\,H_2 + n\,CO \longrightarrow C_nH_{2n+2} + n\,H_2O \qquad (\Delta_R H^0_{298K} = -158.0\ KJ.MOL^{-1}) \qquad (1)$$

The water gas shift (WGS) reaction is a side reaction, which may accompany the Fischer-Tropsch synthesis (mainly with iron-based catalyst). In this reaction CO reacts with water to yield CO_2 and H_2 (Patzlaff et al., 1999).

$$H_2O + CO \longrightarrow CO_2 + H_2 \qquad (\Delta_R H^0_{298} = -41.3\ KJ.MOL^{-1}) \qquad (2)$$

1.1 Historical Background of Fischer-Tropsch Synthesis

In 1902 Sabatier and Sanderens first observed carbon monoxide hydrogenation over a nickel catalyst yielding methane (Sabatier and Sanderens, 1902). The Fischer-Tropsch synthesis is named after by Franz Fischer and Hans Tropsch who observed in 1923 that passing synthesis gas (H_2 + CO) over iron turnings at 100-150 atm. and 400°-450°C, catalysed the production of 'synthol'; a product comprising of hydrocarbons and oxygenates (Fischer and Tropsch, 1923). In 1925 mixtures of cobalt and chromium were found to be more active than the iron based catalysis. The synthesis could be performed at temperature ca. 20°C lower than the iron based catalyst. Low temperature and low pressure cobalt-based catalyst Fischer-Tropsch synthesis was developed and commercialised in Germany during World War II (Storch et al., 1951). At the same time, a medium pressure iron based process was developed. In 1948 the US Bureau of Mines and Oil Industry started a Fischer-Tropsch plant using an iron-based catalyst using fluidised

bed technology, in Bronwsville, Texas in 1948. The synthesis gas for this process was derived from natural gas. The plant was shut down because of economical reasons (Storch et al., 1951).

One of the success stories to date in the Fischer-Tropsch synthesis to date is that of Sasol in South Africa. Sasol began coal based Fischer-Tropsch synthesis in 1955 on a commercial scale using fixed bed reactors with an iron catalyst in Sasolburg. In the early eighties Sasol built and commissioned two new Fischer-Tropsch plants in Secunda (Dry, 1990).

New Fischer-Tropsch process applications for natural gas conversions to liquid fuels have been recently applied on a commercial scale. PetroSA (former Mossgas) in Mossel Bay (South Africa) was commissioned in 1991 using Sasol developed technology for synthesis gas conversion (Dry, 1990; Knottenbelt, 2002). The Shell Middle Distillate Synthesis Process (SMDS) technology was commissioned in Bintulu (Malaysia) in 1993 (Corke 1998; Dawe, 2001; Dry, 2002). A methane-based Fischer-Tropsch plant (Sasol and Chevron venture) is currently in planning Nigeria; Exxon and Sasol have designed similar plants for Quatar (Dry, 2001).

1.2 Economics

The economic viability of the Fischer-Tropsch process depends on the price of crude oil, which has varied considerable over the past 30 years (Dry, 2002). Traditionally gas to liquid (GTL) plants have only been regarded economically feasible at crude oil prices of US $ 30-35/bbl, but the recent development of highly active cobalt-based Fischer-Tropsch catalysts has assisted greatly in the reduction of this target cost of crude oil to US $ 20/bbl (Van Berge et al., 2000). Activity and selectivity among other remain challenging problems to be overcome to make the Fischer-Tropsch process very competitive at crude oil prices below about $US 30 (Adesina, 1996). The largest contributor to the capital investment of a GTL plant is, however, the reforming (60% of the total). Although an economy of scale GTL plant would demand a much larger scale

of reforming than required in traditional applications (Van Berge et al., 2000; Dawe, 2001).

According to Dry (2002), environmental/political considerations are also a key to the success of the process. For example, Fischer-Tropsch diesel is low in sulphur and aromatic content. It is characterised by cetane numbers greater than 70, which makes them ideal for poor diesel upgrade, and use when environmental emission limits puts a restriction on use of oil derived diesel (Knottenbelt, 2002). The economics of Sasol and Shell Fischer-Tropsch plants have been supported by the high prices obtained for its speciality product, such as high quality diesel, hard wax, olefins, and oxygenates (Corke, 1998).

1.3 The Fischer-Tropsch process

The Fischer-Tropsch process is the heterogeneously catalysed hydrogenation of carbon monoxide yielding longer chain hydrocarbons such as paraffins and olefins (Storch et al., 1951). The general block flow diagram for the Fischer-Tropsch process route involves synthesis gas production followed by synthesis gas conversion into hydrocarbons (Fischer-Tropsch synthesis) and product upgrading. Figure 1-1 illustrates the process used by Sasol with synthesis gas produced from coal gasification (Sasol facts, 2001).

At Sasol the Fischer-Tropsch process is performed in two different modes, viz. high temperature and low temperature. In the high temperature (P~20 bar; T~300-350 ^{0}C) Fischer-Tropsch synthesis, broad spectrums of hydrocarbons ranging from C_1-C_{20} are produced (Sasol facts, 2001; Dry, 2000). The products are mainly hydrocarbons in the gasoline boiling range, low molecular weight olefins and some oxygenates. The low temperature conversion (P~20 bar; T~200-240 ^{0}C) is mainly used for the production of high molecular weight linear waxes.

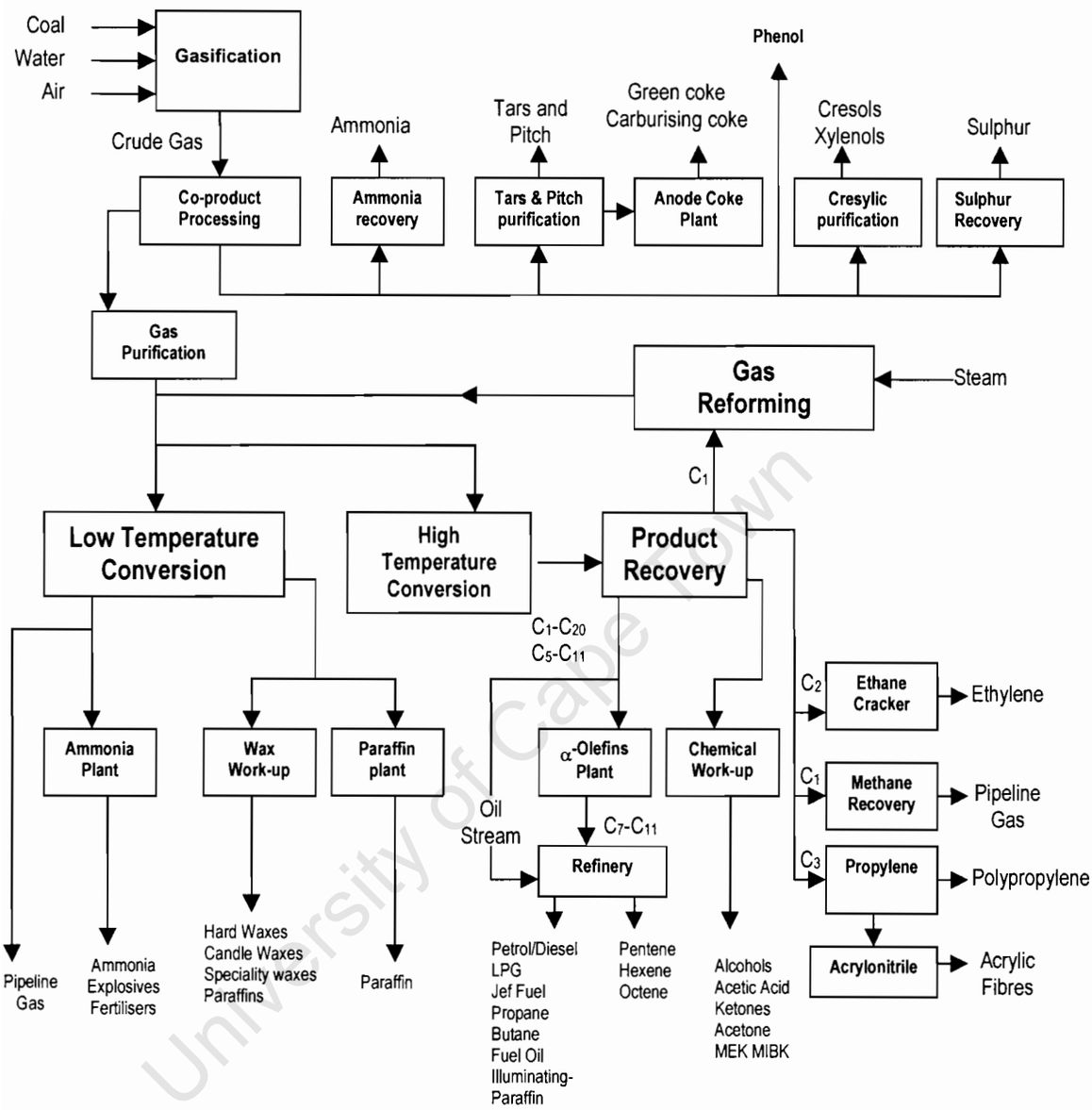

Figure 1-1: The Sasol Fischer Tropsch Process, (Adapted from Sasol facts, 2001)

The Shell Middle Distillate Synthesis (SMDS) process (see Figure 1-2) is commercially applied in Malaysia. Synthesis gas is converted into heavy parrafins over a cobalt-based catalyst in this process (Adesina, 1996; Dawe, 2001). The heavy paraffins are subsequently hydrocracked and distilled to produce high quality gas oil, kerosene and naphtha.

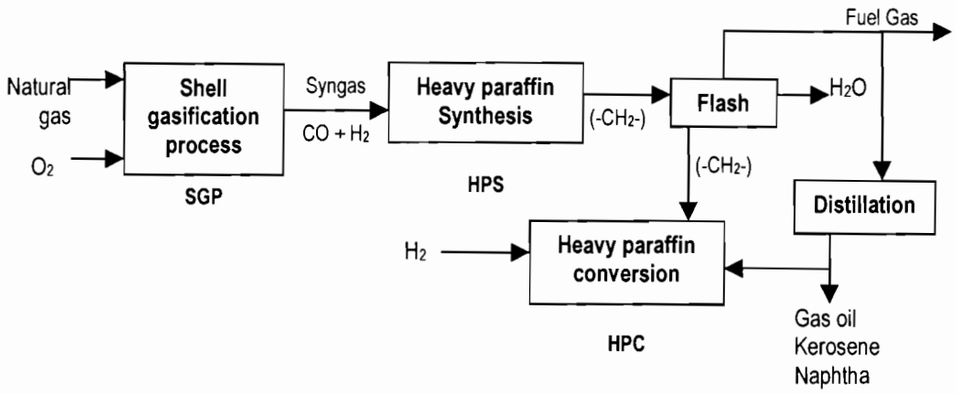

Figure 1-2: A simplified flow scheme -The Shell middle Distillate Synthesis (SMDS) process (Adapted from Dawe, 1999).

Product upgrading differs from application to application and it depends on the type of products produced in Fischer-Tropsch synthesis. Although the basic production and separation principles may be similar, the details of the technologies are very different and the companies have separate patent portfolios (Sasol facts, 2001; Dawe, 2001).

1.4 Synthesis gas preparation

Various methods and technologies can be used to convert different fossil carbon sources (coal, natural gas, shale oil, biomass, etc.) into synthesis gas and ultimately into hydrocarbons and oxygenates (Yakobson, 2000). Coal gasification and natural gas reforming are the most common resource from which synthesis gas is produced. (Cybulky et al., 1993; Basini and Piovesan, 1998).

Some of the commonly used methods for converting natural fossils into synthesis gas are shown in Table 1-1. In methane reforming by autothermal reforming (ATR), 20% of the feed methane is converted to CO_2 whereas with coal gasification this figure is around 30% due to the much lower hydrogen content in coal (Dry, 2002). The Texaco, Lurgi and the Shell/Koppers gasifiers from which synthesis gas is obtained by steam gasification of coal or coal combined with heavy oil produce a synthesis gas with CO/H_2 of about 0.5. Texaco and Shell/Koppers gasifiers produce much more CO_2 compared to the Lurgi gasifier.

Table 1-1: Syngas, production feed stocks, technology and typical compositions

Feed Stock	Process	Component (vol. %)			
		H_2	CO	CO_2	Other
Natural gas, steam	SR[1]	73.8	15.5	6.6	4.1
Natural gas , steam, CO_2	CO_2 –SR[3]	52.3	26.1	8.5	13.1
Natural gas, steam, CO_2 O_2	ATR[2]	60.2	30.2	7.5	2.2
Coal/Heavy oil, steam, oxygen	Gasification[2]	67.8	28.7	2.9	0.6
Coal/Heavy oil, steam, oxygen	Taxaco gasifier[2]	35.1	51.8	10.6	2.5
Coal/Heavy oil, steam, oxygen	Shell-Koppers gasifier[1]	32.1	55.0	10.5	2.4
Coal/Heavy oil, steam, oxygen	BCG-Lurgi gasifier[2]	28.6	54.9	3.4	8.7

SR-Steam reforming, ATR-Autothermal reforming

1. Data from Pay and Patel (1981).
2. Data from Cybulky et al. (1993).
3. Data from Basini and Piovesan (1998).

1.5 Fischer-Tropsch reaction mechanisms

CO hydrogenation via the Fischer-Tropsch synthesis process involves a complex system of series and parallel reaction steps that uses CH_X monomers derived from synthesis gas (Brady and Petit, 1981; van Barneveld and Ponec, 1984). The key reaction steps in Fischer-Tropsch reaction are chain initiation, chain growth and chain termination. Various mechanisms have been put forward to explain the conversion of synthesis gas into higher hydrocarbons.

1.5.1 The Carbide-Carbene Mechanism

The carbide theory was first suggested by Fischer and Tropsch in 1926, the C-C bonds are produced via the polymerisation of methylene species (CH_2) on the metal surface (Storch et al., 1951; Brady and Pettit, 1981). In this mechanism CO is chemisorbed and dissociated on the metal surface yielding chemisorbed carbide and oxygen; the latter hydrogenated to water. The carbide is then hydrogenated to surface methylene groups. Chain growth is accomplished by insertion of an adjacent methylene into the chain initiator (CH_3), with the subsequent hydrogenolysis of the remaining carbon-metal bond (see Figure 1-3) (Brady and Pettit, 1981). Chain growth occurs via the insertion of CH_2-species. Chain termination occurs, either by β hydride abstraction into olefin product or by associative desorption of an alkyl species together with an H-atom into paraffins. Works done by Brady and Pettit (1981) and van Barneveld and Ponec (1984) support this mechanism.

The Carbide-Carbene mechanism main shortcoming is that it does not explain the formation of oxygen-containing products that accompanies the formation of hydrocarbons in Fischer-Tropsch synthesis.

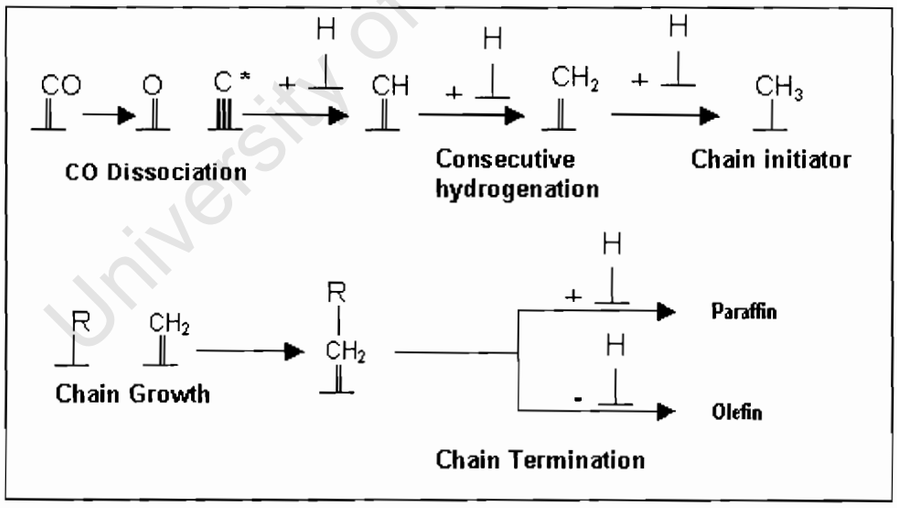

Figure 1-3: Scheme of the Alkyl Mechanism as proposed by Brady and Petit (1980).

1.5.2 Enol Condensation Mechanism

Anderson et al. (1951) postulated another mechanistic route where they suggested that the C-C bonds are formed through a condensation reaction between hydroxy-methylene groups on the catalyst surface (Storch et al., 1951). The mechanism they proposed is depicted in the Figure 1-4. In this mechanism, chain growth is assumed to occur by hydrogenolysis of one of the carbon-metal bonds, thus allowing chain growth. Further hydrogenolysis leads yields alcohols, which upon hydrogenation form hydrocarbons. Olefinic products are thought to originate from the spontaneous breakdown of a longer hydroxylated species into an olefin and the basic surface hydroxy-methylene group. Brady and Petit (1981) used isotope labelling (^{13}CO) experiments to show that experimental Fischer-Tropsch product distribution were incompatible with those proposed by the mechanism predicted by the Enol mechanism.

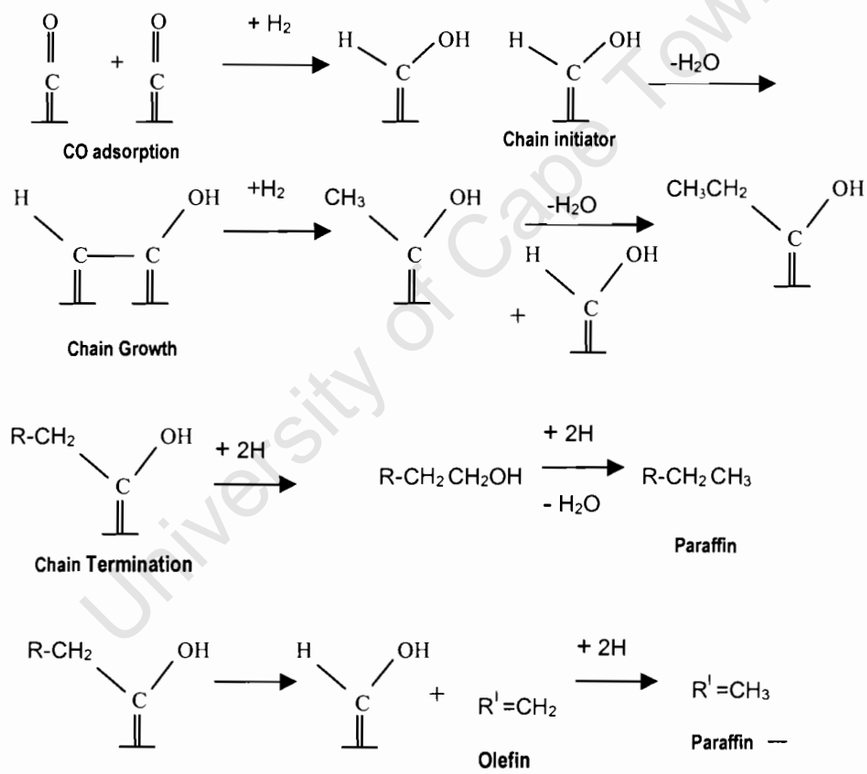

Figure 1-4: Scheme of the Enol Condensation Mechanism (according to Anderson et al., 1951).

1.5.3 CO Insertion Mechanism

Pichler and Schulz (1970) suggested that the C-C bonds arose though the insertion of CO into the metal alkyl bond analogous to the well-known insertion of CO in homogeneous systems. This proposed scheme is shown in Figure 1-5. This mechanism might explain the formation of oxygenates found in Fischer-Tropsch product.

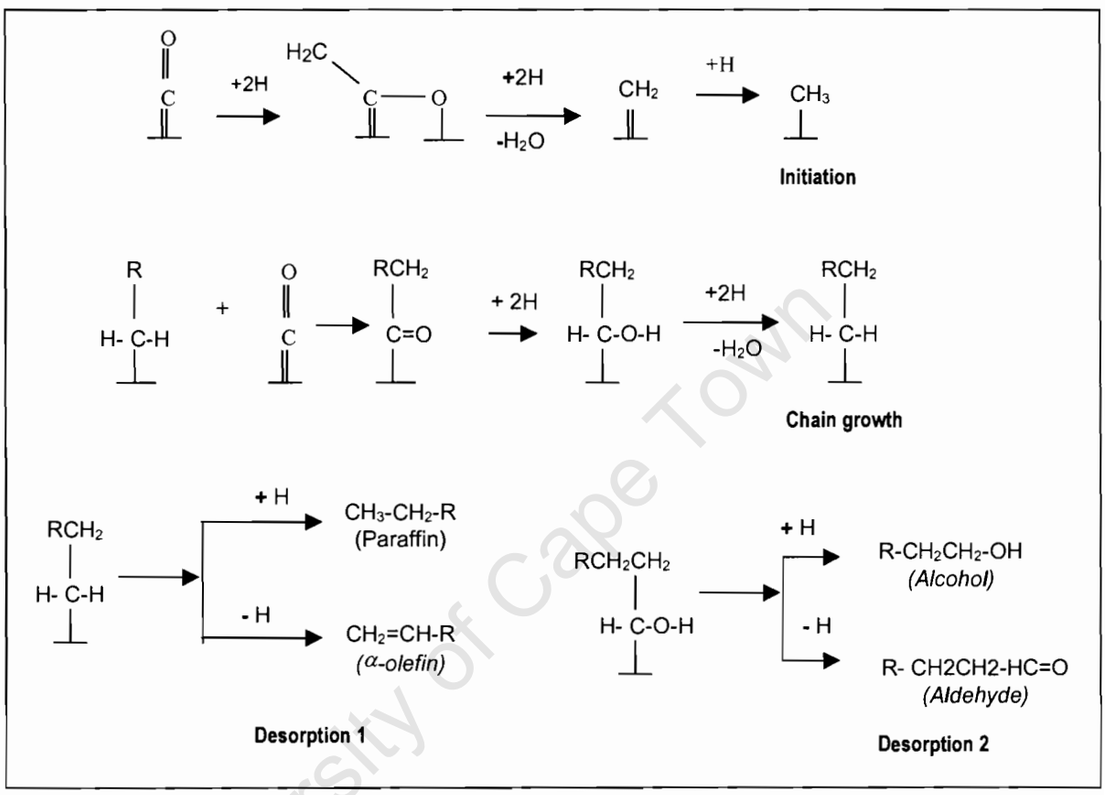

Figure 1-5: Scheme of the CO Insertion Mechanism proposed by Pichler and Schulz (1970).

1.5.4 Alkenyl Mechanism

The most recently reported mechanism was proposed by Maitlis et al. (1996), in which chain growth is initiated by vinyl species as opposed to the generally accepted surface methylene or alkyl species (see Figure 1-4). Chain propagators are alkenyl species rather than alkyl species.

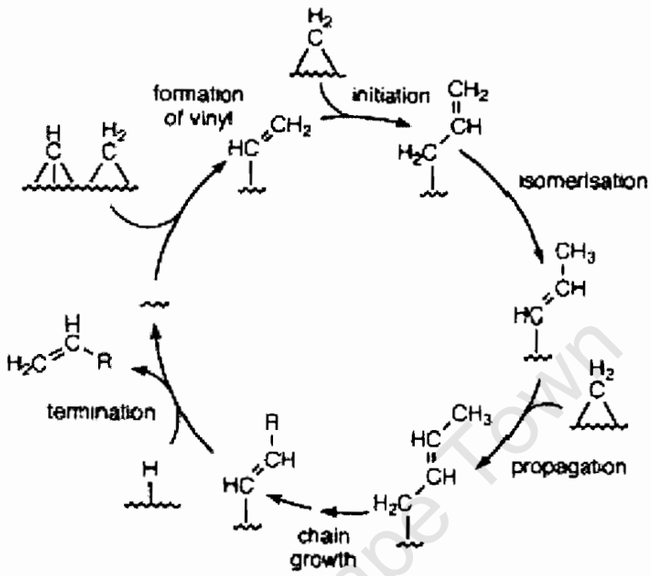

Figure 1-6: Scheme of the Alkenyl mechanism as proposed by Maitlis et al. (1996).

This mechanism has recently been refuted by Ndlovu et al. (2002) where they cited one of the mechanism shortcomings to be its prediction of 100% primary olefin selectivity, which is not observed experimentally. They also did not observe the isomerisation of the allyl to vinyl species claimed in the mechanism proposed by Maitlis et al. to be chain initiators in the Fischer-Tropch synthesis (Ndlovu et al., 2002).

1.6 Fischer-Tropsch product distributions

The variety of compositions of Fischer-Tropsch product comprising of hundreds of individual compounds shows a remarkable order with regard class and size of the molecules (Schulz and Claeys (b), 1999; Dawe, 2001). A number of researchers have come up with mathematical models describing the Fischer-Tropsch product distribution, the Anderson-Schulz-Flory distribution being the basic and the simplest of these kinetic models (Schulz and Claeys (b), 1999; Patzlaff et al., 1999).

The basis of the Anderson-Schultz-Flory (ASF) polymerisation kinetics, is the generally accepted belief that the Fischer-Tropsch reaction proceeds via the addition of a C_1 monomer (Storch et al., 1951, Schulz and Claeys (b), 1999) and may be presented as follows:

$$\mathbf{M_N=(1-\alpha).\alpha^{N-1}} \qquad (3)$$

Where $\mathbf{M_N}$ the molar fraction of the linear products with carbon number **N** and α the chain growth probability (Schulz and Claeys (b), 1999). The so-called Anderson-Schultz-Flory plots are those obtained from plotting log ($\mathbf{M_N}$) versus **N** which according to equation 3, predicts a linear relationship between log ($\mathbf{M_N}$) and **N,** from which the chain growth probability is obtained. This simple model assumes the chain probability to be independent from the carbon number of the growing species, which is not the case in the Fischer-Tropch product distribution (Schulz and Claeys (b), 1999; Patzlaff et al., 1999).

The noted empirical deviations of the Fischer-Tropsch product distribution from the theoretically predicted ASF product distribution are:

- High yield of methane i.e. low chain growth probability for C_1 surface species (Schulz et al., 2002)
- Relatively low ethene yield, which has been explained by strong ethene re-adsorption for chain initiation and chain growth. (Schulz and Claeys (a), 1999; Schulz et al., 2002).

- Increase in chain growth probability in the range of C_7-C_8, indicative of increasing n-olefin re-adsorption for further chain growth (Madon et al., 1991; Schulz et al., 2002).

Figure 1-7 illustrates a typical ASF plot obtained from analysis of a Fischer-Tropsch product distribution.

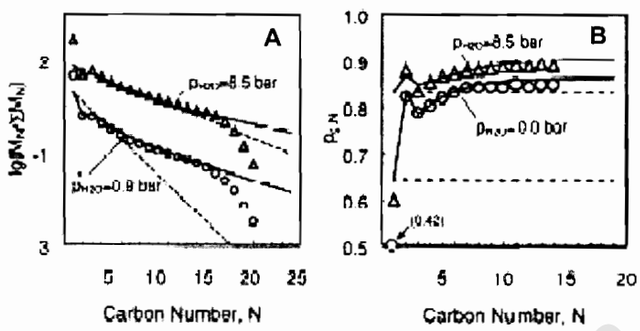

Figure 1-7: (A) Typical ASF distributions from Co-Zr-SiO_2 catalysed Fischer-Tropsch synthesis. **A**-ASF plots, **B**- variation chain-growth probability with carbon number. Dashed lines represent Ideal ASF kinetics without primary product readsorption and solid lines modelled from secondary readsorption considerations. (Adapted from Schulz and Claeys (b). (1999)).

1.7 Transport effects on Fischer-Tropsch Selectivity

Semi-quantitative models on the effect of intra-pellet diffusion on selectivity in the Fischer-Tropsch synthesis catalyst pellets has been developed by Iglesia et al, (1995). The proposed model by Iglesia (1997) could explain Fischer-Tropsch synthesis product data, especially C_{5+} selectivity from cobalt catalysts of different pellet sizes. In the cobalt catalyst Fischer-Tropsch synthesis selectivity of long chain hydrocarbons depends on the transport of CO into pellets reactive sites and the diffusion of product from the active site into the fluid phase (Iglesia et al., 1995).

The model proposed by Iglesia follows a classical engineering approach to transport limitations in heterogeneously catalysed systems. The basis of the model is the effectiveness factor of the catalyst from which a Thiele module is derived. (The Thiele module is an indicator of the rate of reaction relative to intra-pellet transport rates of reactants/products- Fogler, 1992; Iglesia, 1997). A high Thiele module implies that the kinetics of the reacting system is controlled by the diffusion rate, otherwise by surface reaction.

Iglesia and co-workers (1995) showed that the Thiele modulus could be broken down into a structural parameter χ and a diffusional parameter Ψ_{CO}. The diffusional parameter Ψ is compound specific, whereas the structural parameter χ describes catalyst pellet. The proposed by Iglesia et al. (1995) for cobalt catalysts model is briefly shown below:

Thiele Module

$$\Phi_o^2 = \left(\frac{2 \cdot H_{CO} \cdot R^*_{CO}}{C_T \cdot P_T \cdot D_{CO}} \right) * \left(\frac{R_0^2 \cdot \varepsilon \cdot \theta_{CO}}{r_p} \right)$$

With structural parameter χ:

$$\chi = \left(\frac{R_0^2 \cdot \varepsilon \cdot \theta_{CO}}{r_p} \right)$$

And the diffusivity reactive parameter Ψ_{CO} being:

$$\psi_{CO} = \left(\frac{2 \cdot H_{CO} \cdot R^*_{CO}}{C_T \cdot P_T \cdot D_{CO}} \right)$$

Where:

R_{CO}^*	- Rate of CO consumption	[$mol.s^{-1}.g_{cat.}^{-1}$]
P_T	-Total Pressure	[Pa]
C_T	-Molar concentration of liquid phase	[$mol.m^{-3}$]
R_O	-catalyst pellet radius	[m]
D_{CO}	-Effective CO diffusivity within catalyst	[$m^2.s^{-1}$]

H_{CO}	- Henry's constant for CO	[Pa]
r_p	- Mean pore radius	[m]
ε	- Pellet porosity	
χ	-Structural parameter	[m^{-1}]
ϕ_M	-Catalyst site density	[g atom surface Co.m^{-2}]
ψ_i	-Diffusivity reactive parameter for species i.	[m]

(Iglesia, 1995)

The selectivity for higher molecular weight hydrocarbons (C_{5+}) in the Fischer-Tropsch synthesis, depends among other factors, on the structural parameter,χ, of the catalyst (Iglesia et al., 1995). The structural parameter,χ, is a mainly a function of active site density, an extrinsic property that might be changed by modification of the catalyst structure during catalyst synthesis. The diffusional parameter,ψ, remains unaffected by catalyst structural changes; since it depends only on intrinsic kinetic and diffusivity properties of reacting species.

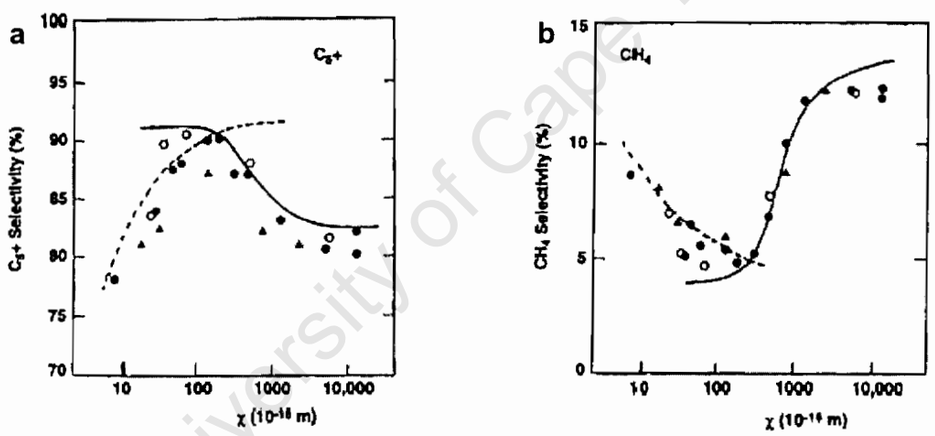

Figure 1-8: The effect of structural parameter (χ) on Fischer-Tropsch synthesis selectivity. Diffusion-enhanced readsorption (-----) and diffusion-inhibited chain growth (-----) simulations and experimental data (O, dispersion/support effects; ▲, pellet size variations; ●, eggshell thickness variations (a) C_{5+} selectivity; (b) CH_4 selectivity. (473K, 2000kPa, H_2/CO=2:,55-65% CO conversion. (Adapted from Iglesia, 1997).

Iglesia et al. (1995) showed structural parameter effects on Fischer-Tropsch synthesis selectivity for cobalt-based catalysts of varying dispersions supported Al_2O_3, TiO_2 and SiO_2. Figure 1-8 depicts the results reported by Iglesia (1997). At small χ values selectivity to C_{5+} products increases (see Figure 1-8 (a)) and the methane selectivity decreases (Figure 1-8 (b)) as χ increases. These observations were attributed to increased diffusion restrictions (an inherent property of increasing χ), which decrease chain termination probabilities because of increased intrapellet olefin concentration and longer intrapellet residence times. This increases the probability of olefin readsorption hence an increase in average chain size (Iglesia, 1997).

At intermediate χ values the increase in C_{5+} selectivity approaches a maximum and subsequently decreases with increasing χ. The structural catalyst properties that control the diffusional removal of α-olefins at low values of χ begin to restrict reactant arrival rates as χ increases further (Iglesia et al., 1995). The methane selectivity at this point begins to increase with increasing χ. Intermediate values of χ limits olefin removal enhancing their secondary readsorption but still permit rapid access of reactants to reaction sites, lead to highest C_{5+} selectivities (Iglesia et al., 1995).

CO transport limitations at high χ values, lead to high effective H_2/CO ratios at catalytic sites, which increase the chain termination probability and the extent of secondary hydrogenation of α-olefins; leading to a more lighter, more paraffinic product (Iglesia et al., 1991). An ideal catalyst is therefore, one with intermediate χ values, which is optimised around dispersion effects and transport limitations for C_{5+} selectivity (Iglesia et al., 1995).

1.8 Fischer-Tropsch Catalysts

All group VIII metals are reported to show a certain amount of Fischer-Tropsch activity. The different metals show varying activities, product distributions, and therefore require different operating conditions (Vannice, 1975; Dry, 1981). Typical Fischer-Tropsch catalysts are iron- (Fe), cobalt- (Co), nickel- (Ni) or ruthenium- (Ru) based. Iron and cobalt based catalysts are commercially applied for the synthesis of hydrocarbons. Nickel is not used as Fischer-Tropsch catalyst commercially because it is more selective to methane at reasonable pressures, while ruthenium is a scarce and expensive metal (Dry, 1990).

1.8.1 Cobalt-based Fischer-Tropsch catalyst.

A good catalyst should not only be active for the desirable reaction but should also be selective and stable to be commercially applied (Le Page, 1997). In terms of synthesis gas efficient usage the cobalt catalyst are preferred since one CO molecule is consumed for every CH_2 produced (Xu et al., 1998). Iron based catalyst show high water gas activity hence some of the CO is consumed in this reaction. Apart from efficient CO usage, cobalt Fischer-Tropsch catalyst have been found to be both active and stable compared to typical industrial iron based Fischer-Tropsch (van Berge and Everson, 1997).

Cobalt catalysts are also well suited for synthesis when high chain growth probability and low branching probabilities are required resulting in high molecular weight linear hydrocarbons (Feller et al., 1999; Dawe, 2001). Cobalt is more expensive than iron, thus necessitating high dispersion on supports and long catalyst lifetime (Iglesia, 1995; Feller et al., 1999). The most significant advantage cobalt based catalyst over the iron based is its low activity for the water gas shift reaction resulting in the low formation rates for CO_2 (Patzlaff et al., 1999; Dry, 2002), and the formation of mainly straight chain hydrocarbons with minimal amount of alcohols (Xu et al., 1998; Dry, 1981).

Iron based Fischer-Tropsch catalyst, which are normally used for the production of high molecular weight hydrocarbons in the high temperature Fischer-Tropsch synthesis, operates at low to intermediate chain growth probabilities to prevent wax accumulation within the catalyst pores (Van Berge and Everson, 1997). This results in large amounts of co-produced methane, ethane and LPG, which have to be recycled (Xu et al., 1998). The Shell Co-based catalyst operates at high chain growth probabilities, thus minimising the formation of unwanted light products making it ideal for maximum diesel production (Dawe, 2001).

1.8.1.1 Activity and stability

Van Berge and Everson (1997) showed the superiority of cobalt-based Fischer-Tropsch catalyst over its iron counterpart at relatively low space velocities and relatively low pressures (see Figure 1-9). The conclusion drawn from Figure 1-9 **(A)** is that at 20-bar operation, the cobalt catalyst outperforms the iron at low relative space velocities. Figure 1-9 **(B)** confirms the notion that cobalt is favoured at low reactor pressures combined with low space velocities, the latter implying conditions favourable for high conversion per pass levels. These observations were attributed to the fact that cobalt based Fischer-Tropch kinetics is not inhibited by reaction water while iron based Fischer-Tropch kinetics is more sensitive to the absolute water partial pressure (van Berge and Everson, 1997).

Van Berge and Everson (1997) also investigated the stability the cobalt-based catalyst and reported a two stage time on stream catalyst deactivation, the first stage within the first 4-days on stream attributed catalyst conditioning. CO conversion was reported to drop by about 5% in 25 days after the conditioning stage; this irreversible catalyst deactivation rate was attributed to sulphur poisoning.

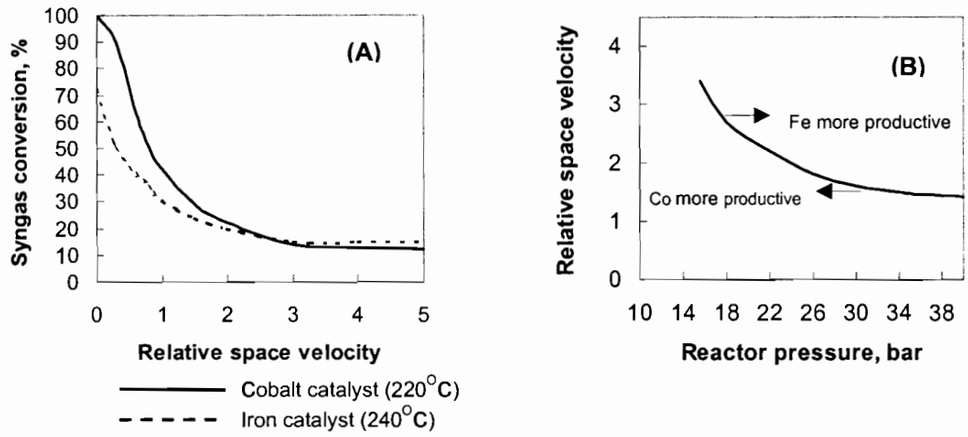

Figure 1-9: (A) Activity comparison between the iron and cobalt catalysts at 20 bar; **(B)** Productivity comparison between the iron catalyst (240^{O}C) and cobalt catalyst (220^{O}C). (Adapted from van Berge and Everson (1997))

1.8.2 Supported Fischer-Tropsch Catalysts

Supports allow the active phase to be cast into a form of coarse particles suitable for use in technical reactors. The active phase usually constitutes between 1 and 20 wt-% of the total catalyst, normally in a form of very small crystallites (1-50 nm). (Doesburg and van Hooff, 1993). The high active metal dispersions on high surface carriers maximises active metal usage (Vannice, 1977; Buonomo et al., 1994). Ideally the support is not supposed to be catalytically active, however, in partnership with the active phase it can participate in the reaction in a number of significant ways. Furthermore, supported metal catalysts also show enhanced thermal stability owing to active metal and support interactions, which increases catalyst life and avoids sintering. (Doesburg and van Hooff, 1993)

Addition of inactive species (structural promoters) to supported catalyst serves to enhance the selectivity/activity or stability of the catalyst. Metal oxides such as ThO_2 have been used as a structural promoter for cobalt catalyst (Anderson et al., 1951; Walsh, 1998). An iron based Fischer-Tropsch catalyst was mentioned by Dry (1981) where Fe supported on SiO_2 was co-promoted with V_2O_5. The catalyst Fe-Cu-SiO_2-V_2O_5 was reported to have a

high activity and a high wax selectivity compared to CaO and Cr_2O_3 promoted catalysts. Feller et al. (1999) showed that promotion of Co/SiO_2 with zirconia resulted in increased Co dispersion. The consequence of increased dispersion was an increase in C_{5+} selectivity, which passed a maximum and a corresponding decrease in methane, which went though a minimum. Similar observations are reported in works by Iglesia et al. (1995) in which they altered the structural parameter of the catalyst by loading a cobalt based Fischer-Tropsch catalyst on TiO_2. Structural parameter changes resulting from metal oxide promotion may involve improved metal dispersions and reduction of intrapellet pore volume of the catalyst. High metal dispersions improve C_{5+} selectivity by availing more sites for readsorption of primary olefins to initiate chains and subsequently grow into long chain products. Pore narrowing leads to longer intrapellet residence times for primary α-olefin to undergo secondary insertion/ readsorption and improve C_{5+} selectivity. Promotion of a Co based catalyst with V_2O_5 coupled with MnO has been patented by Shell recently to improve the C_{5+} selectivity in the Fischer-Tropsch product distribution (Geerlings et al., 1997). Promotion by metal oxides may thus enhance metal dispersion increasing the number of active sites.

1.8.3 Catalyst preparation

Preparation of supported catalyst is still considered as more art than a science (Geus and van Veen, 1993) and can basically be achieved in two ways.

I. selective removal of a component from a non-porous phase containing a precursor of the active component(s) and the support e.g. a co-precipitate, usually achieved by thermal-treatment in reducing atmosphere.

II. separate introduction of a precursor of the catalytically active material (s) onto a pre-existing support, e.g. by impregnation, ion exchange, anchoring, grafting, spreading and wetting,

heterogenoisation of complexes, deposition precipitation (Geus and van Veen, 1993; Che et al., 1997).

Emphasis in this review will focus on ion exchange and wet-impregnation since these play a crucial role in support and catalyst preparation for this study. Other methods and factors to consider in catalyst preparations are well documented in numerous publications (Smith, 1981; Che et al., 1997).

1.8.3.1 Active metal impregnation

Fischer-Tropsch catalysts are usually prepared via precipitation, impregnation, ion-exchange or vapour deposition techniques. Commercial iron and cobalt catalysts have largely been prepared using precipitation techniques, while vapour deposition techniques are promising in that high metal dispersions can be achieved without deactivation through strong metal-support interactions (Iglesia et al., 1995). A well-prepared supported catalyst should exhibit high dispersion of the active metal phase to achieve a large surface area for reaction to occur. For Co-based catalyst, this can be achieved by, synthesis of small crystallites at high local surface densities on the support, and supports that increase the rate per surface cobalt atom area (Iglesia 1997).

Ion exchange involves the electrostatic interaction of a support by ionic species in solution, while impregnation refers to the introduction of the active phase(s) into a high surface area support. During impregnation, a previously dried support of known pore volume is loaded with a precursor of the active phase in such a way that the precursor solution fills the pores of the support. This is termed as dry impregnation, i.e. the pore volume of the support is exactly equal to the volume of the added precursor solution. In wet impregnation, the volume of the precursor is larger than the pore volume of the support (Che et al., 1997). Both ion exchange and impregnation are influenced by a number of parameters such as pH, temperature, starting salt, type of oxide support, and impurities during support/catalyst preparation steps (Geus and van Veen, 1993)

1.8.3.2 pH effects in catalyst preparation

In an exchange procedure pH of the exchange medium is very important because it determines the surface charge of the support and hence whether cationic or anionic specie is adsorbed or exchanged. To fully appreciate the extent of the impact of pH in ion exchange one has to have an insight into the surface chemistry of support oxides and an understanding of the ionic species involved. Under hydrated conditions, the surface of an amorphous oxide is covered by a thin layer of water and its hydroxyl (OH^-) is subject to pH equilibria reactions (Geus and van Veen, 1993; Che et al., 1997; Weckhuysen and Keller, 2003):

$$M\text{-}OH_2^+ \leftrightarrow M\text{-}OH + H_S^+$$
$$M\text{-}OH \leftrightarrow M\text{-}O^- + H_S^+$$
$$H_S^+ \leftrightarrow H^+$$

Where **M**=Si, Al, Zr, Ti, V, or Mg; $\mathbf{H_S^+}$ and $\mathbf{H^+}$ represent surface and solution proton respectively. The resulting surface charge arising from an excess of one type of charged site over the other is a function of the solution pH. There exists a pH for which the net charge of the surface is zero. This value is characteristic for an oxide and is called the Point of Zero Charge (PZC) or the Isoelectric point (Che et al., 1997). When oxide particles are suspended in aqueous solution with pH>PZC, the oxide particles tend to negatively charged, increasing their affinity to adsorb cationic species. Conversely at pH<PZC anion adsorption is favoured (Geus and van Veen, 1993; Che et al., 1997). Figure 1-10 illustrates the variation of zeta potential, which reflects the particle surface charge as a function of pH for alumina and silica. γ-Al_2O_3 is amphoteric and may also adsorb cations as well as anions depending on the pH of the adsorption media.

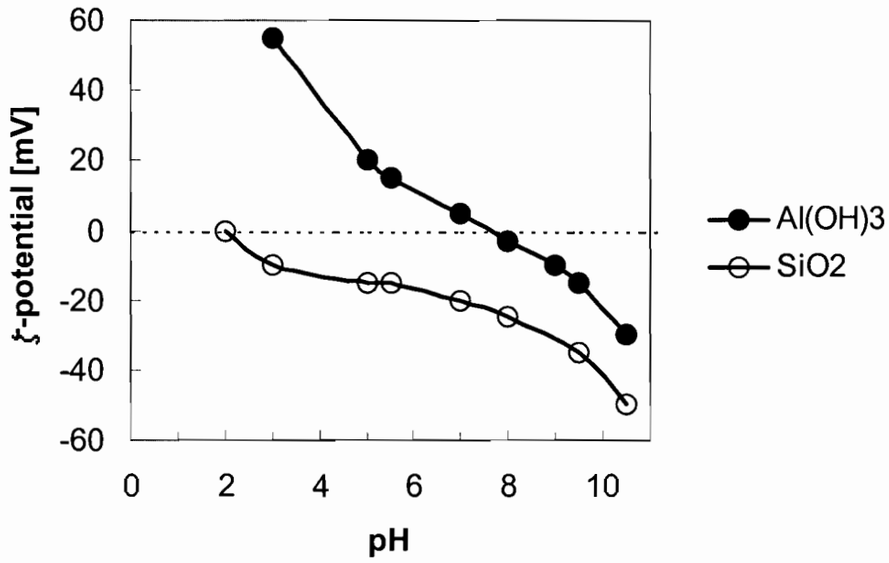

Figure 1-10: Variation of zeta potential of silica and alumina (gibbsite) a function of pH. (Redrawn from Che et al., 1997)

1.9 Vanadium oxide chemistry and speciation

Surface chemical properties of a solid catalyst are very crucial in catalyst and the to the eventual activity of the catalyst. In solution, supported vanadium oxides show chemical and electronic properties, which are entirely different from those found for unsupported vanadium oxides (Clark, 1973; Weckhuysen and Keller, 2003). In this section a brief overview of the behaviour and speciation of the complex array of vanadium oxides in solution will briefly reviewed.

The chemistry of vanadium compounds is related to the oxidation-state of the vanadium. Thus, V_2O_5 is acidic and weakly basic, VO_2 is basic and weakly acidic and V_2O_3 and VO are basic (Woolery, 1997). According to Clark (1973), when vanadium pentoxide is subjected to an aquatic environment anionic species are generated by hydrolysis. The various equilibria involved in hydrolysis maybe formally divided into two categories:

Protonation, e.g. $VO_4^{3-} + H^+ \longleftrightarrow HVO_4^{2-}$

Condensation, e.g. $2HVO_4^{2-} \longleftrightarrow V_2O_7^{4-} + H_2O$.

The most important oxidation states of vanadium in aqueous solution are V^{5+} and V^{4+}. The specific vanadium oxide that can exist depends on the solution pH and the vanadium concentration (Weckhuysen and Keller, 2003; Baes and Mesmer, 1976) as illustrated in Figure 1-11, which shows the different regions in which a particular vanadium oxide is stable. This scheme is generally known as a Poubaix diagram.

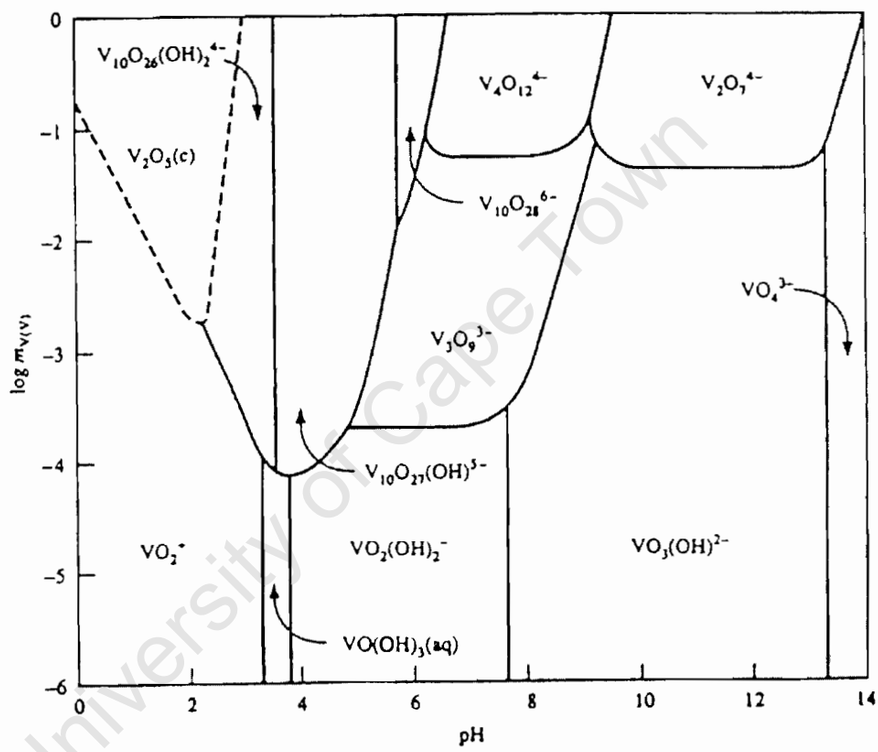

Figure 1-11: The Poubaix diagram of vanadium expressing the vanadium speciation as a function of pH and molality of vanadium at 25^{0}C. (Beas and Mesmer, 1976)

In aqueous solutions, vanadates on acidification undergo a series of complex hydrolysis reactions (Clark, 1973), which is apparent from the Poubaix diagram. In strong alkaline solutions, the VO_4^{3-} ion is the most predominant species. It is a moderately strong base, hydrolysing in solution to form the HVO_4^{2-} species (Clark, 1973; Weckhuysen and Keller, 2003). Clark reported that the VO_4^{3} is likely to condense to the $V_2O_7^{4-}$ ion, which can then be protonated to form the $H_2VO_4^{-}$ ion. The polymerisation reactions of the $H_2VO_4^{-}$ are a still a grey area with most evidence pointing to the formation of both the trimer $V_3O_9^{3-}$ s well as the tetramer $V_4O_{12}^{4-}$ (Clark, 1973; Beas and Mesmer, 1976).

1.9.1 Vanadium on oxide supports

Vanadium oxide can be loaded onto a support by the impregnation method, which is simple and widely used preparation technique. If the support is dipped into an excess amount of solution, the process is called wet impregnation. Precise control over the vanadium oxide loading may be achieved with a technique called dry impregnation, pore volume impregnation or incipient wetness impregnation. The support is then contacted with a solution of appropriate concentration, corresponding in quantity to the total known pore volume of the support, or slightly less. This allows precise control of the concentration of the active vanadium oxide component on the support. However, the maximum loading obtainable in a single impregnation is limited by the solubility of the reagent and if necessary multiple impregnation steps should be applied (Weckhuysen and Keller, 2003).

V_2O_5 has a low solubility (0.08/l) in aqueous solutions and therefore, to achieve high V_2O_5 loadings, impregnating precursors derived from relatively soluble vanadium containing salts like NH_4VO_3 dissolved in water or in aqueous oxalic acid (Weckhuysen and Keller, 2003) should be used. The impregnation process is followed by a drying and heating step in which the vanadium oxide compound is chemically anchored onto the support oxide,

Figure 1-12 illustrates the sequential steps involve in the synthesis of supported vanadia catalysts.

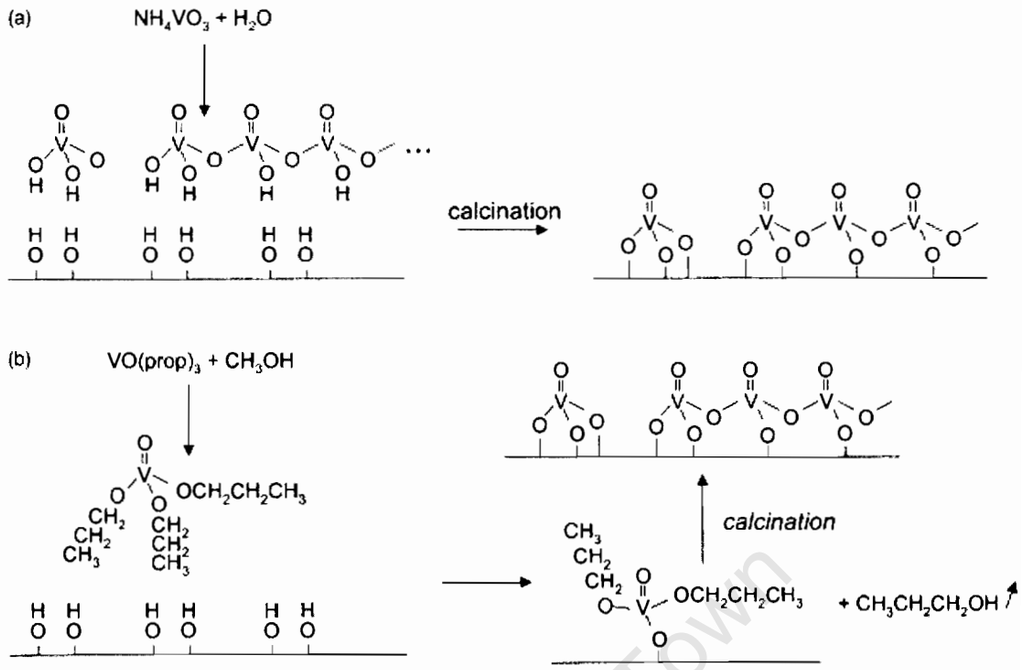

Figure 1-12: Synthesis methods for the preparation of supported vanadium oxide catalysts: (a) impregnation with an aqueous solution of NH_4VO_3, followed by calcination in oxygen and (b) impregnation with $VO(OC_3H_7)_3$ in methanol, followed by calcination in oxygen or air and release of propanol. (Adapted from Weckhuysen and Keller, 2003.)

1.9.1.1 Al_2O_3 - V_2O_5 system

In catalytic applications vanadium oxides are introduced in the system either in bulk or supported form. In this section the behaviour Al_2O_3 - V_2O_5 system in aquatic media would be reviewed.

Various techniques have been used to quantitatively and qualitatively characterize the behaviour of Al_2O_3 - V_2O_5 system. Gil-Llambas et al. (1985) used electrophoresis migration technique to try and quantify the available active surface area in Al_2O_3 and TiO_2 supported V_2O_5 catalyst system. In their experiments they varied the amount of V_2O_5 loading on each support and monitored the pH changes by electrophoresis. They reported an observed

decrease in pH at the point of zero charge (PZC) of each support with increased in V_2O_5 loading (see Figure 1-9 and Table 1-13).

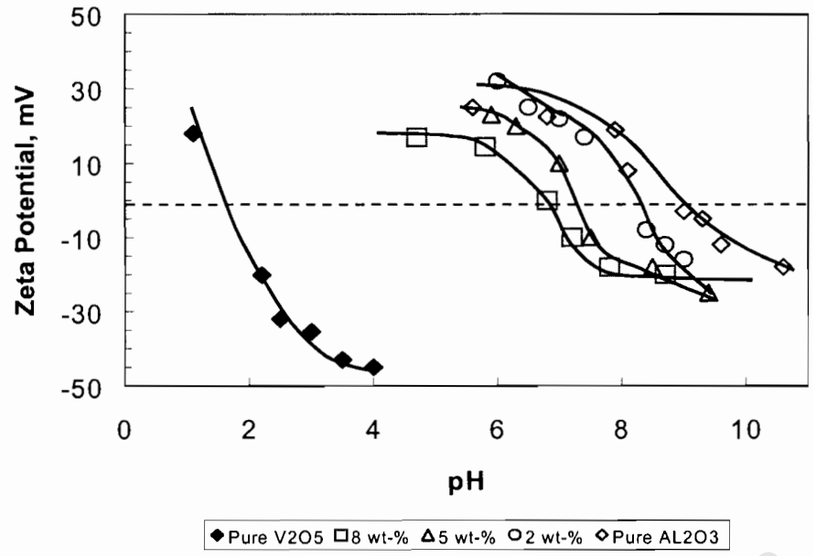

Figure 1-13: Zeta Potential (mV) as a function of pH of the suspension media of V/Al_2O_3 with different V content. (Redrawn from Gil-Llambas et al., 1985).

The Point of Zero Charge (PZC) of aqueous solutions containing oxide materials tends to approach the PZC of the oxide because oxide surfaces are positively charged at pH values below their PZC (Deo and Wachs, 1991). Consequently, under ambient conditions the pH values of the hydrated oxide surfaces present on the oxide supports should be close to PZC of the specific oxide support. Gil-Llambias et al. (1985) and Deo and Wachs (1991) reported pH value at PZC for γ-Al_2O_3 at 8.8 while a value of 1.4 was reported for bulk V_2O_5.

The acidic nature of V_2O_5 in aqueous environment lowers the net surface pH at PZC for the Al_2O_3/V_2O_5 system. Gil-Llambias et al. (1985) have shown that for the Al_2O_3/V_2O_5 and TiO_2/V_2O_5 systems, the pH at PZC of the samples decreases with the vanadium oxide loadings. The effect of the oxide overlayer is specially pronounced at high loadings. Hence, the pH at PZC of supported oxide system is expected to be lower than the pH of the oxide support at high coverages and close to the oxide support at low coverages. Predicted surface

vanadium species based on the net pH at PZC of the surface and the known vanadium oxide phases as per Poubaix diagram are shown in Table 1-3.

Table 1-2: Metal content, Isoelectric Point (IEP), Apparent Surface Coverage (ASC), and Surface Area (BET) and V_2O_5 Surface Area (S).

10^{-14} Molecules V_2O_5 (cm^{-2})	IEP (pH)	ASC[b] (%)	BET (m^2g^{-1})	S[c] (m^2g^{-1})
-	8.80	-	188	-
0.11	8.25	13	180	23
0.21	8.00	18	182	33
0.32	7.64	26	179	46
0.41	7.40	29	179	52
0.83	7.20	33	175	58
1.23	7.05	36	180	65
1.66	6.95	37	171	63
2.29	6.80	40	177	71
[a]	1.4	-	-	-

[a] unsupported V_2O_5

[b] $$ASC = \frac{M_S^{-1} \cdot (IEP_S - IEP_C) \cdot 100}{(M_M^{-1} - M_S^{-1}) \cdot (IEP_C - IEP_S) + M_M^{-1} \cdot (IEP_S - IEP_M)}$$

[c] $S = ASC \cdot S_{BET}$,

M_S - support (Al_2O_3 or TiO_2) molecular weight, M_M-molecular weight of the supported phase (V_2O_5), IEP_S- Isoelectric Point for supports, IEP_C-Isoelectric Point for catalyst, IEP_M-Isoelectric Point for supported phase (V_2O_5) -Gil-Llambias et al. (1985).

At low vanadium oxide surface coverages, the net pH at PZC should closely reflect the specific oxide support, and at high vanadium oxide coverages the net pH at PZC is significantly lowered due to the presence of the vanadium oxide overlayer. The qualitative agreement between the predicted and surface observed surface vanadium oxide species of the different oxide supports as seen in Tables 1-3 (a) and (b), suggest that the net pH at PZC of each support is controlling the structure of these hydrated species (Deo and Wachs, 1991).

Table 1-3: (a) Predicted and observed vanadium oxide species on different oxide supports-high vanadium oxide loadings. **(b)** Predicted and observed vanadium oxide species on different oxide supports for high vanadium oxide loadings. (Deo and Wachs, 1991)

(a) Low coverage			
Oxide Support	**pH**	**Predicted high coverage**	**Observed high coverage**
MgO	11	$VO_3(OH)$,V_2O_7, $(VO_3)_n$	VO_4[a], ,V_2O_7[a], $(VO_3)_n$
Al_2O_3	8.9	V_2O_7 , $(VO_3)_n$	$VO_3(OH)$,$V_{10}O_{28}$[a]
ZrO_2	5.9-6.1	$(VO_3)_n$, $V_{10}O_{27}(OH)$	$V_{10}O_{28}$[a]
SiO_2	6-6.4	$(VO_3)_n$, $V_{10}O_{28}$	$V_{10}O_{28}$[a]
TiO_2	3.9	$V_{10}O_{26}(OH)_2$, V_2O_5	V_2O_5
(b) High coverage			
MgO	11	$VO_3(OH)$	VO_4[a],V_2O_7[a], $(VO_3)_n$
Al_2O_3	8.9	$VO_3(OH)$, $(VO_3)_n$	$(VO_3)_n$[a]
ZrO_2	5.9-6.1	$VO_2(OH)_2$ $(VO_3)_n$	V_2O_7 , $(VO_3)_n$[a] , $V_{10}O_{28}$[a]
SiO_2	6-6.4	$VO_2(OH)_2$ $(VO_3)_n$	$(VO_3)_n$[a] , $V_{10}O_{28}$[a]
TiO_2	3.9	$V_{10}O_{26}(OH)_2$, $VO(OH)_3$	O_h[b]

[a] Major species. [b] Decavanadate-like environment, from solid state NMR

1.9.1.2 Thermodynamic stability of vanadium-oxygen phase under FTS conditions

The conditions in the Fischer-Tropsch reactor are highly reducing because of the high concentration of CO and H_2. It is therefore anticipated that V_2O_5 in the catalyst can be reduced into the lower forms of oxides. Typical reduction equations expected under Fischer-Tropsch conditions are shown below:

Table 1-4: Reduction of different vanadium oxides in the presence of CO

CO Reduction	V_2O_5	+ CO	⇔	$2VO_2$	+	CO_2	
	$4VO_2$	+ CO	⇔	V_4O_7	+	CO_2	
	$3VO_2$	+ CO	⇔	V_3O_5	+	CO_2	
	$3V_4O_7$	+ CO	⇔	$4V_3O_5$	+	CO_2	
	$2V_3O_5$	+ CO	⇔	$3V_2O_3$	+	CO_2	
	V_2O_3	+ CO	⇔	2VO	+	CO_2	
	VO	+ CO	⇔	V	+	CO_2	
Carbide formation	V_2O_5	+ 5CO + $1.76H_2O$	⇔	$2VC_{0.88}$	+	$2.5CO_2$	+ $0.88H_2$

A similar set of reduction equations as the one in Table 1-4 can be formed for H_2 reduction. A common feature to all the above equations is the same equilibrium constant expression for each reduction equation. Thermodynamic data for the species involved in the reduction has been pooled together to come up with the various vanadium oxide phases present at different temperatures. The thermodynamic information is graphically shown in Figure 1-14 and Figure 1-15.

Typical H_2O/H_2 ratio under industrial Fischer-Tropsch conditions ranges between 0.01 and 2 and with the CO_2/CO ratio lying within 0.01-2 range with the CO_2 content even lower after synthesis gas purification. The thermodynamic plots in Figure 1.6 (a) and (b) predicts that under Fischer-Tropsch conditions, the V_2O_3 is thermodynamically preferred oxide to the other oxide phases. The low temperature Fischer-Tropsch operating regime is indicated on the graphs where the doted lines intersect. Of critical importance is whether the V_2O_3 phase will enhance cobalt dispersion and hence C_{5+} selectivity when vanadium is used to promote a supported cobalt catalyst in the Fischer-Tropsch synthesis. Based on calculations, Kp values too small for carburisation reaction [$\sim 10^{-100}$] implying that no vanadium carbide phase forms at Fischer -Tropsch synthesis conditions.

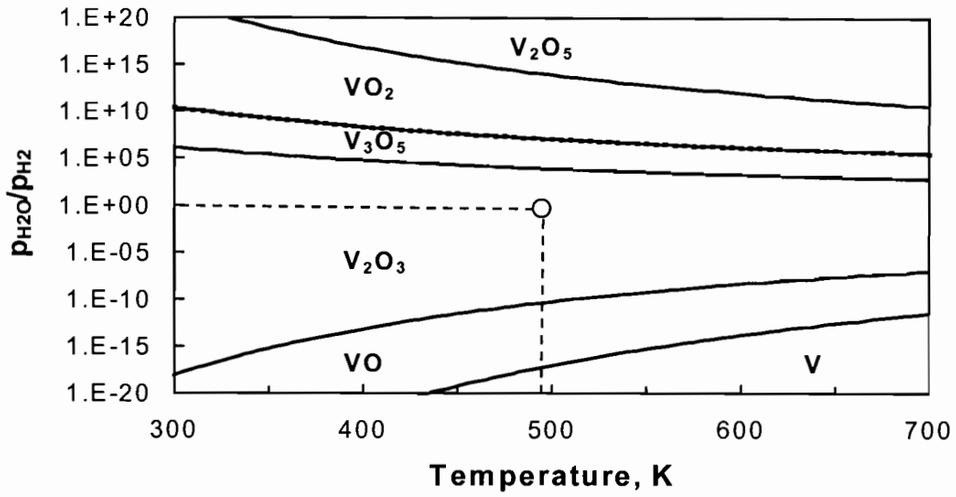

Figure 1-14: Thermodynamic equilibrium plots for V_xO_y reduction by H_2 (Thermodynamic data from Knacke et al., 1991).

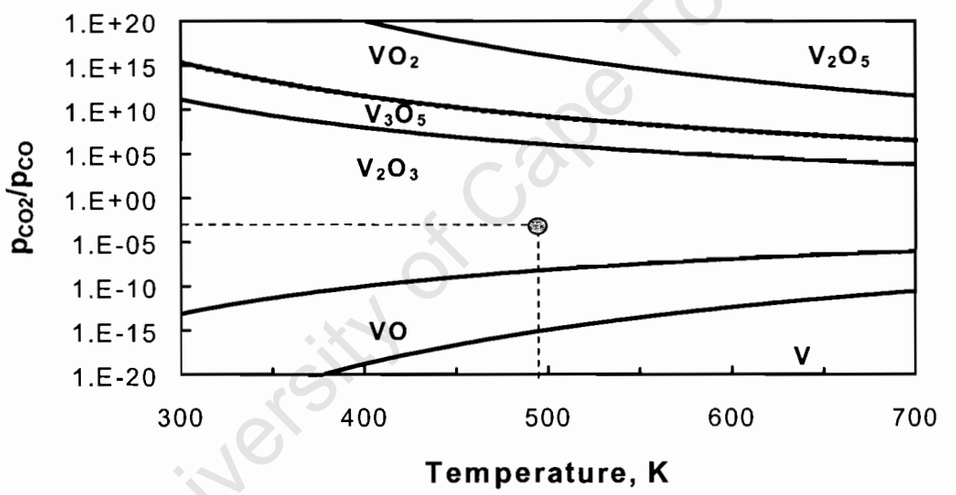

Figure 1-15: Thermodynamic equilibrium plots for V_xO_y reduction by CO (Thermodynamic data from Knacke et al., 1991).

Chapter 2
Experimental

2 EXPERIMENTAL

2.1 Catalyst Synthesis

Catalyst synthesis was composed of two main steps, support preparation and active metal impregnation.

In this work, the support was changed by modifying commercially available alumina with vanadia. Active metal impregnation was carried out by loading cobalt on the supports in $Co(OH)_2$ form obtained via precipitation of cobalt nitrate by ammonium hydroxide as described in the method by Mugalie and Blaise (2001).

2.1.1 Support Preparation

Vanadia was introduced in the catalyst support system by controlled ion exchange between Al_2O_3 surface hydroxyl ions with a metavanadate ion (VO_3^-) from the exchange solution. 50 g of commercially available γ-Al_2O_3 (Sasol Germany Alumina, Puralox ScCa 5-150) with BET surface area of 150m^2/g was loaded with different amounts of vanadium by controlled ion exchange. Appropriate amounts of ammonium metavanadate (NH_4VO_3) (Sigma, 99.8%) were dissolved in 1000ml of de-ionised water to prepare the ion exchange solution as indicated in Table 2-1. Because of the low solubility of NH_4VO_3 in water, ~5g/l at 25^OC, as shown in Figure 2-1, the ion exchange procedure was performed at 40^OC.

Vanadium loading on the γ-Al_2O_3 was based on the assumption that V_2O_5 dominant species anchored on the Al_2O_3 surface. Various vanadia surface coverages on the alumina were targeted.

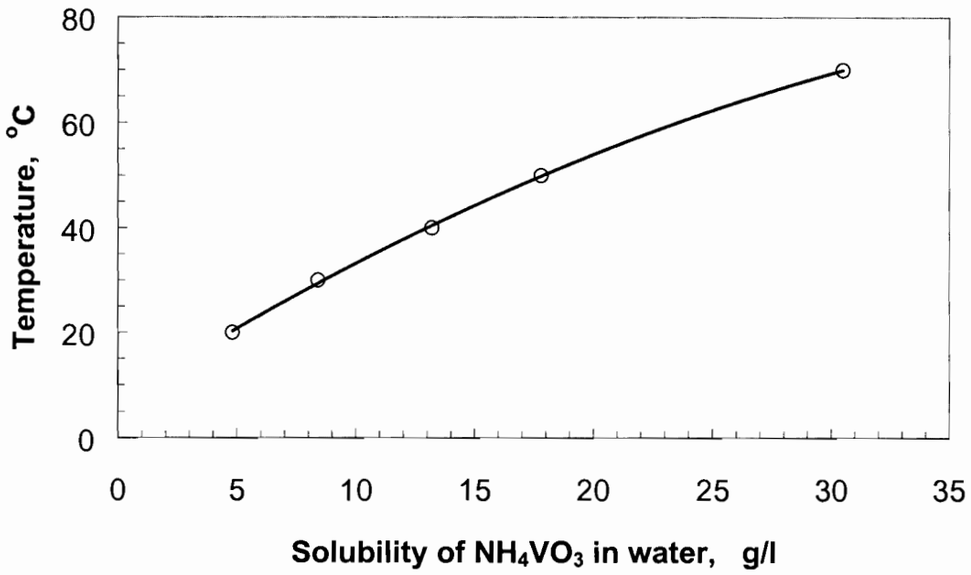

Figure 2-1: Ammonium metavanadate (NH_4VO_3) solubility curve-data from Perry et al. (1997).

Table 2-1 below summarises the targeted (V_2O_5) surface coverage and the corresponding amounts of ammonium vanadate added per litre of de-ionised water.

Table 2-1: Amount of NH_4VO_3 added per litre of water to yield specific V_2O_5 coverage on γ-Al_2O_3 and the expected weight fraction of vanadium on the modified support.

V_2O_5 fractional coverage	NH_4VO_3 in solution [g/l]	Targeted vanadium loading V/(V_2O_5 +Al_2O_3) [wt-%]
0.1 monolayer	1.2	1.0
0.5 monolayer	6	1.9
1 monolayer	12	8.4
2 monolayer[a]	2*12	14.1
5 monolayer[b]	5*12	23.8

[a] Vanadium loading achieved by a 2-step ion-exchange procedure.

[b] Vanadium loading achieved by a 5-step ion-exchange procedure

The 0.1,0.5 and 1-monolayer V_2O_5 on γ-Al_2O_3, were obtained from a single-step controlled ion-exchange procedure at pH ~6. This entailed dissolving the appropriate amount of NH_4VO_3 in de-ionised water at 40-45^{O}C under stirring in a 2-litre glass beaker. When all the NH_4VO_3 had completely dissolved, the pH of the solution was noted (see Table 2-2) followed by addition of 50 grams of γ-Al_2O_3 noting the pH immediately after addition.

The mixture was allowed to continue stirring at this temperature for 2 hours and the pH was measured. The increase in pH as a result of γ-Al_2O_3 addition was corrected by adding drops of 1M of nitric acid while stirring the mixture until pH 6 was attained. The pH-corrected mixture was then put back for about 12 hours at 40^{O}C under stirring to allow the ion exchange to equilibrate at this pH. Vanadate (VO_3^-) cations were exchanged with the surface hydroxyl groups on Al_2O_3 until equilibrium was reached. It was noted that after pH-correction, the pH of the mixture remained steady at pH 6 for the duration of the ion exchange procedure.

Table 2-2: pH variations during the various stages in ion exchange procedure and final colour of for the 0.1.0.5 and 1 monolayer V_2O_5 loading.

V_2O_5 fractional coverage [per 50 g Al_2O_3]	**pH NH_4VO_3 solution**	**pH NH_4VO_3 solution + γ-Al_2O_3**	**pH after HNO_3 correction**	**Resultant support Colour [a]**
0.1 monolayer	6.29 [35^{O}C]	8.30 [40^{O}C]	6.05 [35^{O}C]	Pale yellow
0.5 monolayer	6.18 [44^{O}C]	7.75 [41^{O}C]	6.10 [40^{O}C]	Light yellow
1 monolayer	6.27 [45^{O}C]	7.80 [48^{O}C]	6.27 [45^{O}C]	Yellow

[a] – colour of resultant modified supports after drying and calcination.

After equilibration the vanadium loaded support supports were separated from the supernatant liquid by carefully decanting the liquor. The modified supports were subsequently oven-dried at 120^{O}C for 3 hours and calcined at 550 ^{O}C for 6 hours. Calcination was done in air (60ml/ min, NTP) in a fixed bed reactor. The temperature was ramped (10^{O}C/min) from ambient to 120^{O}C and kept

there for one hour to remove water that might be trapped in the modified support. This step was followed by a temperature ramp (10^{O}C/min) to 550^{O}C, which was maintained for 6 hours before returning to ambient temperature. After calcination the modified supports were stored in 30ml glass bottles and placed in a dessicator.

Preparation for the 2-monolayer V_2O_5 coverage support entailed carrying out two successive ion exchange procedures. Initially, 1-monolayer V_2O_5 coverage was loaded on 50g of pure γ-Al_2O_3 using the procedure outlined above, followed by the drying and the calcination steps. The ion exchange procedure was repeated to load more V_2O_5 on 50 grams 1-monolayer V_2O_5-γ - Al_2O_3 support. Repeating the ion exchange steps 5 times, with drying and calcination steps in between each step, was employed when preparing the 5-monolayer V_2O_5 coverage on γ-Al_2O_3. For these supports the drying, calcination and storage procedures were similar to those described for the single step iron exchanged supports.

Table 2-3 show pH variations for the multi-step iron exchanged supports for the initial and final steps of the multiple step ion exchange procedure. The intermediate ion exchange steps have been omitted because there were no observed pH variations due to addition of support into the ammonium metavanadate solution.

Table 2-3: pH variations during the various stages in ion exchange procedure and final colour of support for the 2 and 5-monolayer V_2O_5 loading.

V_2O_5 fractional coverage [per 50 g Al_2O_3]	**pH NH_4VO_3 Solution**		**pH NH_4VO_3 solution + γ-Al_2O_3 (1st step)**		**pH After HNO_3 correction**		**Resultant support Colour [a]**
2 monolayer	6.01	[48.7^{O}C]	8.28	[39^{O}C]	6.15	[35^{O}C]	Orange
5 monolayer	6.18	[40^{O}C]	8.31	[43^{O}C]	6.10	[40^{O}C]	Orange

[a] – colour of resultant modified support after drying and calcination.

On each of the vanadia loaded supports, cobalt was introduced the slurry impregnation method so as to achieve 10% wt-% Co loading. This method is described elsewhere (Mugalie and Blaise, 2001). 316 ml of 50 g Co/l of $Co(NO_3)_2$ solution was placed in a 500-ml glass beaker into which 10 ml of 4 M sodium hydroxide (NaOH) added. After 15 minutes the resultant greenish colloidal solution was removed from the stirrer. Its pH was measured and was found to consistently lie between 7.6 and 7.9.

The precipitated $Co(OH)_2$ was separated in a Berti centrifuge to separate the $Co(OH)_2$ at 5000 rpm. The pink supernatant liquid was decanted from the bottles leaving the cobalt hydroxide colloid in the bottle. 17.28 grams of support (γ-Al_2O_3 or V_2O_5 loaded) support was weighed and placed into 500-ml glass beaker. The $Co(OH)_2$ colloid was scraped from the plastic bottle using a spatula and added onto the support. Great care was taken to ensure that all the $Co(OH)_2$ was added onto the support. The remnants of $Co(OH)_2$ left in the plastic bottles were rinsed off with 2 ml of the pink supernatant liquid and were also added onto the support-$Co(OH)_2$ mixture. Thorough mixing of the support and $Co(OH)_2$ mixture into a green homogeneous paste was done using a glass rod. The mixed paste was then oven dried at 120^{o}C for 12 hours.

The dried catalyst was then calcined in a fluidised glass tube reactor with air as the fluidising medium (air flowrate=1l/min NTP) at 250^{O}C and atmospheric pressure for 6 hours. After calcination the catalysts were stored in glass storage bottles and were placed in a desiccator. In addition to the V_2O_5 loaded supports a sixth catalyst was prepared using pure γ-Al_2O_3 as a support using the procedure outlined above. The γ-Al_2O_3 supported catalyst served as the base catalyst. After calcination the catalysts were placed in glass bottles and stored in a dessicator.

2.2 Catalyst Characterisation

Catalyst characterisation is a critical step because it provides information about the physical properties and to a smaller extent the chemical properties that are pivotal to catalyst performance. An in-depth understanding the characteristics of the support and the active metal forms a fundamental basis for explaining catalyst performance. Structural, electronic and chemical properties of the support and active metal are derived from a suite of characterisation methods. To obtain an insight about the physical and chemical properties of the synthesised catalysts, the following well established methods were used: ζ-potential measurements, AAS, BET, TEM, CO- chemisorption, XRD, and TPR.

2.2.1 Zeta Potential Measurements.

Zeta potential measurements of the supports were obtained using a Malvern Zetasizer 4. Zeta potential is a measure of the net surface charge of a solid substance when placed in solution. The equilibrium that created by the positive and negative ions on the surface of the solid and the counter ions in solution determines whether the net surface charge is positive or negative. A change in the pH of the solution affects the equilibrium and hence the net surface charges. The sequential steps followed when zeta potential measurements were carried out are outlined below:

- 0.1 gram of each support was finely ground in a pestle and mortar so that it would exist as a suspension in solution.
- The support was placed in 50 ml of 0.05 M KCl solution and was shaken.
- The pH of the suspension was adjusted using hydrochloric acid or potassium hydroxide in the acid and alkaline range, respectively.
- For each pH adjustment 5ml of the suspension was injected into the zetasizer, which was set to give out 4 measurements from which an average zeta potential was determined.

- Data was collected and zeta potential curves were obtained for all six supports.

The Zetasizer4 was operated at 25^{O}C, 50mm electrode spacing of 50 mm, a cell dielectric constant of 79 and the beam position set at 14.6^{O}. Zeta potential and pH data was obtained from the Zetasizer. The zeta potential measurements came in replicates of four for a single pH value. The replicates were averaged to yield a single zeta potential for each pH. From the data plots for zeta potential as a function of pH were drawn from which the Point of Zero Charge for the supports was established.

2.2.2 Atomic Adsorption Spectroscopy (AAS)

Elemental analysis of both the supports and the catalyst was analysed using a Varian AA.30 atomic spectrometer. The amount of aluminium (Al) and vanadium (V) was analysed for the supports while in addition to the aforementioned elements cobalt analysis was added for the catalyst derived from corresponding supports.

Catalysts/supports were finely milled and digested in aqua regia composed of HCl and HF with HCl/HF volume ratio of 4. 0.1 g of sample (catalyst or support) was weighed into a 250ml Erlenmeyer flask into which 10ml of HCl/HF mixture (30 vol.-% HCl) was added and heated to 80^{O}C. 10ml HNO_3 (60%) was carefully added to the flask and the mixture was allowed to evaporate at 80^{O}C until about 2 ml remained in the flask. After this step 5ml of concentrated $HClO_4$ was added into the flask and the mixture was again boiled until 2ml of sample remained in the flask. This was transferred 100ml volumetric flask and made up to 100ml with distilled water. The samples were subsequently read on a Varian AA.30 atomic spectrometer. AAS data atomic spectrometer gave concentration of each of the analysed elements per support or catalyst sample. Elemental compositions in the catalyst samples and supports were obtained by combining oxygen balance and concentration ratios from AAS data.

2.2.3 Transmission Electron Microscopy (TEM)

Transmission electron microscope pictures were taken using a JOEL JEM-200CX, which operated at 120 kV. The supports and the catalysts were finely crushed in 5ml of methanol in 30-ml sample bottles using a blunt but smooth glass road. The fine particles dispersed in the methanol were pipetted out and placed on carbon coated copper grids. The sample loaded copper grids were then placed in de-ionised water with dispersed plastic on the surface. This were then carefully removed from the water surface and placed on a filter paper to dry. After this the samples were viewed at under Transmission Electron Microscope at different magnifications. Pictures were taken for the establishment of the crystal size distribution of cobalt in the catalyst.

The measured Co crystallite diameters from TEM pictures of the different catalysts were used in crystallite size analysis. On average about 250-300 particles were manually and randomly measured from the pictures for each catalyst and size distribution analysis was done by following the method outlined by Bergeret and Gallezot (1997). From the particle count and measurements, plots of the number (n_i vs. d_i) distribution was drawn; where d_i represents the particle diameter of particles i and n_i being the number of particles with diameter d_i. Particles were assumed to be spherical. For each catalyst, the number mean diameter d_{LN} cobalt crystallite was estimated using the following formulae:

$$d_{LN} = \frac{\sum n_i \cdot d_i}{\sum n_i} \qquad (2.1)$$

2.2.4 X-ray Diffraction (XRD)

X-ray diffractometry was used to obtain the physical characteristics of the catalyst. Application of this method is based on the orderliness of the repeating planes that form a particle or crystals. When X-rays are directed on the crystal, they are reflected by these ordered planes yielding a diffraction pattern unique to a specific plane. The diffraction patterns are recorded from which information like, degree of crystallinity of the catalyst material, the position of individual atoms in the particle matrix. Average particle size of the active material can be ascertained.

A Phillips X-ray diffractometer was used to obtain X-ray diffraction spectre for the different catalyst. The operational settings on the difractometer were:

- Voltage 40kV
- Current 20mA
- 2θ range 15-70^{O}
- 2θ step size 0.01 second
- Step duration 0.01 second

X-ray diffraction data was used to identify the phases present in the catalyst and to estimate the mean particle diameter of cobalt crystallites in the catalysts. Phase identification was accomplished by comparing the catalyst XRD patterns with known reference XRD patterns for elements/compounds suspected to be present in the catalysts. Line broadening analysis of the catalysts X-ray spectre was used in mean particle diameter estimation The Scherrer formula was used to estimate the cobalt crystallite diameter. The Scherrer formula:

$$L_{hkl} = \frac{k \cdot \lambda}{\beta \cdot \cos\theta_o}$$ (Bergeret and Gallezot, 1997). (2.2)

Where λ is the wavelength of X-ray radiation employed in the analysis, β is expressed in radians is the full width at half the maximum peak intensity and

θ_o is the angular position of the peak maximum. K was taken to be 0.9 as suggested by Bergeret and Gallezot (1997) because β was estimated at half the peak width.

2.2.5 CO Chemisorption

CO chemisorption experiments were performed to estimate the following catalytic properties: active metal surface area, metal dispersion on support and metal crystallite size.

In this study CO chemisorption was performed on a Micromeritrics ASAP 2000. About 0.5 grams of catalyst sample was loaded into the reactor. The reduction program of the loaded catalyst was started at $25^{O}C$ with the temperature ramped at $5^{O}C$/min to $350^{0}C$ under H_2 flow (50 ml/min NTP). The reduction temperature was kept at $350^{O}C$ for 16 hours. After reduction the system was allowed to cool down to $35^{O}C$ and H_2 flow was stopped. The system was subsequently evacuated to remove gases that might still be trapped within reactor and tubes before CO chemisorption was commenced.

CO chemisorption experiments were performed at $30^{O}C$ by a pre-set program in the apparatus that allowed CO at different pressures to equilibrate with the sample. The chemisorption was initiated at ~5 mmHg with pressure increments of 20 mrnHg up-to 650 mmHg.

2.2.6 Temperature programmed reduction (TPR)

TPR experiments were performed using Micromeritrics Autochem 2910 apparatus. The TPR apparatus is equipped with a detachable quartz tube housed in a temperature programmable furnace and a thermocouple positioned in the quartz tube used for temperature control purposes. The quartz cell can be removed from the apparatus gas line loop to load sample and reconnected. A thermal conductivity detector (TCD) is connected after the quartz tube for measuring concentration of gases though the reactor. During the TPR experiment, time, conductivity and temperature measurements are captured and recorded and stored in a computer for later analysis.

About 0.3 grams of catalyst sample was loaded in the quartz tube with the catalyst bed sitting on silane treated glass wool. The quartz cell is connected in a way that the gas flows though the bed when the TPR program is run. The TPR procedure was programmed in the apparatus software that is linked to the gas supply system. The program steps were as follows:

- Pre-treatment step- Argon line supply valve was programmed to open and allow argon to flow at 50 ml/min (NTP). Temperature was ramped at a 10^{O}C/min from 25^{O}C to 120 ^{O}C. Temperature was kept at 120^{O}C for 1 hour after which the system was allowed to cool down to ~50^{O}C.
- Gas supply was switched from Ar to a 5 vol.% H_2-Ar (50 ml/min, (NTP)) mixture. The temperature was then ramped at 10^{O}C/min from ~50^{O}C to 1000^{O}C and was kept at this temperature for 1 hour. Conductivity, temperature and time data was recorded as soon as the temperature ramp- step commenced. After 1 hour the furnace was allowed to cool down to ambient temperature and the program was stopped. The accumulated data was automatically saved in the computer after every run. From TPR data, TPR profiles for the catalysts were plotted. Peak areas from the TPR profiles where quantitatively used to identify the phases present is catalysts and supports.

2.3 Fischer Tropsch synthesis

2.3.1 Experimental set-up

The experimental set-up used to test the Fischer-Tropsch catalyst performance is shown in Figure 2-2. The set-up is made up of three distinct zones; gas feed lines, reaction zone and the product section. Appropriate CO and H_2 flow rates for Fischer-Tropsch synthesis are set using Brooks Series 9650 mass-flow controllers. The CO and H_2 flowrates are set to obtain (H_2/CO) mole ratio of 2. The hydrogen and the carbon monoxide streams are premixed before the 4-way valve. Also going into the 4-way valve is an argon stream. Argon in introduced for the purpose of pressurising the system to the desired operating pressure. The pressure regulator connected on argon line was used to regulate and maintain the reaction zone pressure at 20 bar (abs). The 4-valve is used for directing synthesis gas though the reactor while argon flows via the bypass line or through the reactor.

A U-tube fixed bed type of reactor (6-mm diameter; 180-mm length) was used for the Fischer-Tropsch. The reactor feed-line from the 4-way valve is preheated to reaction temperature (220^0C) before entry into the reactor. An aluminium heated furnace houses the reactor has an imbedded thermocouple connected to a programmable controller for monitoring and controlling the reactor temperature. Details of the reaction zone are shown in Figure 2-3. Connected to the exit line of the reactor is the bypass line from the 4-way valve for the purpose of pressurising the system. The exit line and the reactor are lagged by glass wool to prevent heat loss.

Heavy products of the Fischer-Tropsch reaction were removed from the product mixture by a wax trap situated immediately after the reactor. The wax trap temperature was controlled by temperature controller and was set at 190^OC to facilitate the removal of high molecular weight hydrocarbons from the product stream. The wax trap is surrounded by a aluminium block equipped with external electrical heating, which is connected to a temperature

controller. A needle valve is positioned immediately after the wax trap for purpose of pressure regulation. Heating the whole downstream line up to the ampoule sampling station using a coil prevented product condensation in the lines. The coil was also linked to a temperature controller, which kept the temperature constant slightly at 190°C. During the course of the Fischer-Tropsch reaction on samples were taken using, online GC TCD sampling in conjunction with ampoule sampling technique for compound analysis for hydrocarbon product analysis.

2.3.2 Catalyst Loading

Catalyst performance for each of the synthesised catalysts in Fischer-Tropsch above was evaluated using the apparatus described above. 0.5 grams of the calcined catalyst (size range 50-150μm) was initially mixed with 1 gram of ~400-μ silicon carbide (SiC). The purpose of mixing the catalyst with SiC was to ensure an even distribution of the catalyst in the reaction zone. Mixing the catalyst with SiC lowered the beds pressure drop and also aided in eliminating temperature gradients. When loading the catalyst care was taken to ensure that the catalyst filled the same height in each leg of the U-tube reactor.

After loading the reactor, both sides of the reactor were plugged using glass wool to both ends of the reactor as shown in Figure 2-3. This step was necessary to prevent catalyst from moving away from the isothermal zone or being blown out of the reactor. The loaded reactor was then connected appropriately and a pressure test was performed to check for gas leaks.

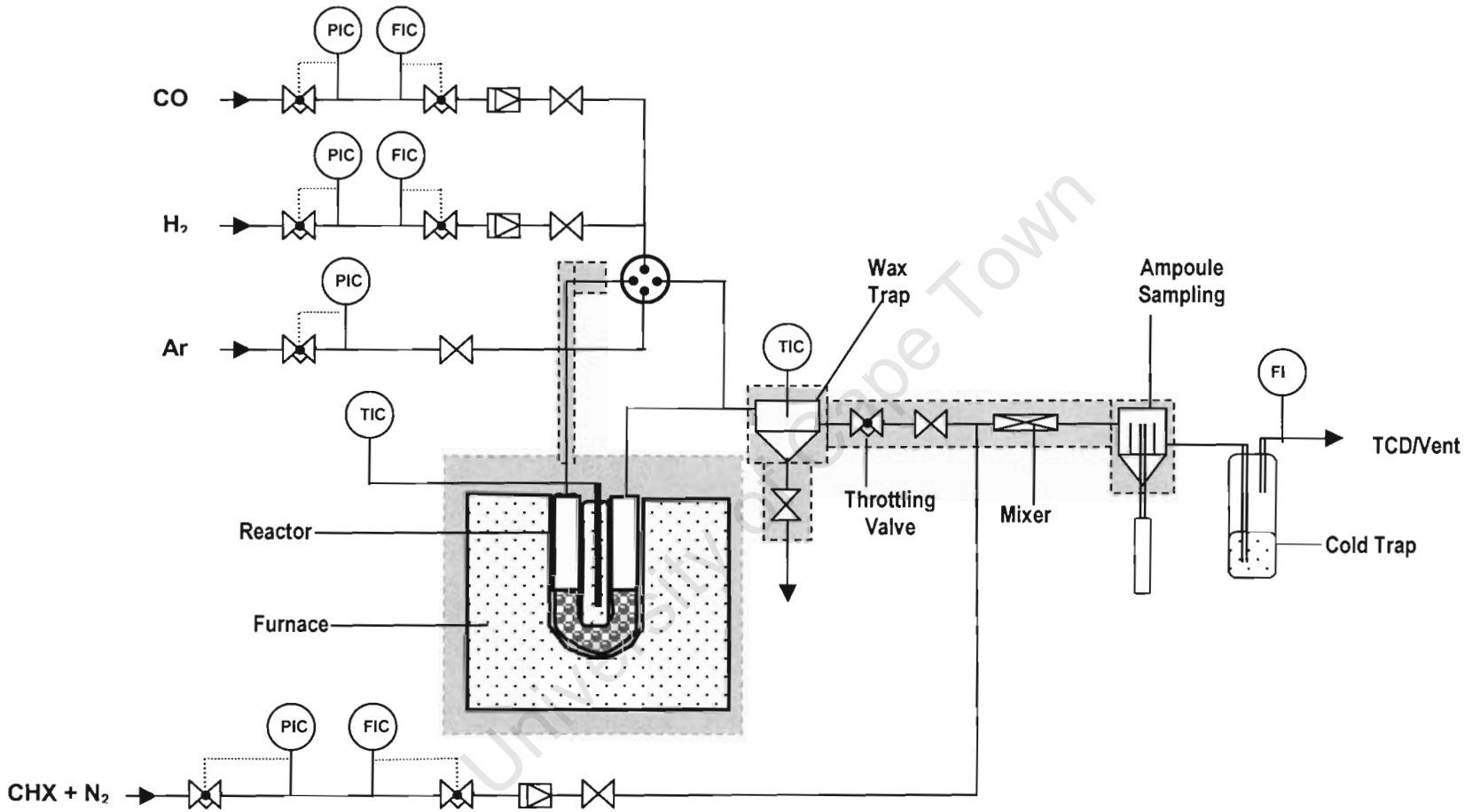

Figure 2-2: Experimental set-up for testing catalyst performance in Fischer-Tropsch synthesis reaction.

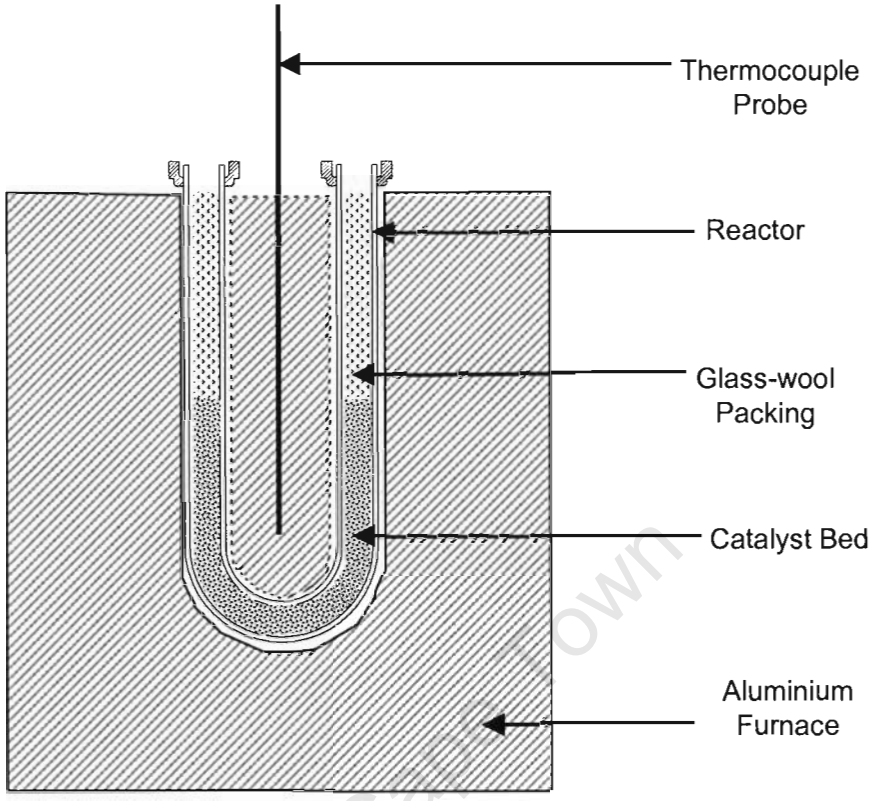

Figure 2-3: Cross-sectional view of the reactor zone

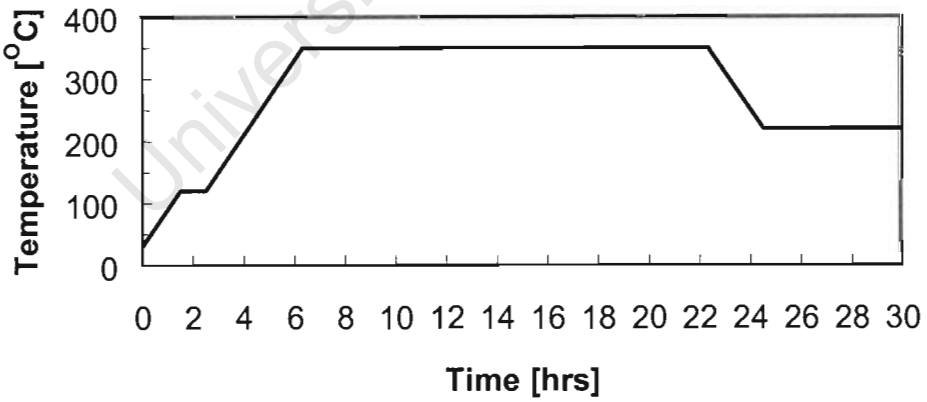

Figure 2-4: Temperature program for catalyst reduction.

2.3.3 Catalyst Activation

To obtain the active Co metal face for the Fischer-Tropsch reaction, in-situ reduction carried out under hydrogen (60 ml/min NTP) and at atmospheric pressure. The 4-way valve is positioned at the reactor pathway .The reduction step involved ramping up the temperature from room temperature at $1^{O}C$/min to $120^{O}C$. The temperature was kept at $120^{O}C$ for an hour, a step that allowed for the removal of water from the catalyst before the actual reduction commenced. After this step, the temperature was again ramped at $1^{O}C$/min to the reduction temperature of $350^{O}C$. The reduction was done at this temperature for 16 hours then the temperature was allowed top drop to reaction temperature ($220^{O}C$) in 2 hrs 10 minutes. The reaction temperature was maintained for 200 hours to perform the synthesis reaction. Figure 2-4 shows the reduction program of the catalyst.

2.3.4 Reaction Start-up

Upon completion of the reduction procedure Fischer-Tropsch reaction was carried out. Initially the 4-way valve was set to bypass so that the reactants did not pass though the reactor before proper synthesis gas setting were done. Proper flow settings were adjusted in the flow controllers so as to get hydrogen to carbon monoxide ratio (H_2/CO) of 2. The reaction zone was pressurised with argon to 19-bar (gauge) using the pressure regulator and the throttle valve. The total flowrate of the synthesis gas (H_2 + CO), reference gas and argon was set to be about 60 ml/min (NTP) using the bubble meter. The reference gas was made up of a mixture of 0.15 mol-% cyclohexane in nitrogen. Table 2-4 summarises the reaction conditions. When all settings were done the exit gas was analysed in a Varian 3700 gas chromatography with a thermal conductivity detector (TCD). This was to confirm if the desired H_2/CO ratio of 2 was obtained. Also from the TCD analysis amounts relative of the reactants to the reference gas from which conversion and selectivity calculations were based.

Table 2-4: Reduction and Fischer Tropch reaction conditions.

Reduction	
Reduction Temperature(^{O}C)	350
Reduction Time (hours)	16
Hydrogen flow (ml/min)(NTP)	60
Reaction conditions	
Mass catalyst (g)	0.5
Mass SiC (diluent)	1
Reaction pressure (bar (abs))	20
Reaction temperature (^{O}C)	220
Wax-trap and exit line temperature (^{O}C)	190
Flowrates (ml/min)(NTP)	
H_2	15
CO	7.5
Reference gas (0.15 mol-% cyclo hexane in N_2)	7.5

After satisfactory TCD analysis (5 replicate results) the 4-way valve was switched to reactor to start the reaction.

2.3.5 Product Analysis

Gas chromatography was the major analytical tool employed in analysing the Fischer-Tropsch reaction products. Gas conversion measurements were obtained and online product gas analysis on a Varian 3700 Series GC with a thermal conductivity detector (TCD) equipped with 80/100 carbosive S II column of 3m length and 3.175 mm inner diameter. Argon was used as a carrier gas in this analysis. Sampling was carried out at a frequency of 10 minutes after reaction was started in the first hour and less frequently in the subsequent hours. Conductivity data was captured in and recorded in a chromatogram using an HP 3393A integrator. The TCD data was used to calculate conversion of synthesis gas during the course of the Fischer-Tropsch reaction.

Organic product content of the Fischer-Tropsch reaction was obtained the analysis of ampoule samples in another GC (Varian 3400 Series) equipped with a flame ionisation detector (FID). This GC was installed with a cryogenic system a feature which enabled product analysis to be performed over a wide temperature range (-60^{0}C to 280^{0}C). Data capture was obtained from a HP 3396 Series II integrator connected to the FID in a form of peak area reflecting the relative weights of hydrocarbon compounds. Column specifications and operating conditions of the GC's used conditions are depicted below.

Table 2-5: Gas chromatography and their Column specifications

	Analysis of permanent gases	**Analysis of organic product compounds**
GC	Varian 3700 Series	Varian 3400 Series
Stationary Phase	carbosieve SII	Polydimethyl siloxane
Detector	TCD	FID
Carrier Gas	Argon	Hydrogen
Column Length [m]	~3	100
Column diameter [mm]	3.2	0.25
Column Pressure [bar, abs)]	2	45
Column Temperature [^{O}C]	170	-60 - 280

2.3.5.1 Fischer-Tropsch synthesis data analysis

0.15 mol-% cyclohexane and nitrogen was used as an internal standard for both conversion and yield calculations. CO and H_2 conversion and was calculated from a calibrated TCD gas chromatograms. TCD calibration was done by injecting a mixture of H_2, CO, CH_4, N_2, and CO_2 of known composition. The response factors for each gas were calculated based on N_2. Using CO as an example, the response factor ($R_{F,i}$) for each gas was calculated from the peak areas and the content of each gas as follows:

$$R_{F,CO} = \left(\frac{\%\cdot CO}{\%\cdot N_2}\right) \times \left(\frac{A_{N_2}}{A_{CO}}\right) \quad (2.3)$$

Where A_{CO} and A_{N2} are the CO and N_2 peak areas, respectively obtained from the TCD trace. The CO conversion (X_{CO}), methane yield (Y_{CH4}), and methane selectivity (S_{CH4}) definitions and equations used to analyse data are given next.

X_{CO} is defined as the amount of CO converted into organic product and CO_2 from Co mass balance X_{CO} is given by:

$$X_{CO} = \frac{\left(A_{CO}/A_{N2}\right)_{Bypass}\cdot R_{F,CO} - \left(A_{CO}/A_{N2}\right)_{\text{Re actor}}\cdot R_{F,CO}}{\left(A_{CO}/A_{N2}\right)_{Bypass}\cdot R_{F,CO}} \quad (2.4)$$

Methane yield (Y_{CH4}) is defined as the fraction of the CO converted to methane.

$$Y_{CH_4} = \frac{\left(A_{CH_4}/A_{N2}\right)_{out}\cdot R_{F,CH4}}{\left(A_{CO}/A_{N2}\right)_{feed}\cdot R_{F,CO}} * 100\% \quad (2.5)$$

Methane selectivity (S_{CH4}) is the fraction of product that goes to methane per total hydrocarbon product.

$$S_{CH_4} = \frac{\left(A_{CH_4}/A_{N2}\right)_{out}\cdot R_{F,CH4}}{X_{CO}\cdot\left(A_{CO}/A_{N2}\right)_{feed}\cdot R_{F,CO}} * 100\% = \frac{Y_{CH_4}}{X_{CO}} \quad (2.6)$$

The yield of total organic product and the selectivity of the products were determined using FID gas chromatograph. The fraction of each organic product based on the known molar fraction of cyclohexane in the reference

gas (0.15 mol-% cyclohexane in nitrogen). The relative response factors for all hydrocarbon products were similar except for oxygenates, which needed correction. FID data, which was on mass basis from the GC, was converted into mole by dividing each peak area of a hydrocarbon product with the products carbon number, N_C.

Mass corrections, alcohols and Aldehyde ketones
Response of carbon (C) with a single bond to oxygen (O): 0.55
Response of carbon (C) with a double bond to oxygen (O): 0
Peak area correction with A_{Ti} being the true area and A_i the area obtained directly from the chromatogram.

$$A_T = A_i \cdot f_O \tag{2.7}$$

Where f_O if given by

$$f_O = \frac{N_{C,i}}{N_{C,0} + 0.55 \cdot N_{C,0,O}}$$

N_{Ci}-Number of Carbon atoms in molecule i.
$N_{C,0,o}$ - Number of carbon atoms not bonded to oxygen
$N_{C,0}$ –Number of carbon atoms bonded to 1 oxygen with a single bond

ASF distribution curves were plotted from linear hydrocarbon fraction only per carbon number. Chain probability growth was estimated between C_{11} and C_{14} and this was used to extrapolate to the total molar amount of products formed (Schulz and Claeys (a), 1999). The area of all linear hydrocarbons carbon number 14 (A_{14}) with is related to the area of all linear hydrocarbons carbon number 15 (A_{15}) by the following relationship:

$$A_{15} = \alpha \cdot A_{14} \cdot \frac{15}{14} \tag{2.8}$$

This relationship holds if one assumes that the value of α remains constant up to infinite carbon numbers. The peak areas of the subsequent carbon numbers beyond C_{15} were established up until C_{30}. The sum of the areas from C_1 to C_{30} was obtained for the linear hydrocarbons.

C_{5+} Selectivity (S_{C5+}) defined as the fraction of organic product with carbon numbers (N_C) greater than or equal 5, was calculated from subtracting from 100% the sum selectivity of products with carbon numbers ranging from 1 to 4, a assuming closure of mass balance.

$$S_{C_{5+}} = 100 - \sum_{1}^{4} S_{C_i} \qquad (2.9)$$

The selectivity for the C_2, C_3 and C_4 products were obtained by comparing FID areas of all products per carbon number, to the selectivity of methane obtained from TCD data. As an example the selectivity for the C_2 product fraction (S_{C2}) based on the methane selectivity is given by:

$$S_{C_2} = \frac{A_{C_2}}{A_{C_1}} \cdot S_{C_1} \qquad (2.10)$$

Where S_{Ci} and A_{Ci} represent the selectivity and total area obtained from an FID chromatogram for a product with carbon number i respectively. It should be noted that the selectivity obtained this way were mass basis.

2.3.5.1.1 n-Olefin content

The olefin content in the product was expressed as a percentage of the total sum n-olefins with carbon number N per total sum of linear hydrocarbons with carbon number N:

$$S_{n-Olef.,N} = \frac{\sum A_{n-Olef.,N}}{\sum A_{LHC,N}} \cdot 100\ \% \qquad \text{(mol-\%)} \qquad (2.11)$$

Where $S_{n\text{-}Olef.,N}$ is the olefin content in linear product with carbon number N , $\Sigma A_{n\text{-}Olef.,N}$ is the total FID area of all linear olefins with carbon number N and $\Sigma A_{LHC.,N}$ is the total FID area of all linear hydrocarbons with carbon number N.

2.3.5.1.2 1-olefin content

1-olefin content in the olefin fraction per carbon number N was expressed as a percentage of the total linear olefin product with carbon number N:

$$S_{1-Olef.,N} = \frac{\sum A_{1-Olef.,N}}{\sum A_{n-Olef.,N}} \cdot 100\ \% \qquad \text{(mol-\%)} \qquad (2.12)$$

$S_{1\text{-}Olef.,N}$ is the 1-olefin content in linear olefin product with carbon number N , $\Sigma A_{1\text{-}Olef.,N}$ is the FID area of the linear 1-olefin with carbon number N and $\Sigma A_{n\text{-}Olef.,N}$ is the total FID area of n-olefins with carbon number N.

2.3.5.1.3 Oxygenate content

Oxygenate content per carbon number fraction was also expressed as a percentage of the total linear hydrocarbon plus oxygenate product of a corresponding carbon number:

$$S_{Ox,N} = \frac{\sum f_{Ox,i} \cdot A_{Ox,N}}{\sum A_{LHCO,N}} \cdot 100\ \% \qquad \text{(mol-\%)} \qquad (2.13)$$

$S_{Ox.,N}$ is the oxygenate content in linear product with carbon number N , $\Sigma A_{ox.,N}$ is the total FID area of all oxygenates with carbon number N, $f_{Ox,\ i}$ - the correction factor for oxygenate product i and $\Sigma A_{LHCO.,N}$ is the sum of all linear hydrocarbons and oxygenates with carbon number N.

2.3.5.1.4 Branching

The content of branched products in product was expressed as a percentage as a fraction of the total linear hydrocarbon product:

$$S_{Brch.,N} = \frac{\sum A_{Brch.,N}}{\sum A_{LHC,N}} \qquad (2.14)$$

$S_{Brch.,N}$ is the content of branched carbon number N, $\Sigma A_{Brch.,N}$ and is the total FID area of all branched products with carbon number N and $\Sigma A_{LHC.,N}$ is the sum of all linear hydrocarbons with carbon number N.

Chapter 3
Results

3 RESULTS

All the catalysts in this study were prepared by modifying a γ-Al_2O_3 support with different amounts of V_2O_5, followed by impregnating these modified supports with the same amount of cobalt per unit weight of support. The prepared catalysts were characterised and their catalytic performance was tested using Fischer-Tropsch synthesis reaction.

3.1 Catalyst Characterisation

3.1.1 Zeta potential Measurements

Surface charge as a function of pH was measured using a Malvern Zetasizer 4. Zeta potential measurements were done on pure γ-Al_2O_3, the five V_2O_5-γ-Al_2O_3 supports and on pure V_2O_5. Figure 3-1 shows the experimentally observed shift in the PZC for the supports under study. The point of zero charge (PZC) shifts from the high pH for pure Al_2O_3 towards the low pH for pure V_2O_5 with increasing vanadia loading on the supports. This is in agreement with the observations reported by GiL-Llambias et al. (1985) on the V_2O_5-γ-Al_2O_3 system. The pH at PZC for pure V_2O_5 and Al_2O_3 were reported at (1.5–2.5) and 8.8, respectively and the pH at PZC for the V_2O_5 doped Al_2O_3 supports sandwiched between those of pure V_2O_5 and Al_2O_3 (Gil-Llambias et al., 1985).

The observed shift in PZC to lower pH values with increased V_2O_5 loading might be indicative for increased acidity contribution with addition of the more acidic V_2O_5 onto the relatively basic γ-Al_2O_3 support. Beyond 1-monolayer V_2O_5 loading, the pH at PZC expected to mimic that of pure V_2O_5 assuming that the entire γ-Al_2O_3 surface has been covered by V_2O_5 after 1-monolayer V_2O_5 coverage. However, the pH at PZC for the 2-monolayer and 5-monolayer V_2O_5 loaded supports does not coincide with the pH at PZC for pure V_2O_5. This result indicates that beyond the monolayer surface V_2O_5 coverage on γ-Al_2O_3, there is still a surface charge contribution to the V_2O_5-modified supports that may arise from an exposed γ-Al_2O_3 or a synergistic contribution from both V_2O_5 and γ-Al_2O_3.

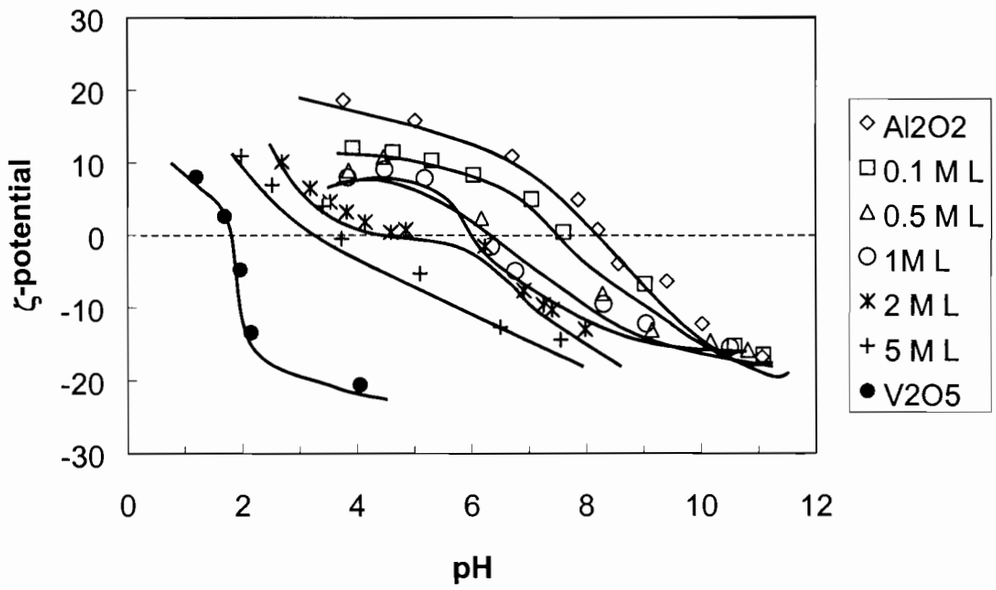

Figure 3-1: Zeta Potential as a function of pH for different V_2O_5 loading on Al_2O_3 for modified supports.

3.2 Atomic Adsorption Spectroscopy (AAS)

Atomic adsorption spectroscopy was used to ascertain the elemental compositions in both the modified supports and the catalysts. The modified supports were analysed for aluminium (Al) and vanadium (V), while for the complete catalysts in addition to the aforementioned elements cobalt (Co) was analysed. Figure 3-2 shows a comparison of the theoretical and experimentally evaluated V_2O_5/Al_2O_3 ratios for both supports and catalysts. The experimental V_2O_5/Al_2O_3 ratio the supports and catalysts were plotted against the theoretically calculated V_2O_5/Al_2O_3 ratio. The experimental V_2O_5/Al_2O_3 ratio for the for both supports and catalysts was expected to increase linearly with an increase in V_2O_5 loading as indicated by the solid line on Figure 3-2.

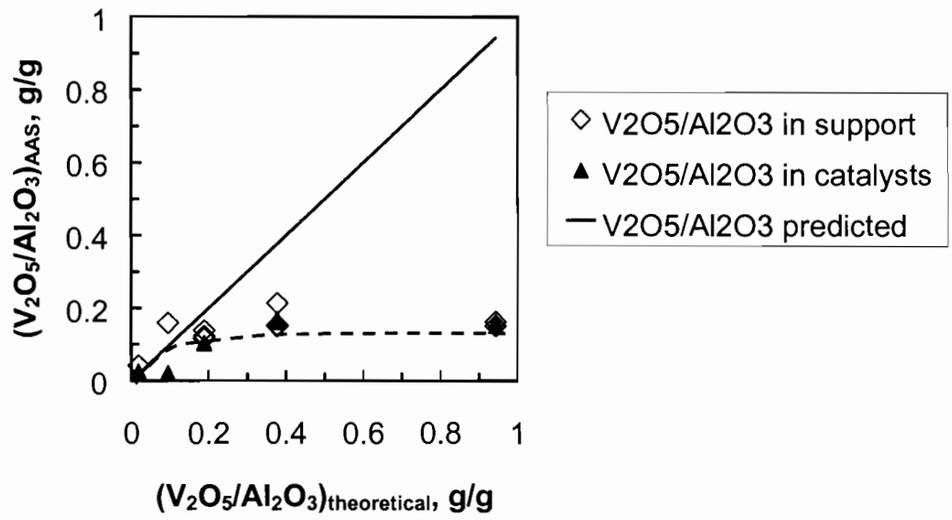

Figure 3-2: Theoretical (V_2O_5/Al_2O_3) mass ratio against theoretically calculated (V_2O_5/Al_2O_3) mass ratio for modified supports and catalysts.

Figure 3-2 show that at low V_2O_5 loading, the experimental V_2O_5/Al_2O_3 ratio varies linearly with an increase in V_2O_5 content with the exception of the 0.5-monolayer doped catalyst. Significant deviations occurred at V_2O_5 loadings beyond 1-monolayer V_2O_5 coverage. The ratio for 2-monolayer V_2O_5 coverage is lower than expected and far too low for the 5-monolayer V_2O_5 coverage for both the supports and catalyst.

The results indicate that the step ion-exchange procedure used to introduce V_2O_5 beyond 1-monolayer V_2O_5 coverage on γ-Al_2O_3 supports did not work. This is however, a surprising observation because the colours of supports changed from light yellow to deep orange from the lowly V_2O_5 loaded support to the support with high V_2O_5 content, which could be interpreted as a an indicator for increased in vanadia loading on each support. Furthermore, zeta-potential measurements indicate a difference in the surface charges of the different catalysts.

A possible explanation for the observed deviation may be that, after 1-monolayer V_2O_5 coverage on γ-Al_2O_3, the concentration of surface hydroxyl groups becomes less thus reducing the number of metavanadate ions (VO_3^-) exchanged with the modified γ-Al_2O_3 surface. The flattening nature of the curves beyond 1-monolayer V_2O_5 coverage suggests that an ion-exchange equilibrium is reached, hence no V_2O_5 uptake occurs beyond this equilibrium.

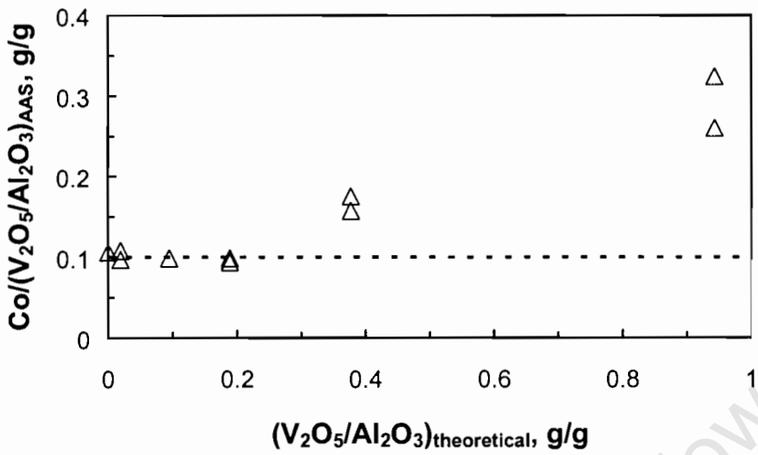

Figure 3-3: Theoretical and experimental Co/(V_2O_5+Al_2O_3) mass ratio against theoretically calculated V_2O_5/Al_2O_3 mass ratio in the synthesised catalysts.

Figure 3-3 shows a plot of the experimental (Co/V_2O_5+Al_2O_3), $_{AAS}$ mass ratio against the theoretical (V_2O_5/Al_2O_3),$_{Theory}$ mass ratio for each catalyst. Theoretically the (Co/ V_2O_5+Al_2O_3) ratio is expected to remain constant at 10 wt-% as indicated by the dotted line on Figure 3-3. The experimental results are in agreement with the theory with increase in V_2O_5 up to 1-monolayer V_2O_5 coverage. A marked increase in (Co/ V_2O_5+Al_2O_3) ratio was observed for the catalyst containing more than 1-monolayer V_2O_5. This is linked to the observations from Figure 3-2; the sudden increase in the (Co/V_2O_5+Al_2O_3) ratio beyond 1-monolayer V_2O_5 coverage is a direct consequence of the low vanadia content in the 2 and 5 monolayer catalysts. From Figure 3-2 and 3-3 it can be inferred that beyond 1-monolayer V_2O_5 coverage on γ- Al_2O_3, vanadia loading on the supports becomes difficult because of equilibrium limitations.

Table 3-1 shows theoretically expected (V_2O_5/Al_2O_3) ratio, vanadium (V) content (wt-%) and (V_2O_5/Al_2O_3) ratio obtained from AAS results for all the six catalysts. This table is included because even though the desired monolayer loadings on the catalysts were not achieved, the monolayer (ML) nomenclature will be retained throughout this work for the purpose of easy data presentation.

To avoid confusion and incorrect interpretation of the monolayer (ML) notation, an asterix (*) will be added to identify or mark supports/catalysts which showed lower vanadia loadings than theoretically expected i.e. the supports and catalysts which were supposed to contain 2 and 5 monolayers of V_2O_5. A fold in leaflet of the same table has been included in the appendix to enable the reader easy reference to the true vanadia loadings found in the supports and catalyst under study.

Table 3-1: Theoretical vanadium (V) content, theoretically determined (V_2O_5/Al_2O_3) mass ratio and experimentally determined (V_2O_5/Al_2O_3) mass ratio in the six catalysts under study.

V_2O_5 coverage	$(V)_{Theory}$ wt-%	$(V_2O_5/Al_2O_3)_{Theory}$ g/g	$(V_2O_5/Al_2O_3)_{AAS}$ g/g
0 ML	0	0	0
0.1 ML	1	0.02	0.04
0.5 ML	5	0.09	0.15
1 ML	5	0.18	0.12
***2 ML**	15	0.37	0.18
***5 ML**	27	0.93	0.17

*-Catalysts showing V_2O_5/Al_2O_3) mass ratios below theoretical predictions.

ML- V_2O_5 monolayers on g-Al_2O_3 surface.

Note: All catalysts contained 10 wt-% Co.

3.3 BET Area and Pore Volume

BET analysis was carried out to establish the surface area and pore volumes of the supports and the catalyst (Figures 3-4 and 3-5). The corresponding amount of V_2O_5 (theoretical and experimental) in each support/catalyst are shown in Table 1-1.

Figure 3-4 shows the overall effect of increasing the amount of V_2O_5 on supports and catalysts on the BET surface area. At low vanadia loadings (0.1 and 0.5ML), the BET surface area for the supports increases compared to the bare γ-Al_2O_3 support. At higher V_2O_5 loadings BET surface area of the supports decreases with increasing V_2O_5 loading to about 140 $m^2.g_{cat}^{-1}$. The loss of surface area for supports at V_2O_5 loadings above monolayer coverage may have been caused by vanadia the phase blocking the pores causing a decrease in the overall surface area for modified supports.

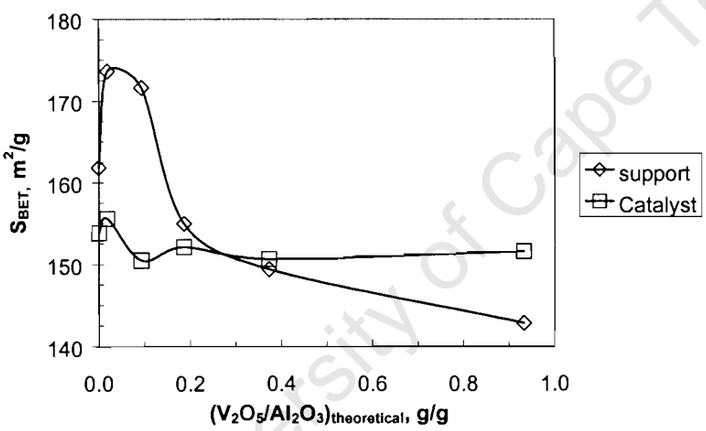

Figure 3-4: BET surface area variation as a function theoretical (V_2O_5/Al_2O_3) ratio for supports and catalysts.

The BET surface areas for the bare γ-Al_2O_3 and to 0.1-monolayer V_2O_5 coverage supports are similar (~155 $m^2.g_{cat}^{-1}$). The effect of vanadia addition on the BET surface area of the supports is pronounced for the 0.5-monolayer V_2O_5 coverage support which show a decrease slight in BET surface area (~150 $m^2.g_{cat}^{-1}$). Figure 3-4 shows that beyond 0.5-monolayer V_2O_5 coverage, an increase in V_2O_5 does not affect the catalyst BET area supports and the surface area remains constant at about 150 $m^2.g_{cat}^{-1}$. The relatively high surface areas for the catalyst as compared to the supports is attributed to the extra surface area provided by the cobalt phase added onto the supports.

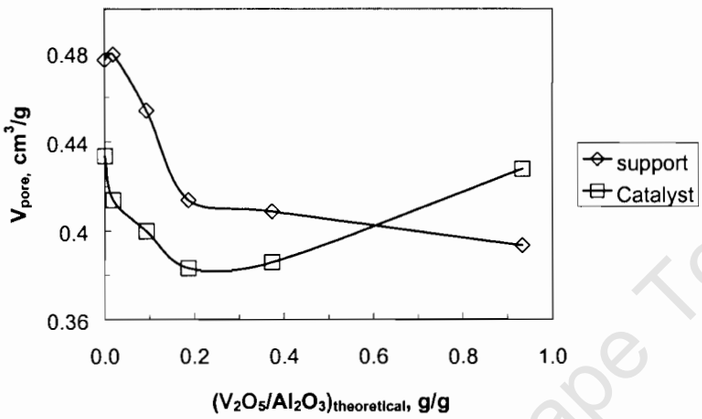

Figure 3-5: Pore volume variation as a function theoretical (V_2O_5 / Al_2O_3) ratio for supports and catalysts.

Figure 3-5 shows the effect of increasing the amount of V_2O_5 loading on the pore volume of both the catalyst and the supports. The pore volume of the supports decreases with increasing V_2O_5 loading. The decrease in pore volume is indicative of pore narrowing within the support structure caused by the cumulative addition of vanadia layers. Catalyst shows a further decrease in pore volume. Ideally, the pore volume should decrease with increasing vanadia loading. However, for the catalyst with 0.93 g/g V_2O_5/ Al_2O_3 ratio (*5 ML) the pore volume of the catalysts is larger than that of support. The addition of the cobalt phase seems to have caused an increase in the pore structure of the catalyst with high V_2O_5 loadings.

3.3.1 CO Chemisorption

CO chemisorption experiments were performed to estimate active metal surface area, metal dispersion and metal crystallite size. CO chemisorption experiments for each catalyst at constant temperature ($30^{O}C$) in an apparatus previously evacuated to remove gases that might still be trapped in the apparatus. The volume/pressure data obtained from the analysis was fitted in the single and dual-site Langmuir isotherm models, to evaluate CO volume The difference between CO uptake in catalysts and supports was obtained so as to evaluate the amount of CO adsorbed by the cobalt phase only.

Figures 3-6 and 3-7 show that both supports and catalysts adsorb appreciable amounts of CO. A closer inspection of the isotherms from both figures shows that at low pressures CO uptake increases sharply with an increase in pressure. With increasing pressure in CO uptake increases at a lower rate even at high pressures. Ideally at high pressures the isotherms should be independent of pressure variations since all the adsorption sites would be occupied if these systems obey Langmuir-adsorption kinetics.

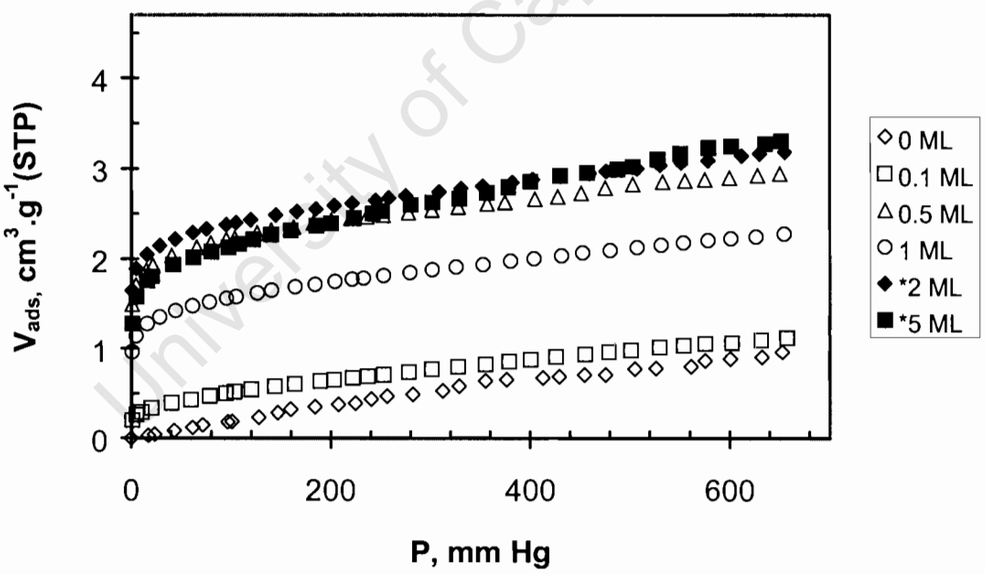

Figure 3-6: Experimental CO volume uptake as a function of pressure for supports with varying vanadia-loading. (T_{ads}= $30^{O}C$, $m_{Supp.}$ = ~0.5 g).

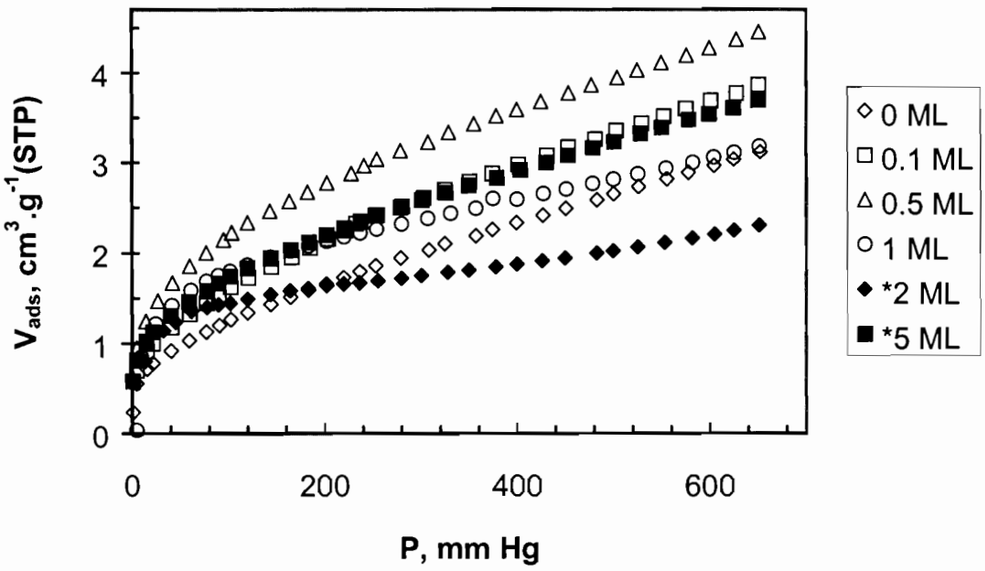

Figure 3-7: Experimental CO volume uptake as a function of pressure for catalyst with varying vanadia-loading. (T_{ads}= 30^{O}C, $m_{cat.}$ = ~0.5 g).

Figure 3-8 shows the isotherms obtained from the difference in CO uptake between the catalyst and their corresponding supports. The CO uptake in the catalysts seemed to decrease with an increase in V_2O_5 content in the catalysts. The difference of CO uptake between the catalyst and the supports yielded negative values. The *2-ML catalyst adsorbed less CO compared to its corresponding support resulting in negative volume differences at different pressures. It is for that reason that the data points for the *2-ML catalyst-support curve does not appear in Figure 3-8. It seems that addition of the cobalt phase on the modified supports lowered the amount of CO adsorbed.

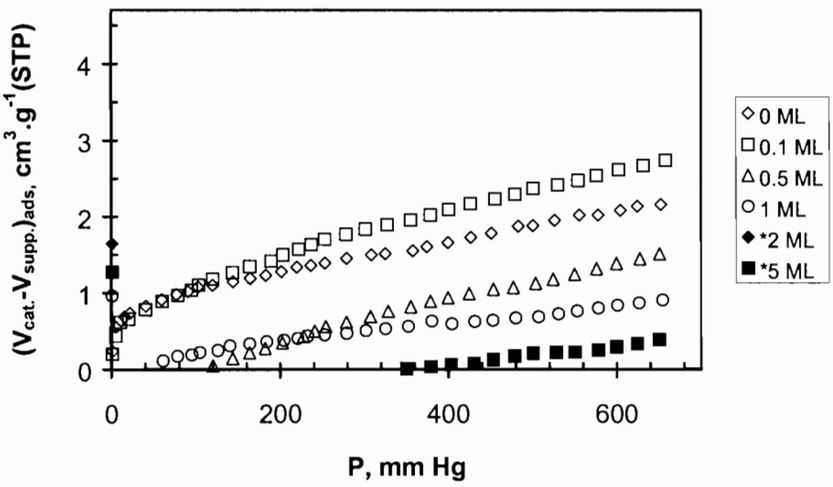

Figure 3-8: Difference in CO uptake of catalysts and supports as a function of pressure for catalysts with varying vanadia-loading. (T_{ads}= 30^{O}C, $m_{cat.}$ = $m_{supp.}$ = ~0.5 g).

3.3.1.1 Single site Langmuir isotherm model

Data for the catalysts with low V_2O_5 content (0 ML and 0.1 ML) were fitted in single site Langmuir model for the purpose of estimating the saturation volume, v_m. These two catalysts were chosen because they reasonable differences in CO uptake between the catalyst and support in the whole pressure range. Figure 3-9 shows the isotherms obtained from fitting experimental volume differences - pressure data for the two catalysts in a single-site Langmuir isotherm adsorption model. The parameters obtained from this regression are reported in Table 3-3.

Table 3-2: Saturation volume (v_m), the equilibrium adsorption (K) and the regression coefficient (R^2) obtained from modelling single-site CO adsorption Langmuir isotherm. (T_{ads}= 30^{O}C, $m_{cat.}$ =$m_{supp.}$ =~0.5 g).

Catalyst	v_m [$cm^3.g_{cat.}^{-1}$]	K mm Hg^{-1}	R^2
0 ML	1.39	0.15	0.91
0.1 ML	1.52	0.15	0.88

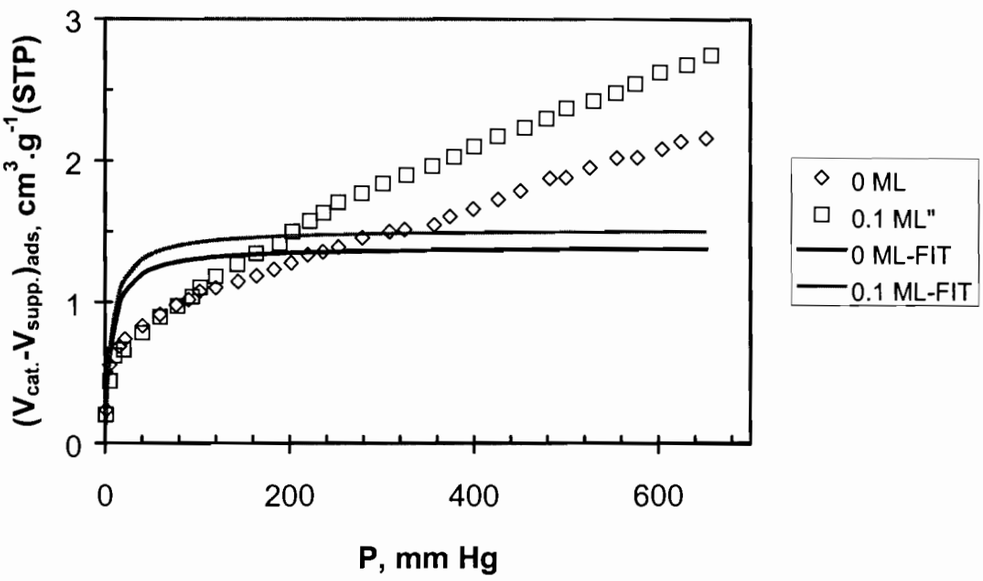

Figure 3-9: Difference in CO uptake of catalysts and supports as a function of pressure, experimental and single-site Langmuir model curves for 0 and 1-monolayer-catalyst/support system. (T_{ads}= 30^{O}C, $m_{cat.}$ = $m_{supp.}$= ~0.5 g).

Single-site Langmuir adsorption model: $\theta = \frac{K \cdot P_{CO}}{1 + K \cdot P_{CO}} = \frac{v}{v_m}$ (Smith, 1981).

Figure 3-9 clearly shows that the single-site Langmuir model does not fit the experimental data well, a fact further emphasised by the poor regression coefficient (R^2) obtained when fitting data (see Table 3-2) to the linearised Langmuir model. At high pressures CO uptake in the catalyst deviates strongly from Langmuir isotherm model. At high pressures, CO uptake should be constant after monolayer gas coverage indicating complete coverage of active sites. This deviation from the anticipated Langmuir isotherm behaviour suggests that different adsorption kinetics govern CO adsorption in these catalytic systems. The values of saturation volume estimated from the single site Langmuir model for the two catalysts are comparable which was expected since both catalysts contained the same amount of cobalt. In view of the poor regression coefficients they are of no use is as far as average crystallite size estimation is concerned.

3.3.1.2 Dual-site Langmuir adsorption model results

The collapse of the single site Langmuir model necessitated the need to explore the dual site Langmuir isotherm model for the purpose of evaluation of v_m, an important parameter in the estimation of average particle size from chemisorption data. Figure 3-10 shows isotherms from experimental data points and those obtained from regressing experimental data in the dual-site Langmuir isotherm model (DSL).

It is evident from Figure 3-10 that the dual-site Langmuir isotherm models the experimental data well, regression coefficients are sufficiently close to1. Also, the model curves and experimental points are well matched. All the parameters extracted from the model are of the same order of magnitude. The values of the saturation volume (v_m) estimated from dual-site Langmuir model fitting (see Table 3.3) are almost twice those from the single-site Langmuir estimates.

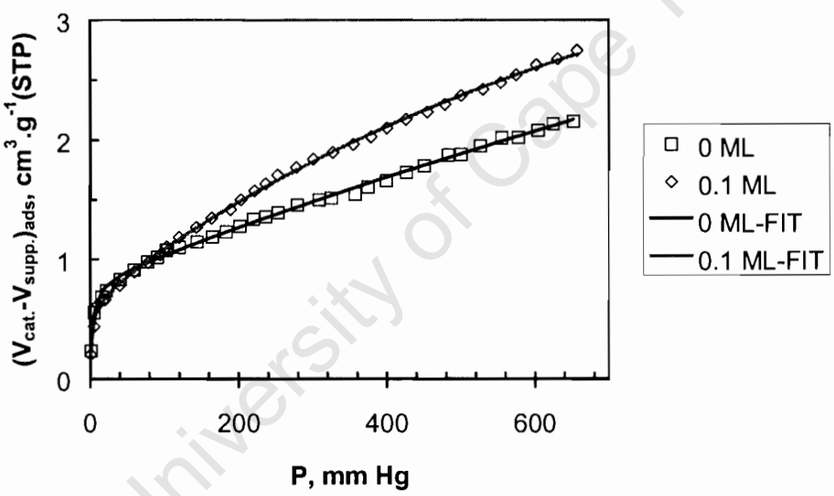

Figure 3-10: Difference in CO uptake of catalysts and supports as a function of pressure, experimental and Dual-site Langmuir model curves for 0 and 1-monolayer-catalyst/support system. (T_{ads}= 30^{o}C, $m_{cat.}$ = $m_{supp.}$= ~0.5 g).

Dual-site Langmuir adsorption model: $\theta = \frac{\theta_1 \cdot K_1 \cdot P_{CO}}{1 + K_1 \cdot P_{CO}} + \frac{\theta_2 \cdot K_2 \cdot P_{CO}}{1 + K_2 \cdot P_{CO}} = \frac{v}{v_m}$ (Krishna et al., 1998).

Table 3-3: Model parameters obtained from regression analysis of supports CO chemisorption data in a dual-site Langmuir isotherm model. (T_{ads}= 30^{O}C, $m_{cat.}$ =$m_{supp.}$ =~0.5 g).

Catalyst	Parameter	Value	Standard-dev.	R^2
0 ML	Vm ($cm^3.g_{cat.}^{-1}$)	3.68	2.13E-04	0.998
	θ_1	0.22	4.67E-05	
	K_1 ($mm.Hg^{-1}$)	0.31	7.21E-04	
	K_2 ($mm.Hg^{-1}$)	2.26E-04	4.27E-08	
0.1 ML	Vm ($cm^3.g_{cat.}^{-1}$)	2.73	6.42E-02	0.999
	θ_1	0.23	3.89E-03	
	K_1 ($mm.Hg^{-1}$)	0.43	6.07E-02	
	K_2 ($mm.Hg^{-1}$)	8.68E-04	6.87E-05	

3.3.1.3 Crystallite size estimation from CO chemisorption

Active metal surface area, metal dispersion metal dispersion and average crystallite sizes were calculated based on the saturation volume, v_m obtained from the dual-site Langmuir isotherm model. The results are reported in Table 3-4.

Table 3-4: Active metal surface area (A), metal dispersion (D), and average Co_3O_4 crystallite diameter for 0 and 0.1 ML catalysts estimated from CO chemisorption experiments. (T_{ads}= 30^{O}C, $m_{cat.}$ =~0.5 g).

Catalyst	A ($m^2g_{cat}^{-1}$)	D (%)	d_{VA} (nm)
0 ML	6.5	9.7	10.3
0.1 ML	4.8	7.2	13.9

The Co crystallite diameter for the 0 and 0.1 ML catalysts were estimated to be 10.3 and 13.9 nm respectively. The estimated value of active metal area is between 5 - 6 $m^2.g_{cat}^{-1}$ while metal dispersion was estimated between 7-10% for these two catalysts. It is difficult to conclude about effect of V_2O_5 content on crystallite size (d_{VA}) as well as the other estimated parameters based on the results in Table 3.4 because only two catalysts were considered.

3.3.2 Transmission electron microscopy (TEM)

TEM photographs were taken for the supports and catalyst with varying vanadia loading. TEM images of all the supports and corresponding catalysts are shown in Figures 3-11 to 3-16. The γ-Al_2O_3 support composed of oblong shaped homogeneous particles of roughly 4-nm in diameter. All the vanadia modified supports images show dark islands of what is assumed to be the vanadia phase in a pool of the Al_2O_3. This might indicate that vanadia was not evenly spread on γ-Al_2O_3 surface to form continuous monolayers as anticipated. The fine texture of the vanadia modified supports might be a result of imply that some of the vanadia which was not anchored on the γ-Al_2O_3 surface. These free vanadia crystallites fill the spaces in between γ-Al_2O_3 crystallites resulting in the fine texture of the modified supports pictures.

The TEM images for the 10-wt% Co-V_2O_5-γ-Al_2O_3 catalysts showed needle-like crystallite structures. These needles were not observed on the images of plain γ-Al_2O_3, on all the vanadia modified γ-Al_2O_3 supports, certainly not the on the non-promoted 10-wt% Co-γ-Al_2O_3 catalyst. The needle-like structures on the catalysts are suspected to originate from the dissolution of the unanchored soluble V_xO_y phases. V_2O_5 is known to be soluble in water (0.8g/l at 25^{O}C), therefore during introduction of the active Co phase by wet impregnation, the unanchored V_2O_5 might dissolve, yielding the observed spindle structures on the TEM images. The needle-like structures are therefore assumed to be soluble V_xO_y phase(s) on the catalysts. The dark spherical spots on the TEM images are thought to be cobalt crystallites as labelled on Figures 3-11 to 3-16.

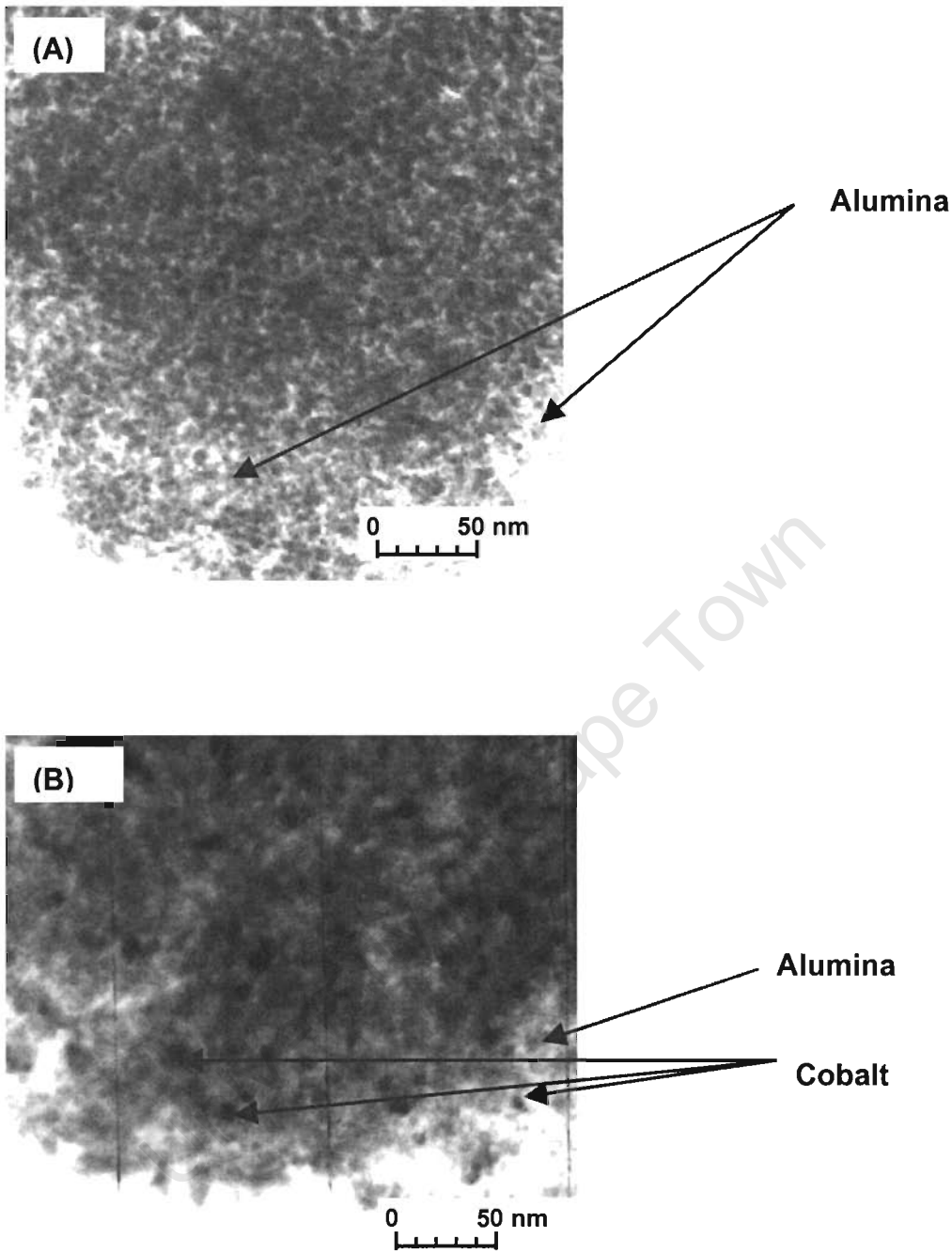

Figure 3-11: TEM images for support and corresponding catalyst, (A) γ-Al_2O_3 support, (B) 10 wt-% Co/Al_2O_3 catalyst.

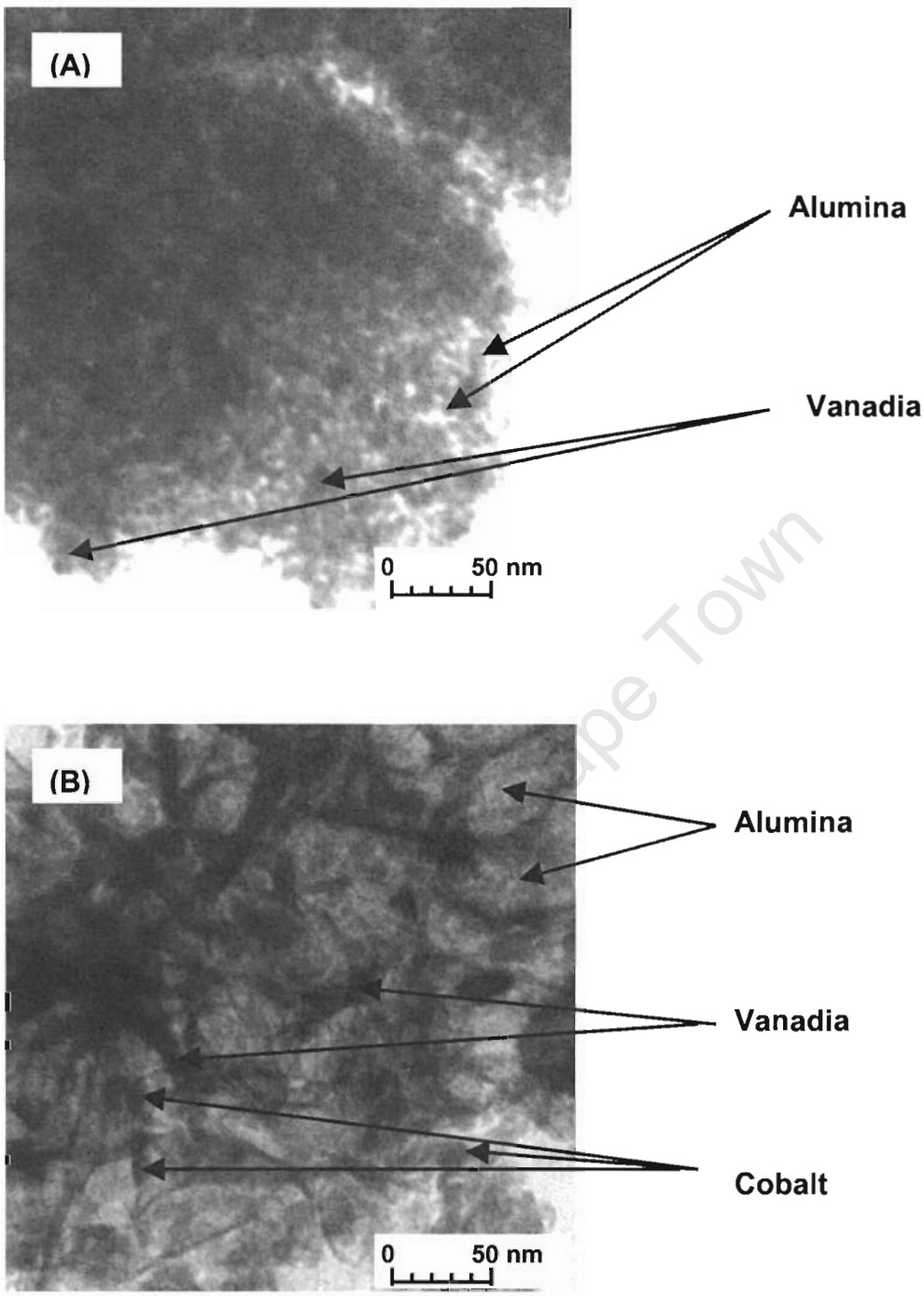

Figure 3-12:TEM images for support and corresponding catalyst, (A) 0.1-ML V_2O_5-γ-Al_2O_3 support, (B) 10 wt-% Co/0.1-MLV_2O_5-Al_2O_3 catalyst.

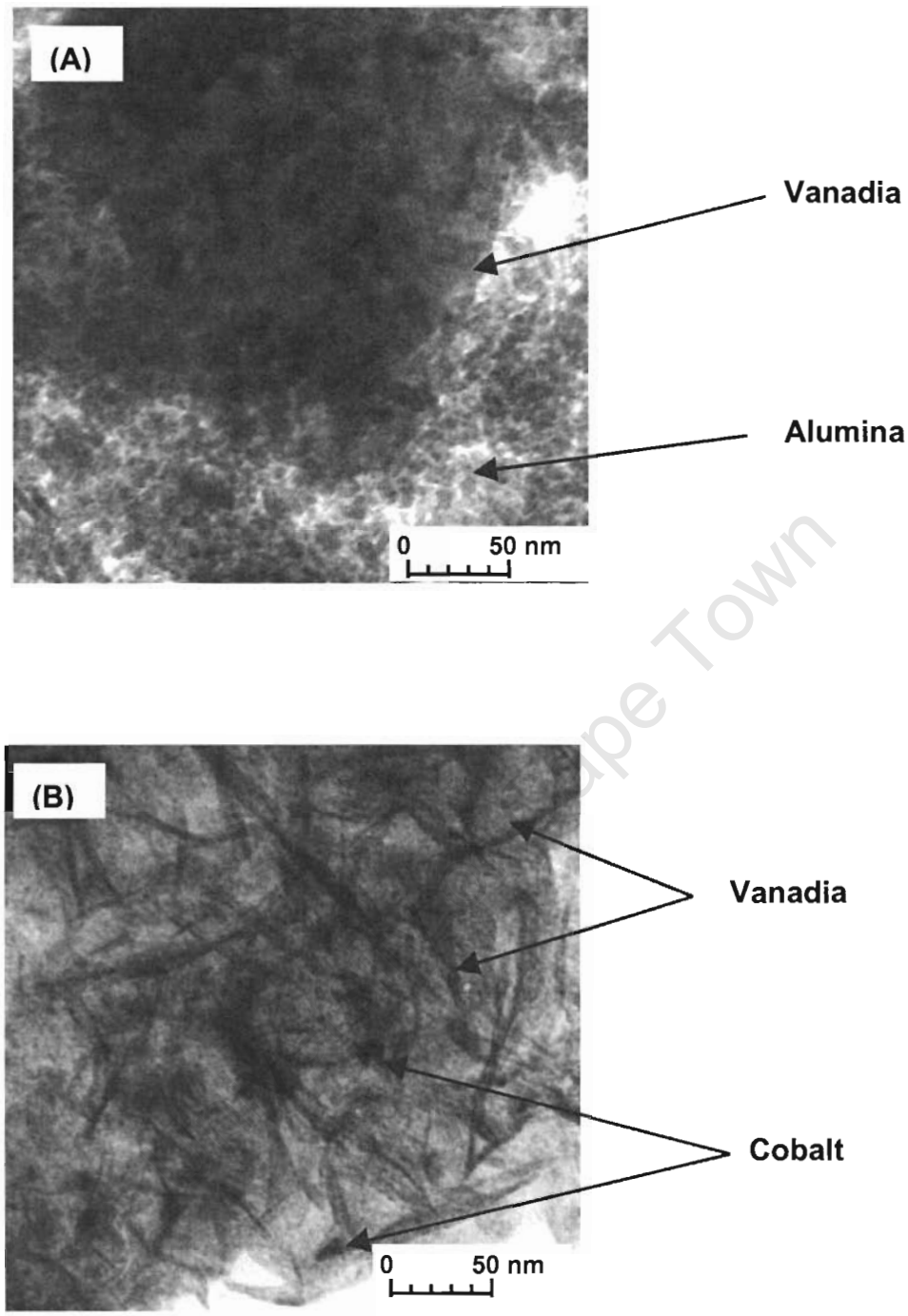

Figure 3-13: TEM images for support and corresponding catalyst, (A) 0.5-ML V_2O_5-γ-Al_2O_3 support, (B) 10 wt-% Co/0.5-ML V_2O_5-Al_2O_3 catalyst.

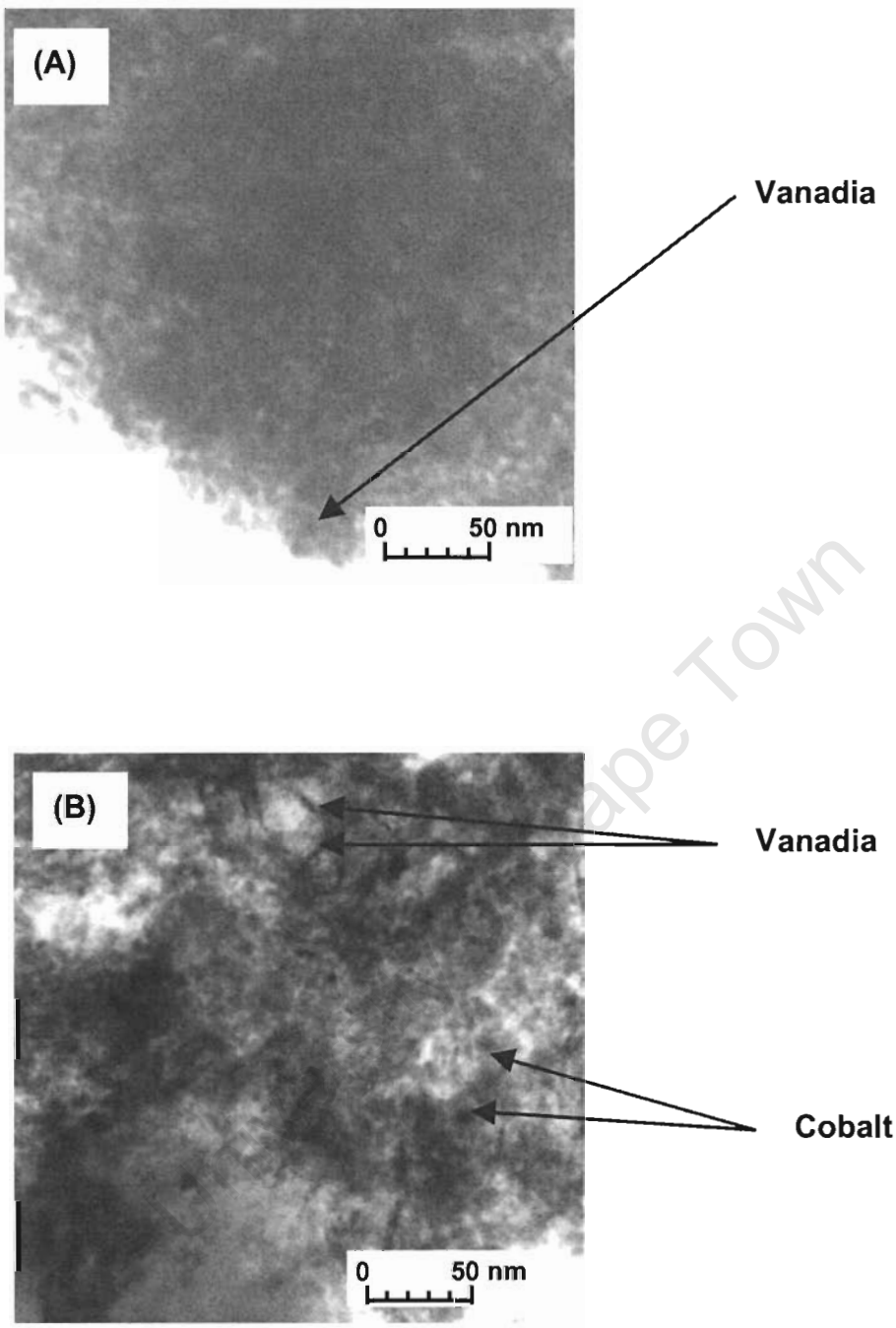

Figure 3-14: TEM images for support and corresponding catalyst, (A) 1-ML V_2O_5-γ-Al_2O_3 support, (B) 10 wt-% Co/1-ML V_2O_5-Al_2O_3 catalyst.

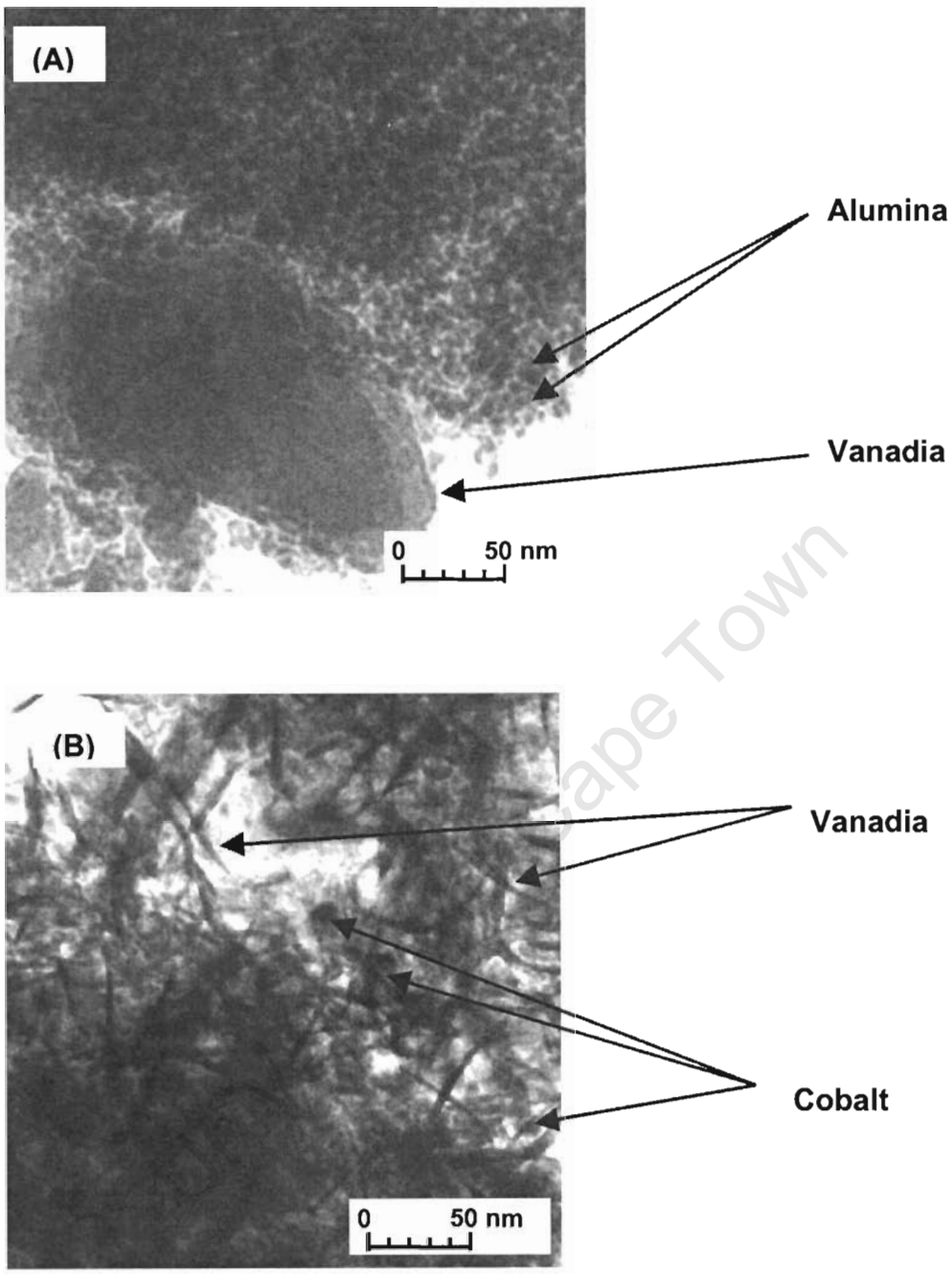

Figure 3-15: TEM images for support and corresponding catalyst, (A) *2 ML V_2O_5-γ-Al_2O_3 support, (B) 10 wt-% Co / *2 ML V_2O_5-Al_2O_3 catalyst.

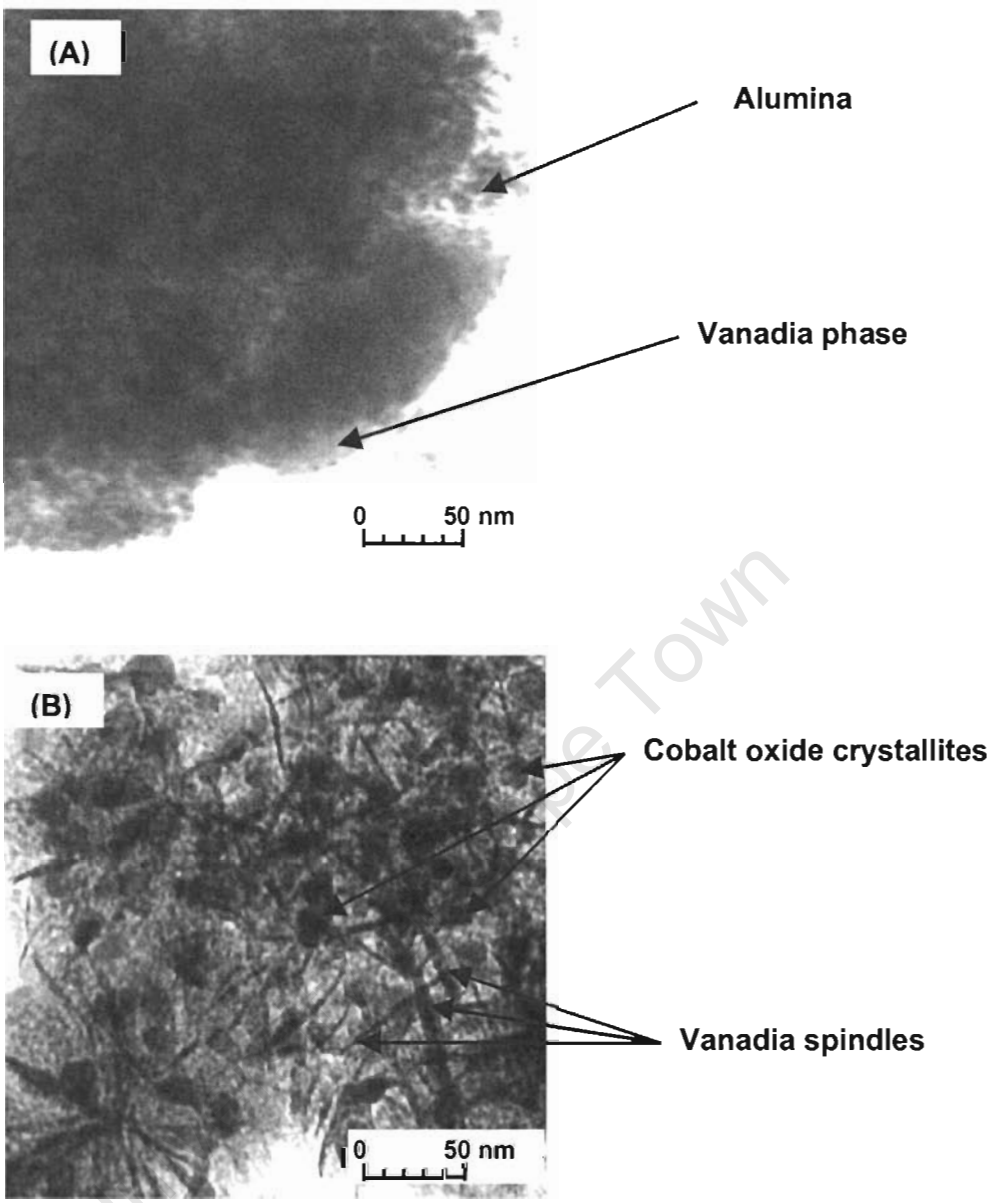

Figure 3-16: TEM images for support and corresponding catalyst, (A) *5 ML V_2O_5/Al_2O_3 support, (B) 10 wt-% Co / *5 ML V_2O_5/Al_2O_3 catalyst.

Crystallite size distributions were obtained performed by measuring crystal diameters from TEM pictures of the different catalysts. On average about 200-300 particles were manually and randomly measured from the pictures for each catalyst and size distribution analysis was done by following the method outlined by Bergeret and Gallezot (1998).

Table 3-5: Number of particles counted (n), mean-number diameter (d_{LN}) for calcined catalysts with varying vanadia loading.

Catalyst	n	d_{LN}, nm
0 ML	311	11.2
0.1 ML	399	10.9
0.5 ML	225	10.5
1 ML	258	9.8
***2 ML**	226	10.2
***5 ML**	230	10.4

The results in Table 3-5 show that the mean length-number diameter (d_{LN}) of the active phase crystallites within catalyst was around 10 nm and was independent of vanadia loading. Figure 3-17 and Figure 3-18 enforce the results shown in Table 3-5. These figures show number distribution (n_i vs. d_i) plots from the crystal counts. The catalyst samples show a wide particle size distribution with dominant size range lying within 9-13 nm size fractions. Table 3-6 shows the mean-number diameter $\mathbf{d_{LN}}$, and standard deviation, σ_x estimated from the crystal count data. The σ_x values are large which confirms that the size distribution is spread widely.

Table 3-6: Mean-number diameter, d_{LN} and standard deviation, σ_x calculated from crystal count population data for catalyst with varying vanadia loading.

Catalyst	d_{LN}, nm	σ_x
0 ML	11.2	5.8
0.1 ML	10.9	5.2
0.5 ML	10.5	4.5
1 ML	9.8	4.3
***2 ML**	10.2	7.6
***5 ML**	10.4	7.6

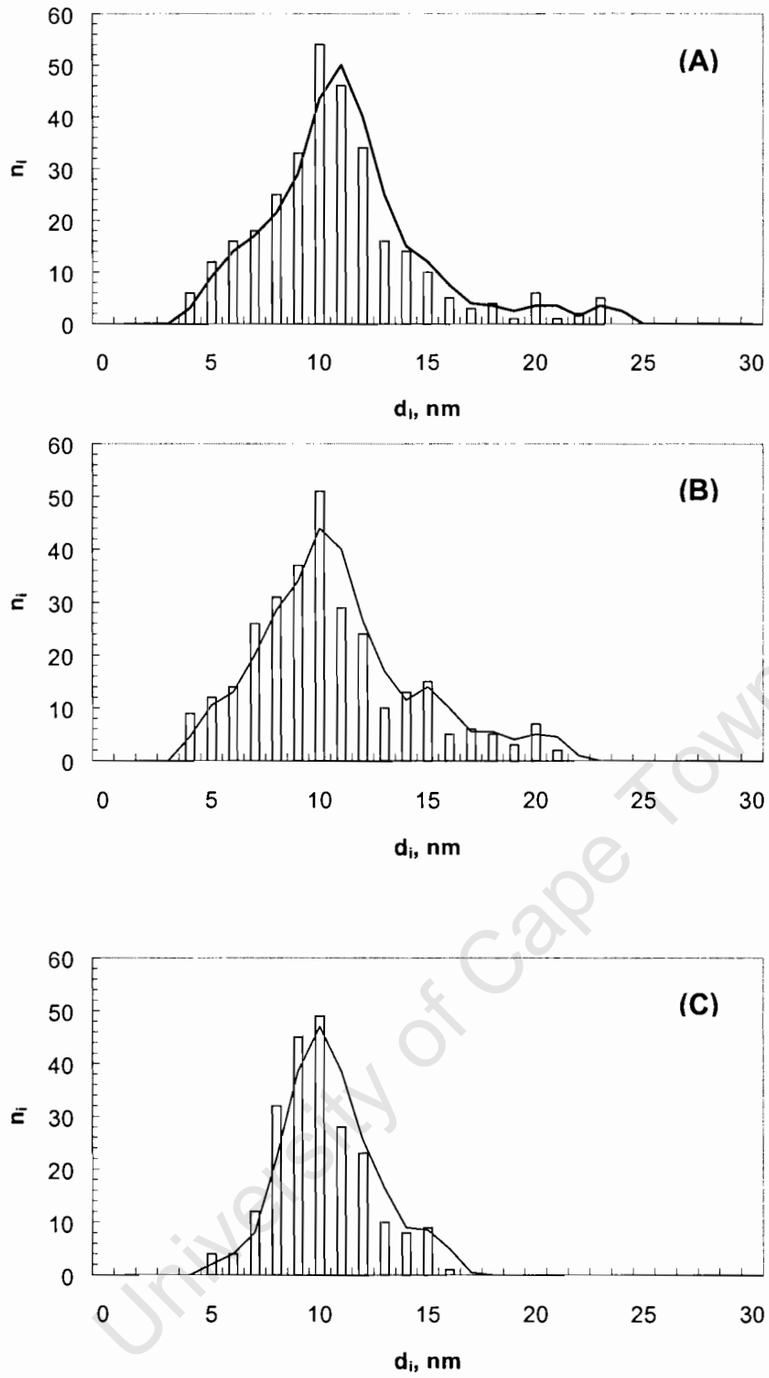

Figure 3-17: Crystallite size distribution curves for catalysts with varying vanadia loading. (A) 10wt-% Co/Al_2O_3, (B) 10wt-% Co/0.1 ML V_2O_5/Al_2O_3, (C) 10wt-% Co/0.5 ML V_2O_5/Al_2O_3.

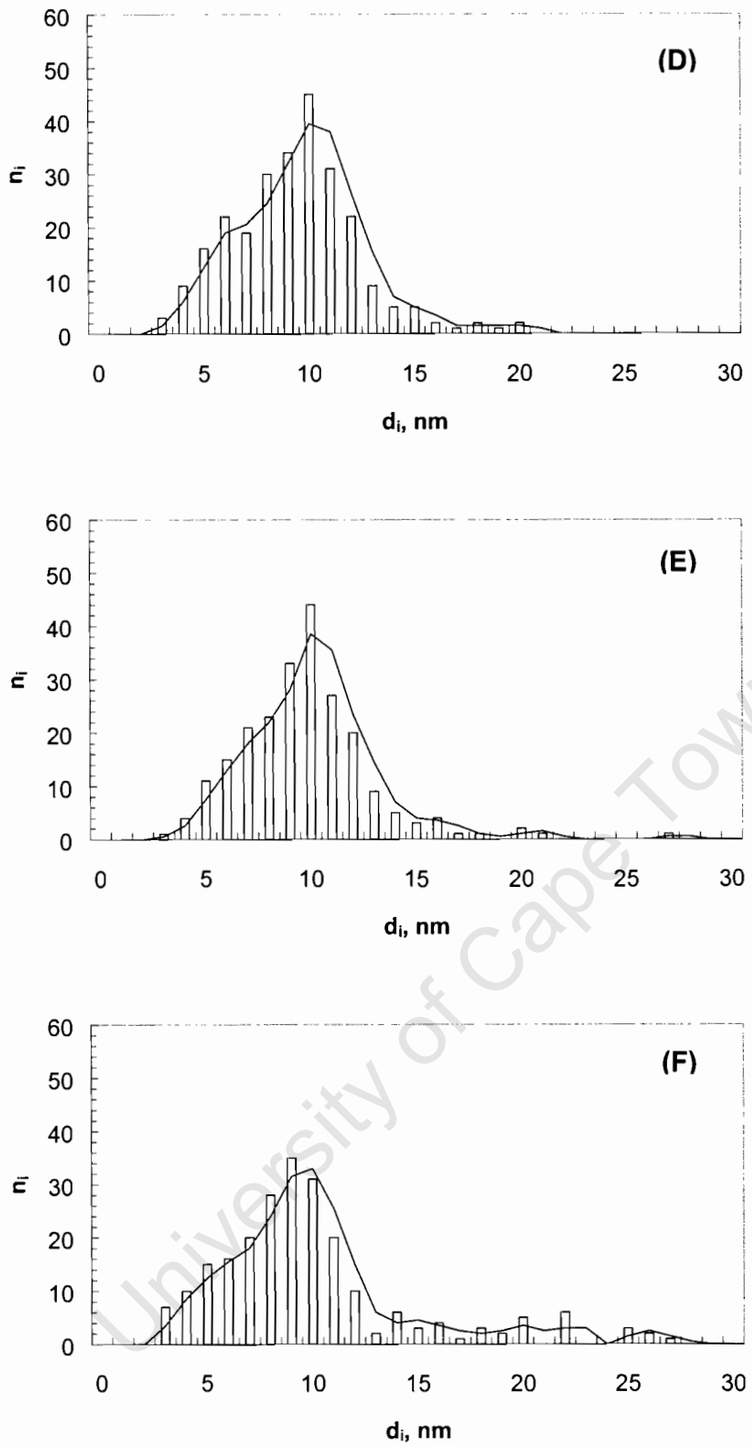

Figure 3-18: Crystallite size distribution curves for catalysts with varying vanadia loading. (D) 10wt-% Co/1 ML V_2O_5-Al_2O_3, (E) 10wt-% Co/*2 ML V_2O_5-Al_2O_3, (F) 10wt-% Co/*5 ML V_2O_5-Al_2O_3.

3.3.3 Temperature programmed reduction (TPR)

Temperature programmed (TPR) experiments were carried out to study the reduction behaviour of the catalysts under study. The reduction behaviour of the catalyst was monitored by the amount of hydrogen consumed during the course of the TPR experiments. Figure 3-19 and 3-20 show TPR profiles for supports and catalysts, respectively. The amount of hydrogen consumed for the supports and catalysts, respectively, is given in Tables 3-7, 3-8 and 3-9.

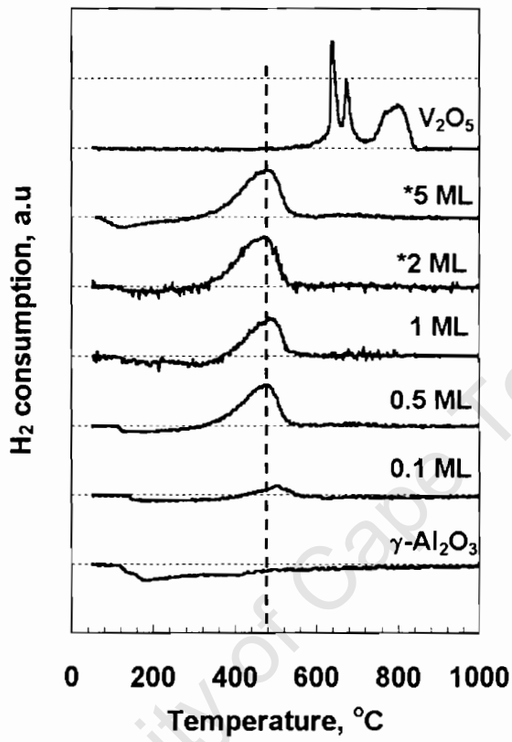

Figure 3-19: TPR profiles for supports with varying vanadia content. Supports calcined in a fixed bed under air (50 ml/min, NTP) at 550^{O}C, 1 atmosphere (γ-Al_2O_3 not calcined). (TPR-$m_{support}$=~0.3g, ramping rate 10^{O}C.min^{-1}, H_2-Ar flowrate 50ml/min (NTP).

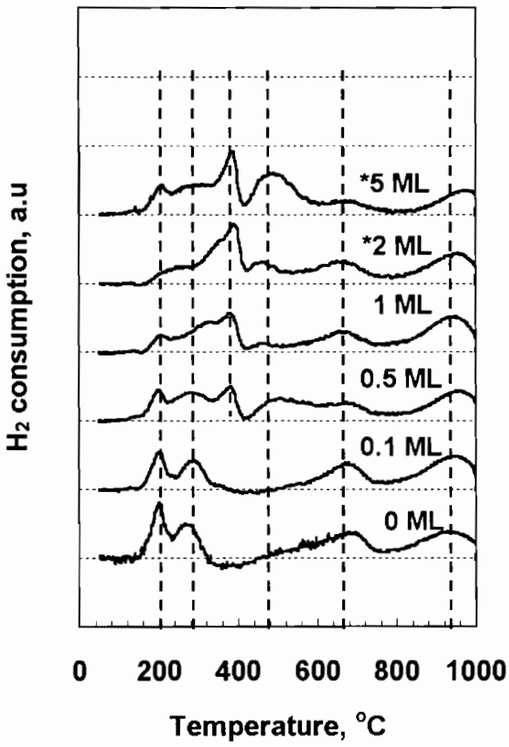

Figure 3-20: H_2 consumption TPR profiles catalysts with varying vanadia content. Catalysts calcined in a fluidised bed under air (1 l.min^{-1}, NTP), at 250 ^{O}C, 1 atmosphere. (TPR- $m_{cat.}$ ~0.3g, ramping rate 10^{O}C.min^{-1}, H_2-Ar flowrate 50ml/min (NTP).

Table 3-7: H_2 consumption amount during TPR experiments for the supports with varying vanadia content. (m_{suppt} = ~0.3g, ramping rate=10^{O}C.min^{-1}, H_2-Ar flowrate 50ml.min^{-1} ,STP).

Support	H_2/V_2O_5 (mol/mol)
0 ML	0
0.1 ML	0.85
0.5 ML	6.20
1 ML	1.13
***2 ML**	2.22
***5 ML**	1.80
Bulk V_2O_5 [a]	1.92

[a] m_{V2O5} = ~0.03 g

NB: vanadia content based on AAS results for all supports

Table 3-8: H_2 consumption amount during TPR experiments for catalysts with varying vanadia content. (Co content =~ 9 wt-%[a], $m_{cat.}$ = ~0.3g, ramping rate =10^{O}C.min^{-1}, H_2-Ar flowrate 50ml.min^{-1}, NTP).

Catalyst	$H_2/g_{cat.}$ (mmols/g)	$H_2/(Co+V_2O_5)^{\#}$ (mol/mol)	$H_2/Co^{\#}$ (mol/mol)
0 ML	2.096	1.24	1.24
0.1 ML	2.028	1.26	1.35
0.5 ML	2.557	1.62	1.73
1 ML	2.353	1.20	1.58
***2 ML**	2.609	1.46	1.87
***5 ML**	2.791	1.35	1.74

[#] vanadia and cobalt content based on AAS results

The TPR profile of bulk V_2O_5 (see Figure 3-19) shows 3 intense reduction peaks at 640 ^{O}C, 680 ^{O}C and at 800^{O}C. Chary et al. (2003) reported a similar TPR profile for bulk V_2O_5. These reduction peaks were attributed to the sequential reduction of V_2O_5 to V_2O_3 in the following manner:

$$2H_2 + 3V_2O_5 \rightarrow V_6O_{13} + 2H_2O \quad (1)$$

$$H_2 + V_6O_{13} \rightarrow V_2O_4 + H_2O \quad (2)$$

$$3H_2 + 3V_2O_4 \rightarrow 3V_2O_3 + 3H_2O \quad (3)$$

The peak at 640 ^{O}C corresponds to the reduction of V_2O_5 toV_6O_{13}, the peak at 680 ^{O}C is associated with the reduction of V_6O_{13} to V_2O_4 and peak at 800^{O}C corresponds to the reduction of V_2O_4 to V_2O_3 (Chary et al., 2003). Gallie et al., (1995) also reported reduction peaks at temperatures higher than 600^{O}C for bulk V_2O_5. Theoretically, the H_2/V_2O_5 mole ratio of for the reduction V_2O_5 to V_2O_3 is 2 mol/mol. The TPR results (see table 3-7) show ratio this ratio to be1.92 mol/mol (4% lower than theoretical prediction) which is in agreement with the observations made by Chary et al (2003). Also the experimentally determined hydrogen consumption distribution between the three peaks are close to theoretically expected distribution ratio of 0.33:0.17:0.5 for peaks 1, 2 and 3 respectively as shown in Table 3-9.

Table 3-9: H_2 consumption for V_2O_5 TPR experiments. (m_{V2O5}=0.0305g, ramping rate =10^{O}C.min^{-1}, H_2-Ar flowrate 50ml.min^{-1}, NTP).

V_2O_5 reduction Peaks	H_2 consumption (mmols)	(H_2/V_2O_5)ratio [a] (mol/mol)	Distribution (%)
1	0.121	0.72	37
2	0.058	0.35	18
3	0.143	0.86	44
Total→	0.322	1.92	100

Figure 3-19 shows the TPR profile for the supports only. γ-Al_2O_3 TPR profile shows no reduction peaks during the entire TPR experiment, indicating that γ-Al_2O_3 was thermally stable in H_2-atmosphere upto 1000^{O}C. The results signal for the reduction of γ-Al_2O_3 dropped below the baseline at 150 ^{O}C and remained there until ~750^{O}C indicating that something came off the γ-Al_2O_3 during the course of the TPR experiment. γ-Al_2O_3 and V_2O_5 were not calcined before performing the TPR experiment might be that the negative signal was caused by desorption of some other adsorbed species in the γ-Al_2O_3.

All the other V_2O_5 modified supports show reduction in the temperature range 320-560 ^{O}C with peak maxima at ~480^{O}C. The size of these reduction peak increases with V_2O_5 loading up to 1-monolayer V_2O_5 coverage after which they remain constant (see Table 3-7; 0.5 ML results must be regarded as an outlier). This suggests that H_2 consumption is due to the reduction of vanadium oxide species introduced during support modification. Gallie et al. (1995) observed TPR reduction peak for V/Al catalyst between 300^{O}C to 600^{O}C (T_{max}= 475^{O}C) which was attributed to the reduction of surface vanadium species. The TPR profiles of the V_2O_5 doped supports does not show the reduction peaks of V_2O_5 at temperature above 600^{O}C. The absence of the V_2O_5 reduction peaks on the profiles of modified supports suggests that the vanadia on the supports exist in other i.e. V_xO_y forms other than V_2O_5.

Figure 3-20 and Table 3-10 show TPR profiles and the quantitative TPR H_2/Co consumption ratios for the catalysts, respectively. The TPR profiles for catalysts show a higher degree of complexity than those for supports. Catalysts with low vanadia content (0 and 0.1 ML) show four distinct reduction peaks having H_2/Co mole ratios of 1.24 to 1.35 mol/mol, respectively. The theoretical H_2/Co consumption ratio for Co_3O_4 to Co reduction is 1.33 mol/mol. These two catalysts show H_2/Co mole ratio close to the theoretically predicted ratio. Arnoldy and Moulijn, (1985) reported this ratio to vary between 1 and1.3 mol/mol observed for the reduction of Co/Al_2O_3 catalyst. Van Steen et al. (1996) reported H_2/Co mole of 1.2 mol/mol for Co/SiO_2 catalyst systems.

The other catalysts (0.5, 1, *2, and *5 ML catalysts) show 6 reduction peaks. The H_2/Co mole ratio for these catalysts varies between from 1.58 to 1.74 mol/mol (higher than 1.33 predicted by theory). This lead to the speculation that despite subtraction of the H_2 consumption by supports from the corresponding catalyst H_2 consumption, there still might be some vanadium species contribution in the total hydrogen consumption for the catalysts.

The TPR profiles for catalysts show two low temperature reduction peaks with peak maxima at 220^{O}C and 280 ^{O}C. These peaks are initially intense for catalysts with low vanadia content and loose their intensity with increasing vanadia content. The reduction peaks in this temperature region is characteristic of stepwise cobalt oxide reduction into metal Co ($Co^{3+}\rightarrow Co^{2+}\rightarrow Co^{0}$). Arnoldy and Moulijn (1985) reported peak maximum at 320^{O}C and 340^{O}C for Co_3O_4 and CoO, respectively, for $Co\text{-}Al_2O_3$ catalysts.

Table 3-10: H_2 consumption for individual reduction peaks during TPR experiments for catalysts with varying vanadia content. (Co content =~ 9 wt-%, $m_{cat.}$ = ~0.3g, ramping rate= 10^{O}C.min^{-1}, H_2-Ar flowrate 50ml.min^{-1}, NTP)

Temp. range, ^{O}C →	100-230	230-340	340-440	430-630	630-800	800-1000
Catalyst ↓	H_2 consumption distribution , mol -%					
0 ML	19	15	0	0	33	33
0.1 ML	14	15	0	0	28	43
0.5 ML	10	16	11	21	14	27
1 ML	7	16	13	9	19	36
***2 ML**	9	13	16	15	18	29
***5 ML**	7	18	18	27	11	19

Table 3-9 shows the H_2 consumption of the individual reduction peaks over the entire TPR temperature range. The first two peaks accounts for 34 mol-% of the total H_2 consumption for the non-promoted catalyst. There is an observed decrease in H_2 consumption on the low temperature peaks. There is no clear distinction between the second and the third low temperature peaks. With increasing vanadia loading on the catalysts, the intensity of the third peak increases, and the percentage area of the first 3 peaks increases from 34 to 41%. The appearance of the third peak indicates the existence of reducible V_xO_y species at low temperature which reduces at T_{max}= 400^{O}C.

The fourth peak at T_{max} = 490 ^{O}C, only appear on the 0.5, 1, *2, and *5 monolayer vanadia loadings. The intensity of the peak increased with increasing vanadia content except for the 1 ML catalyst, as indicated by the percentage of the total H_2 consumption corresponding to this peak (see Table 3-9). The increase in H_2 consumption with increasing V_2O_5 content on the catalysts suggests presence of surface vanadium species present in these catalysts. This is in agreement with the observations made by Gallie et al. (1995), who reported reduction of vanadium oxide surface species of V_2O_5/Al_2O_3 catalyst systems in this temperature range. The only peak observed on TPR profiles for supports falls within this temperature range.
Broad peaks between 600^{O}C-750^{O}C are shown by the TPR patterns of all the catalysts. The intensity of these peaks decreases with increase in V_2O_5 content in the catalysts. Arnoldy and Moulijn (1985) attributed these high

temperature peaks the reduction of Co^{2+} surface species (Co_2-Al-oxide). The high temperature reduction peak at 950^{O}C corresponds to the reduction of crystalline phase Co-Al_2O_4 reported to occur at high a temperature above 900^{O}C.

3.3.4 X-ray diffractometry, XRD

XRD experiments were carried out for the purpose of identifying phases present in the catalysts and for estimation of the average crystal size of the cobalt phase in the prepared catalysts. The XRD patterns for the catalysts prepared in this study are depicted in Figure 3-21. In addition to the catalyst XRD profiles, γ-Al_2O_3 and pure V_2O_5 XRD patterns were obtained from XRD experiments of these compound without pre-treatment.

Catalysts patterns showed characteristic main diffraction peaks for Co_3O_4 at 2θ =31.2^{O}, 36.7^{O}, 59.7^{O} and 65.9^{O}. This indicated the presence of cobalt (II, III) oxide phase in the catalysts. γ- Al_2O_3 is present in the catalysts. None of the diffraction peaks for V_2O_5 are observed on the catalyst patterns probably because the V_2O_5 phase on the catalyst samples is X-ray amorphous. There is no evidence on the catalyst patterns pointing towards the presence of crystalline aluminium vanadium oxide phase ($AlVO_3$ or $AlVO_4$). The Co_3O_4 peak intensity decreases with an increase in V_2O_5 loading on the catalysts. From the XRD patterns it can be concluded that the V_2O_5 is well dispersed on the γ-Al_2O_3 such that its crystallite size was below XRD detection limits.

Co_3O_4 crystallite size was estimated by line broadening analysis, using the Scherrer equation (β estimated from the width at half the height of the Co_3O_4 peak). The Co_3O_4 diffraction peak at 2θ=59.17^{O} was chosen for estimating β values because is free from interference from γ-Al_2O_3 diffraction peaks.

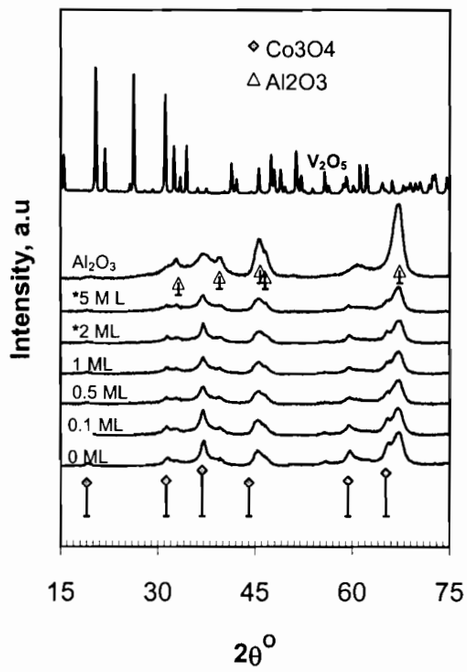

Figure 3-21: XRD patterns of 10-wt.% Co-V_2O_5/Al_2O_3 catalysts with varying vanadia content (catalysts calcined at 250°C, V_2O_5 and Al_2O_3 uncalcined).

Table 3-11: Co average crystallite sizes in catalysts with varying vanadia content estimated using line broadening analysis of XRD data ($2\theta = 59.17^{O}$).

Catalyst	Crystal size nm
0 ML	11.0
0.1 ML	10.1
0.5 ML	9.8
1 ML	12.6
***2 ML**	13.2
***5 ML**	13.2

The estimated Co crystallite sizes in the catalysts range from 11-13 nm (see Table 3-10) There are no observed trends pointing towards an effect of vanadia loading on the Co_3O_4 crystallite size in the catalysts.

3.4 Fischer-Tropsch synthesis

The effect of vanadia promotion on the catalytic performance of a $Co/V_2O_x/Al_2O_3$ catalyst was tested under Fischer-Tropsch conditions in a plug flow reactor. Perfomence characterisation was based on activity and selectivity data obtained from reactions run for each of the synthesised catalyst in this study. Catalyst activity was reflected by the amount of converted CO under test conditions.

3.4.1 Time on stream results CO conversion

The time on stream perfomance of the catalysts was monitored for each run by calculation the CO conversion as a function of reaction time. Figure 3-22 depicts the time on stream CO conversion plots for the six runs; each run corresponding to a catalyst with different vanadia content.

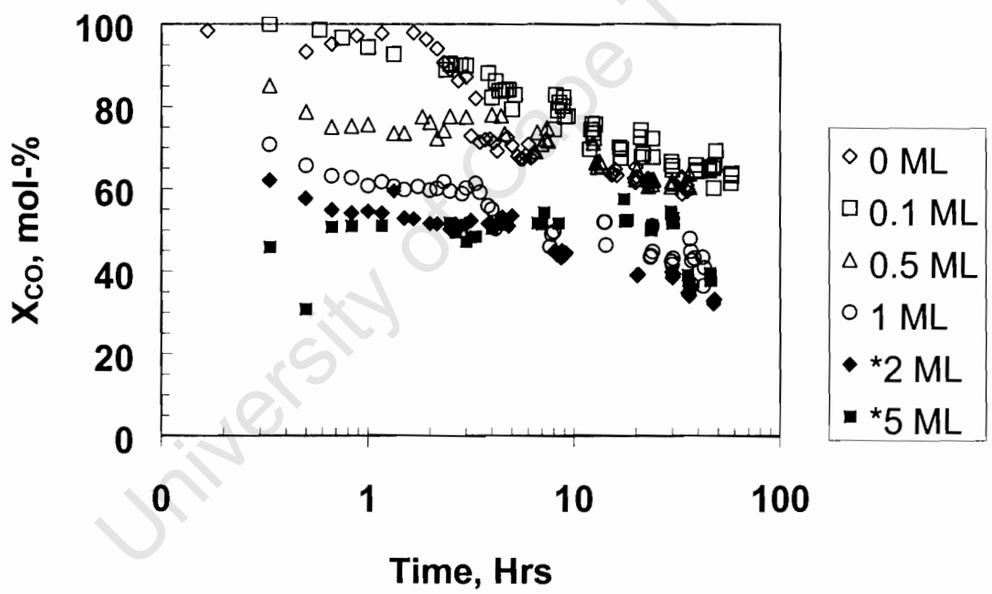

Figure 3-22: Time on stream CO conversion (X_{CO}) from Fischer-Tropsch synthesis for the six catalysts (m_{cat}~ 0.5g, T=220^{O}C, P=20 bar (abs), H_2:CO=2:1, WHSV=1.125 g_{CO}/g_{cat}.hr)

Vanadia in the catalyst affects the initial catalyst activity before attaining steady state during Fischer-Trospch synthesis. The base case (0 ML) and the 0.1 ML catalysts show high CO conversion (~100 mol-%) within the first 20 minutes of the reaction. The observed high conversions exhibited by these two catalysts might not be real. These high initial conditions might have been caused by the bigger dead space in these catalyst which which required relatively longer times and more synthesis gas to fill. As a consequence of this no synthesis gas is picked up by the GC during the initial stage of the synthesis.

The initially high conversion then drops steadily with time on stream until steady state conversion is attaneined between 24-36 hours for all catalysts, however, that the catalysts with high vanadia loading seem to deactivate at a faster rate beyond 36 hours time on stream this range. The deactivation after this range might indicate that high vanadia contents decreases catalyst life during Fischer Tropsch synthesis.

The steady state values CO conversion for the catalysts with low vanadia content (0ML, 0.1ML, and 0.5 ML catalysts) show steady state conversions of about 60 mol-%. The initial conversios for the catalyst with relatively high vanadia contents (1ML, *2ML and *5ML catalysts) showed a marked decrease as compared to the catalysts with low vanadia content (see Figure 3-18 and Table 3-12). Steady state conversions for 1ML, *2ML and *5ML catalysts were 44, 40 and 50 mol-% ,respectively, after 24 hors time on stream. It seems that the increasing vanadia content in the catalysts resulted in lower steady state CO conversions. The *5-ML catalyst however showed steady state CO conversions with much more scatter than with 1 and *2 ML catalysts, albeit a higher degree of scatter was obtained with this catalyst.

Table 3-12: Steady state CO conversion, X_{CO} and methane, CH_4 selectivity after 24 and 30 hours Fischer-Tropch synthesis for the catalysts with varying vanadia loading. $m_{cat.}$=0.5g, T=220^{O}C, P=20 bar, H_2;CO=2:1

Catalyst	24 Hours		30 Hours	
	X_{CO}, mol-%	S_{CH4} , C-%	X_{CO}, mol-%	S_{CH4} , C-%
0 ML	62	9.4	62.3	11.5
0.1 ML	67	6.7	65	7.2
0.5 ML	61	8.3	60	8.0
1 ML	44	8.1	42	11.5
***2 ML**	40	9.9	36	9.7
***5 ML**	51	7.3	50	7.5

3.4.2 Methane selectivity

Figure 3-23 shows the time on stream variation of methane selecticity (S_{CH4}) for the six catalysts during Fischer-Tropsch synthesis. The 0ML, 0.1ML and 0.5 ML catalysts show low methane selectivities during the initial stages of the reaction (catalyst precondition step) which increases to a steady state values of about 7 to 9 C-% after 24 hours. This is consistent with the high steady state CO conversions observed observed for these three catalysts. Generally, the methane selectivity at steady state is high for the catalyst with high CO conversions and seem to vary with CO conversion . All the vanadia promoted catalyst show relatively lower initial methane selectivities as compared to the base case catalyst. This seem to indicate that the vanadia in the catalyts enhances the hydrogenation propeties in the initial stages of the reaction.

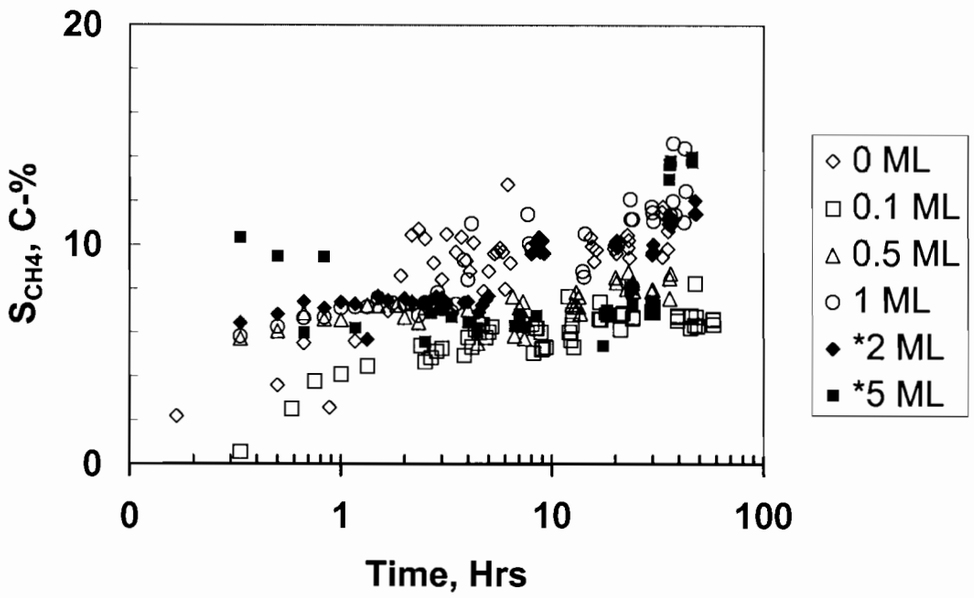

Figure 3-23: Time on stream methane selectivity (S_{CH4}) from Fischer-Tropsch synthesis for the six catalysts (m_{cat}~ 0.5g, T=220^{O}C, P=20 bar (abs), H_2:CO=2:1, WHSV=1.125 g_{CO}/g_{cat}.hr).

The effect of vanadia loading on the methane selectivity cannot be easily escertained from Figure 3-23 because of the different steady state conversions exhibited by the six catalyts. Figure 3-24 shows a plot of CO conversion (X_{CO}) agaist methane selectivity. On this plot all the vanadia promoted catalyst show low methane selectivities compared to the base case catalyst at steady state conversions (40-60 mol-%). From this it can be concluded that vanadia addition lowers the methane selectivity during Fischer-Tropsch synthesis.

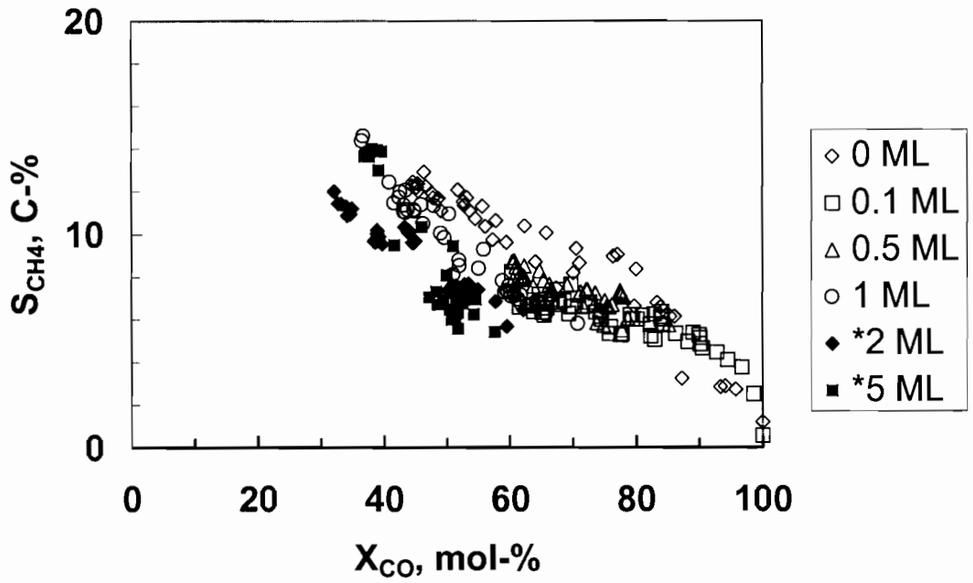

Figure 3-24: CO conversion (X_{CO}) vs. methane selectivity (S_{CH4}) from Fischer-Tropsch synthesis for the six catalysts (m_{cat}~ 0.5g, T=220^{O}C, P=20 bar (abs), H_2:CO=2:1, WHSV=1.125 g_{CO}/g_{cat}.hr).

3.4.3 Anderson-Schulz-Flory (ASF) product distributions

Anderson-Schulz-Flory distribution plots were used to calculate the chain growth propabilities of each of the six catalyst from FID data. The chain growth propabilities were calculated from slope of the linear hydrocarbon ASF plots between C_3 and C_9 . Table 3-13 shows values of chain growth propabilities for each catalyst obtained for the 24 and 30 hours time on stream analysis. Figures 3-25 (A) and (B) illustrates the ASF plots for the 24 and 30 hours time on stream analysis, respectively.

The 24 hours time on strean results show that the chain growth probability is not affected by vanadia content on the catalysts . The chain growth probability values varied between 0.84 to 0.88 with the 0.1, 1 and *2 ML catalysts showing high chain growth probabilities. Chain growth probabilities between 0.81 and 0.84 were obtained after 30 hours time on stream. The chain growth probability for 30 hours time are slightly less than those from the 24 hours analysis for all vanadia promoted catalyts. The chain growth

probability for the non promoted catalyst remained constant for the 24 and 30 hours time on stream analysis.

Table 3-13: Chain growth propabilities (α) for the six catalysts with varying vanadia content at different times on stream, 24 and 30 hours.(m_{cat}~ 0.5g, T=220^{O}C, P=20 bar (abs), H_2:CO=2:1, WHSV=1.125 g_{CO}/g_{cat}.hr).

Catalyst	24 Hours	30 Hours
	α	α
0 ML	0.84	0.84
0.1 ML	0.88	0.85
0.5 ML	0.87	0.82
1 ML	0.85	0.83
***2 ML**	0.87	0.82
***5 ML**	0.85	0.81

The ASF plots for the 6 catalysts (see Figures 3-25) match each other closely between C_1 and C_{10}, hence the estimated chain growth probabilities were were also very close to each other. All ASF plots for the 6 catalysts show the characteristic high C_1 content and low C_2 content normally observed in Fischer-Trosch synthesis. Beyond C_3 , the product content then decreases steadily with an increase in carbon number. The 24 hour time on stream ASF plots (Figure 3-20 (A)) demonitrates this well , while the 30 hours data shows some scatter. The 0.1- ML catalyst shows relatively high hydrocarbon content beyond C_8 which drops again at C_{10} to coincide with the ASF plots for the other catalysts. This might been caused by product build-up in the ampoule breaker as a result of wax accumulation. Another anormalty in the 30 hours time on stream ASF plot is the rather high C_2 content for the 0.5-ML catalyst which cannot be explained at present.

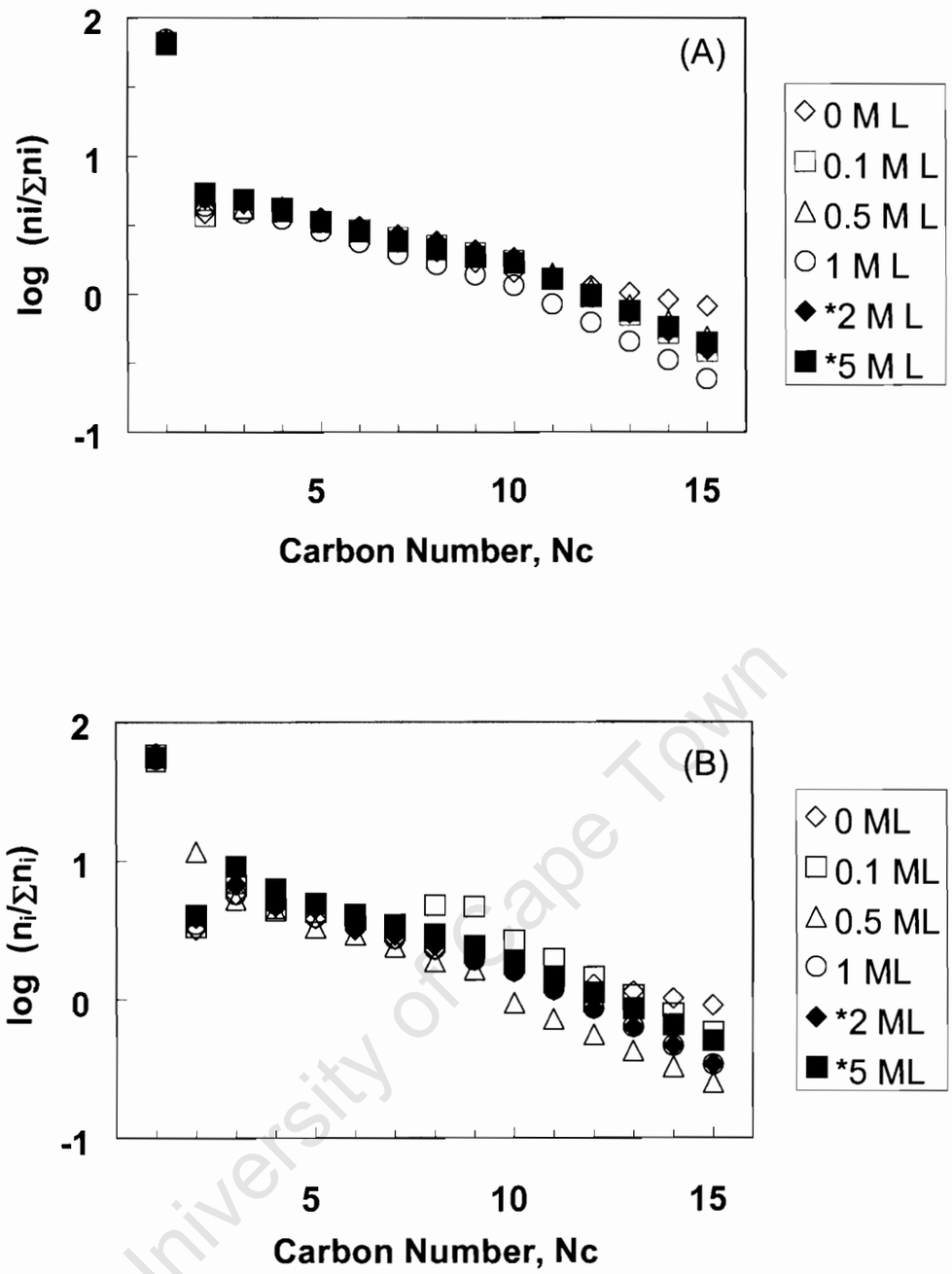

Figure 3-25: Anderson-Schultz-Flory product distribution for the catalysts with varying vanadia content at different time on stream, (**A**) 24 hours (**B**) 30 hours. (m_{cat}~ 0.5g, T=220^{O}C, P=20 bar (abs), H_2:CO=2:1, WHSV=1.125 g_{CO}/g_{cat}.hr)

3.4.4 C_5+ Selectivity

The selectivity of the catalysts towards the formation of linear products greater than or equal to C_5 was evaluated combining TCD and FID data. The peak areas (C_1 to C_4) from the FID trace were used in conjunction with the methane selectivity calculated from TCD data to calculate the selectivities for C_1-C_4 and hence C_{5+} selectivity. The results obtained are shown in Table 3-14 .

Table 3-14: C_{5+} selectivity in the Fischer-Tropsch synthesis after 24 and 30 hours time on stream for the catalysts with varying vanadia content. (m_{cat}~ 0.5g, T=220^{O}C, P=20 bar (abs), H_2:CO=2:1, WHSV=1.125 g_{CO}/g_{cat}.hr)

Catalyst	24 Hours		30 Hours	
	X_{CO}	S_{C5+}, wt-%	X_{CO}	S_{C5+}, wt-%
0 ML	62	85.3	62.3	80.3
0.1 ML	67	89.6	65	87.2
0.5 ML	61	86.4	60	83.4
1 ML	44	87.9	42	79.1
***2 ML**	40	83.9	36	82.8
***5 ML**	51	88	50	84.4

Figure 3-26 shows a plot of C_{5+} selectivity against theoretical (V_2O_5/Al_2O_3) mass ratios for each of the six catalysts. The results from Table 3-14 and Figure 3-26 reflect slighly higher C_{5+} selectivities for the vanadia promoted catalysts compared to the base case catalyst. C_{5+} selectivities for the 24 hours on stream data vary between 85-90 wt-% whilst it varies between 80 to 85 wt-% for the 30 hours time on stream results. C_{5+} selectivity in vanadia promoted catalysts seem to fall within the scatter of the data. This is especially pronounced in the 30 hours time on strean data. The low chain growth probabilities for the 30 hours time on stream results might indicate that the catalysts are deactivating over time during the course of the reaction. Overall, there is no trend in the C_{5+} selectivity that can be attributed to the variation of vanadia content in the catalysts.

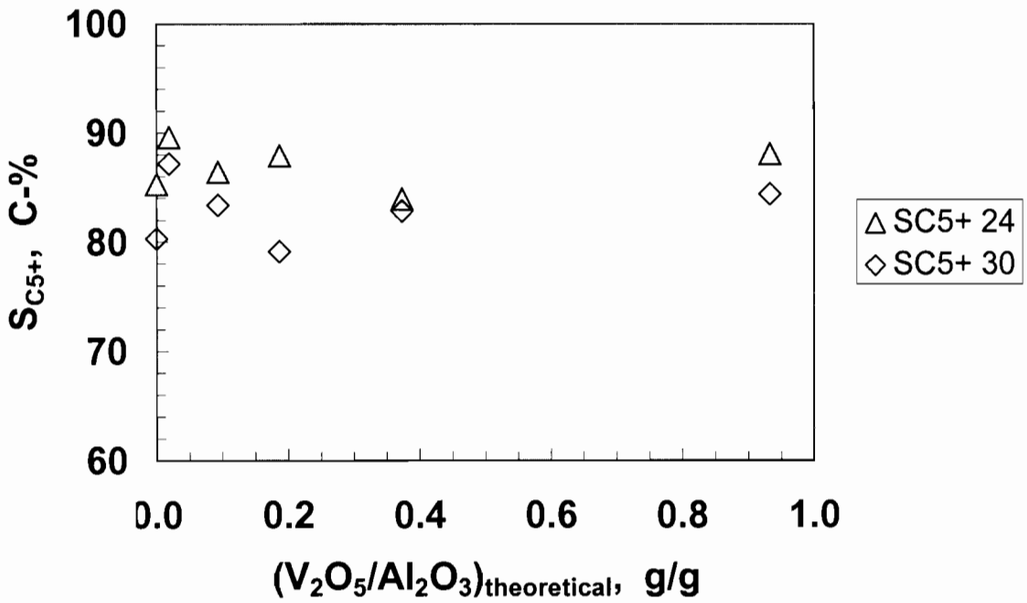

Figure 3-26: Effect of vanadia content in catalysts the C_{5+} selectivity in Fischer-Tropsch synthesis. (m_{cat}~ 0.5g, T=220^{O}C, P=20 bar (abs), H_2:CO=2:1, WHSV=1.125 g_{CO}/g_{cat}.hr).

3.4.5 Linear olefin content

n-Olefin content was calculated based on the total linear hydrocarbon product per carbon number for each catalyst. The results for this analysis are shown in Figure 3-27, which shows the variation of olefin content with an increase in carbon number.

Figure 3-27 shows that the a low n-olefin content for C_2 linear hydrocarbons followed by a high content in C_3–fraction for all the catalysts. The lower content at C_2 is indicative of the higher reactivity of ethene in secondary reactions, e.g. secondary hydrogenation. Schulz and Claeys (a) (1999) reported the reactivity ethene to be 10-40 times higher than the reactivity of other olefins. Beyond C_3 , the n-olefin content decreases gradually with carbon number to smaller fraction at C_{11} and beyond. The decrease in n-olefin with increasing carbon number is attributed to secondary reactions of primary formed 1-olefins. 1-Olefins are also believed to act as chain initiators,

that in conjunction with their hydrogenation of olefins leads to the decrease is olefin content (Schulz and Claeys (a), 1999) .

For both 24 and 30 hours time on stream results, the n-olefin for the different catalyst varied parallel to each other with an increase in carbon number. V_2O_5 content in the catalysts affects the olefinicity of the Fischer-Tropsch product. With increase in vanadia loading the n-olefin content increases with the exception *2-ML catalyst . This is observed clearly on the 30 hours time on stream n-olefin plots (see Figure 3-27 (B)) where all the vanadia promoted catalyst show high olefin content compared to the unpromoted catalyst except for the *2-ML catalyst which show rather low n-olefin contents. The 24 hours data is inconclusive because the order of increase n-olefin content is erratic and does not follow a pattern or trend which can be linked to the vanadia content in the catalyst. The C_3 fraction has been chosen to demontrated n-olefin content variation with vanadia content at both 24 and 30 hours time on stream. These results are reported in Table 3-15.

Variation between 24 and 30 hours time on stream results indicates that steady state in as far as secondary reactions are concerned has not been reached. The 30 hours time on stream results show a clearer trend ; catalysts with high vanadia content show the highest n-olefin content. The observed increased n-olefin contents might also be due to the low steady state CO conversions. Low CO conversions results in relatively high n-olefin contents.

The n-olefin content results seem to suggest that vanadia promoted catalysts show decreased activity in secondary n-olefin reactions in the Fischer-Tropch reaction.

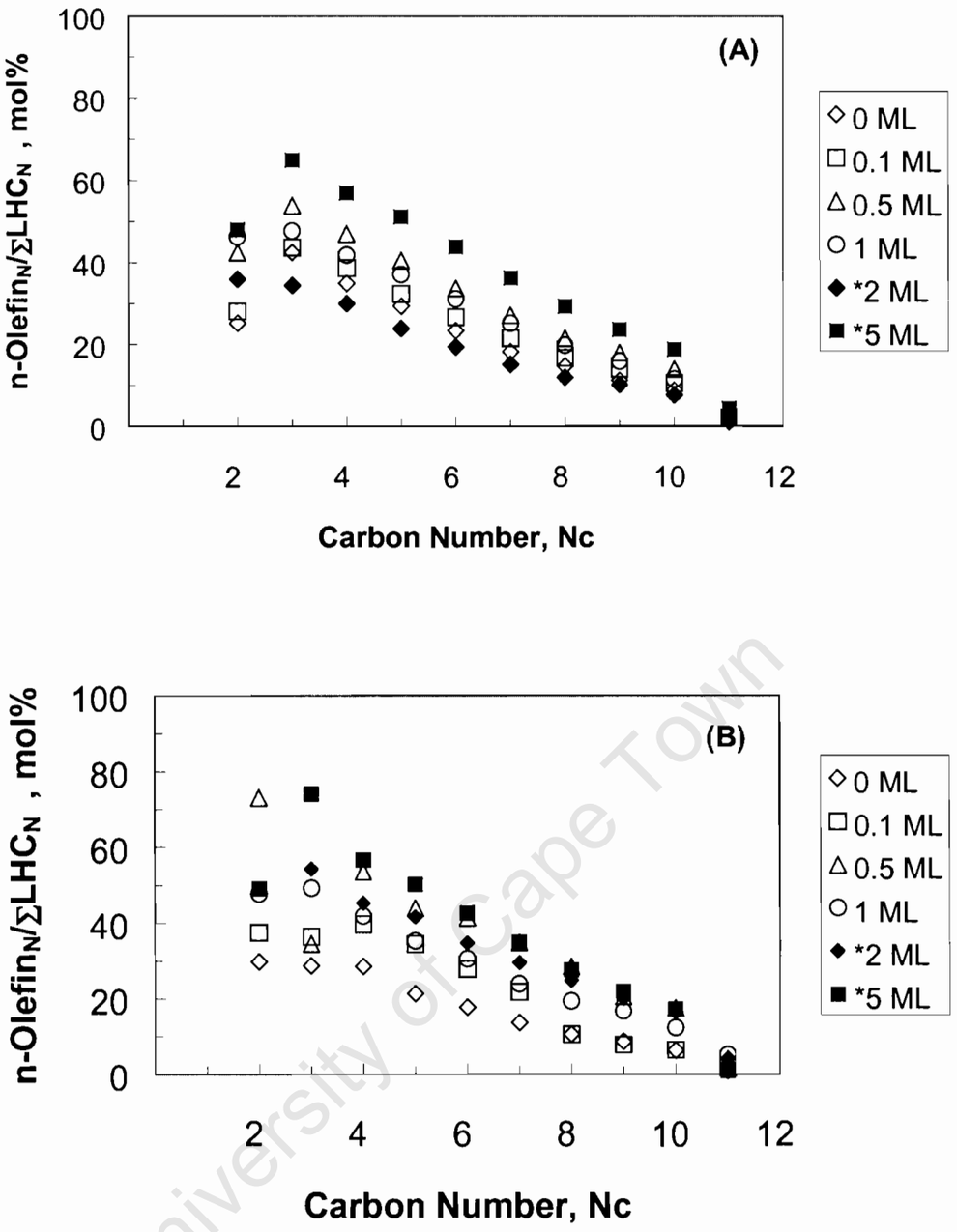

Figure 3-27: Variation in n-olefin in the fraction of linear hydro-carbons as a function of carbon number for the catalysts with varying vanadia content at different times on stream, (A) 24 hours (B) 30 hours. (m_{cat}~ 0.5g, T=220^{O}C, P=20 bar (abs), H_2:CO=2:1, WHSV=1.125 g_{CO}/g_{cat}.hr).

Table 3-15: C_3 linear hydrocarbon fraction n-olefin content after 24 and 30 hours time on stream for the catalysts with varying vanadia content.(m_{cat}~ 0.5g, T=220^{O}C, P=20 bar (abs), H_2:CO=2:1, WHSV=1.125 g_{CO}/g_{cat}.hr).

Catalyst	24 Hours		30 Hours	
	X_{CO}	n-olefin content, C_3 mol-%	X_{CO}	n-olefin content, C_3 mol-%
0 ML	62	42.5	62	28.7
0.1 ML	67	43.7	65	36.4
0.5 ML	61	53.9	60	44.0
1 ML	44	47.7	42	49.3
***2 ML**	40	34.5	36	54.3
***5 ML**	51	64.8	50	74.1

3.4.6 1-olefin content as a fraction of total olefins

1-Olefin content was calculated as the mol-% fraction of linear 1-olefin in the total linear olefin hydrocarbon product. Figure 3-28 shows the variation of 1-olefin selectivity with an increase in carbon number for the 24 and 30 hours time on stream product samples.

Figure 3-28 (A) shows no clear trends indicating the effect of vanadia content on the 1-olefin content per carbon number. The results are erratic and cannot be directly linked to the vanadia content on the catalysts. Olefinicity for the different catalysts varied in a parallel fashion from C_4 to C_{10}, with the 1-olefin content decreasing gradually with an increase in carbon number. The decrease in olefinicity with increasing carbon number reflects the depletion of 1-olefins via secondary reaction i.e. incorporation, chain initiation and hydrogenation. The 1-olefin content curves to not decrease to zero at high carbon numbers (minimum of 30 mol- % at C_{10}). This result show that a considerable amount of the linear n-olefins have internal double bonds arising from double bond-isomerisation of the primary 1-olefins.

Table 3-16: 1-Olefin content in the fraction of C_4 linear olefins after 24 and 30 hours time on stream for the catalysts with varying vanadia content. (m_{cat}~ 0.5g, T=220^{O}C, P=20 bar (abs), H_2:CO=2:1, WHSV=1.125 g_{CO}/g_{cat}.hr)

Catalyst	24 Hours		30 Hours	
	X_{CO}	1-olefin content, C_4 mol-%	X_{CO}	1-olefin content, C_4 mol-%
0 ML	62	83.9	62	71.8
0.1 ML	67	79.0	65	83.6
0.5 ML	61	82.8	60	84.8
1 ML	44	85.1	42	83.4
***2 ML**	40	74.8	36	72.4
***5 ML**	51	89.1	50	90

Table 3-16 shows the 1-olefin content in the C_4 fraction for the 24 and 30 hours analysis. The *2ML catalyst shows a rather low 1-olefin content compared to the other promoted catalyst, which is consistent with n-olefin content results and low CO conversion. The 1-olefin trends in the C_4 fraction indicated in Table 3-14 hold in the whole C_4 to C_{10} carbon number range.

The 30 hours time on stream results (see Table 3-16 and Figure 3-28 (B)) show that increasing vanadia content on the catalyst caused a high 1-olefin content. The observed trend suggests that vanadia promotion suppress secondary double bond isomerisation of 1-olefin into internal olefins.

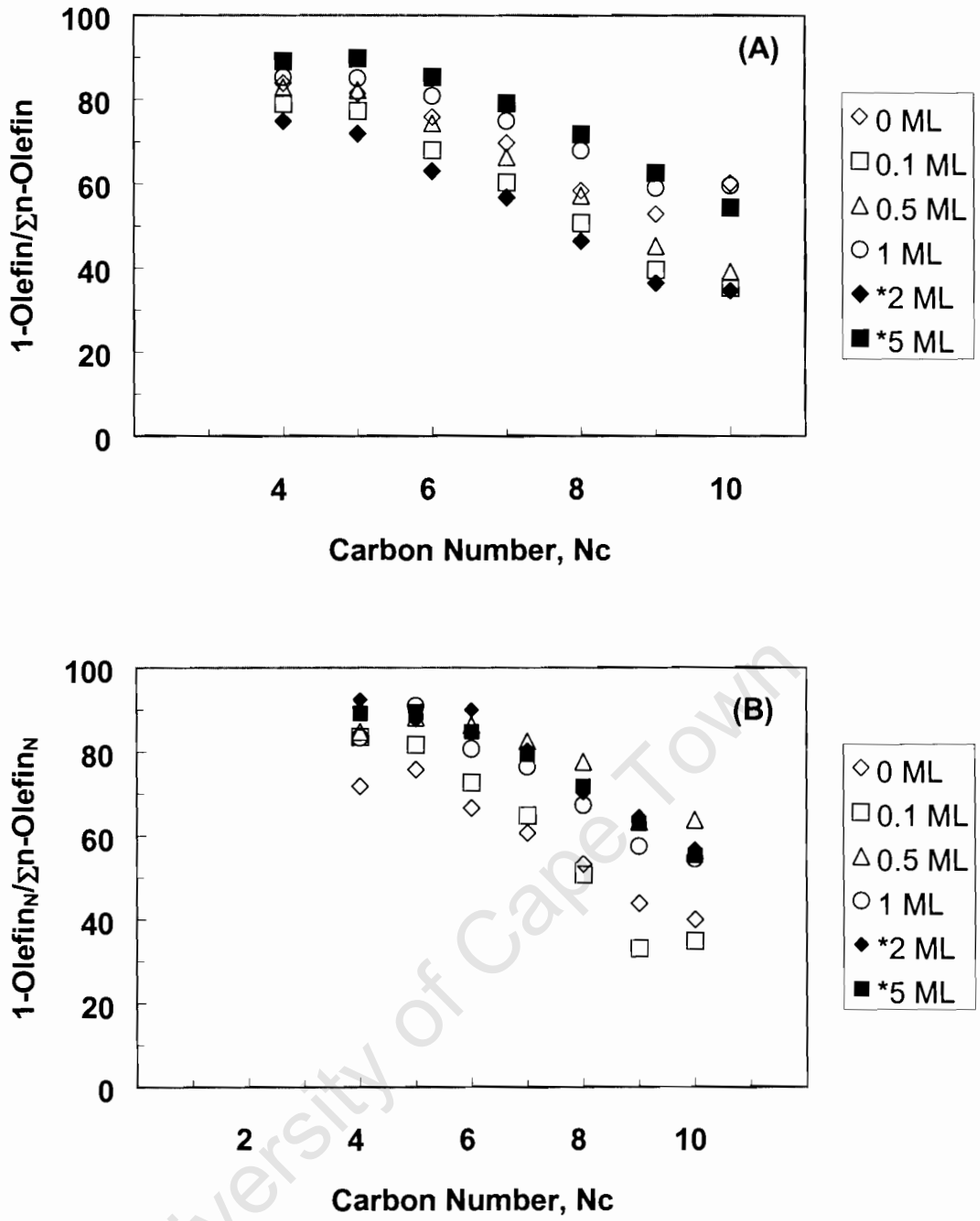

Figure 3-28: Variation in 1-olefin content in the fraction of linear olefins with increase in carbon number for the catalysts with varying vanadia content at different times on stream, (**A**) 24 hours (**B**) 30 hours. (m_{cat}~ 0.5g, T=220^{O}C, P=20 bar (abs), H_2:CO=2:1, WHSV=1.125 g_{CO}/g_{cat}.hr).

3.4.7 Branching

The effect on vanadia promotion on product branching was investigated by analysis of the content of branched products in C_5 hydrocarbon fraction. The molar content of iso-C_5 from each catalyst synthesis results was plotted against vanadia content in the catalyst. Figure 3-29 illustrates the results obtained upon analysis of 24 and 30 hours time on stream samples.

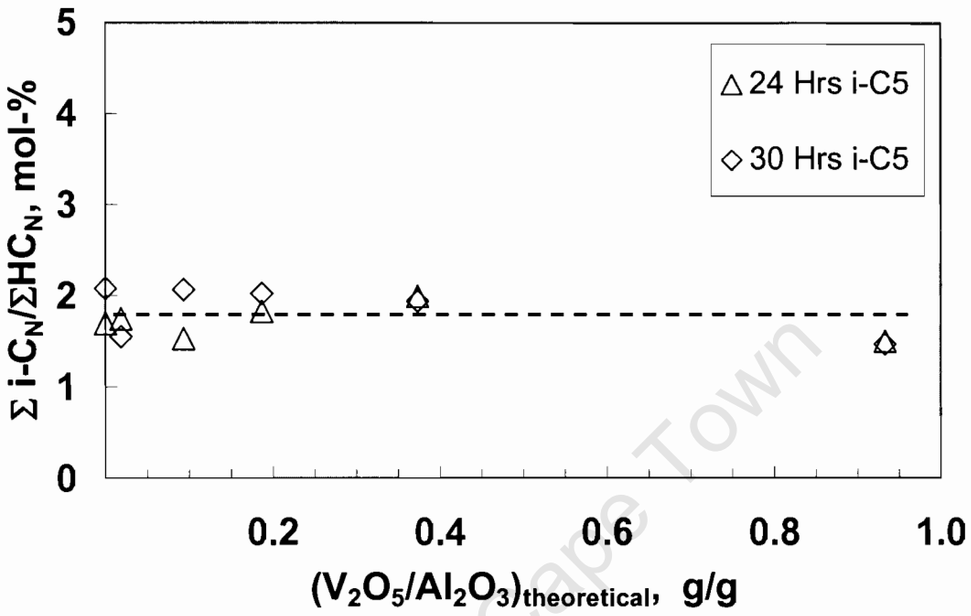

Figure 3-29: Effect of vanadia content in catalysts on content of iso-C_5 in the C_5 hydrocarbon fraction. (m_{cat}~ 0.5g, T=220^{O}C, P=20 bar (abs), H_2:CO=2:1, WHSV=1.125 g_{CO}/g_{cat}.hr).

The results in Figure 3-29 indicate that chain branching is not affected by vanadia content in the catalyst during Fischer-Tropsch synthesis. The iso-C_5 content remains around 2 mol-% irrespective of the increase in vanadia content in the catalysts. The results suggest that acidic character imparted by V_2O_5 on the catalyst systems is not dominant, probably the more basic V_2O_3 phase becomes dominant during the reaction hence secondary skeletal isomerisation reactions are suppressed in the Fischer-Tropsch synthesis.

3.4.8 Oxygenate content

Vanadia promotion effects on the oxygenate content of the Fischer-Tropsch product was investigated by evaluating the oxygenate content in the C_5 and C_9 product fractions. The C_5 and C_9 oxygenate content were then plotted against V_2O_5 content in the catalyst for 24 and 30 hours time on stream data, as illustrated in Figure 3-30.

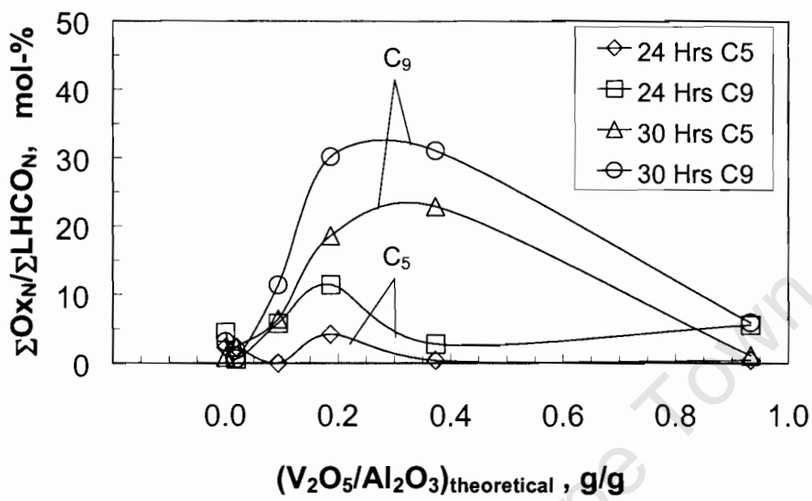

Figure 3-30: Effect of vanadia content in catalysts on the formation of oxygenate product in the C_5 and C_9 fractions. (m_{cat}~ 0.5g, T=220^{O}C, P=20 bar (abs), H_2:CO=2:1, WHSV=1.125 g_{CO}/g_{cat}.hr).

The results clearly shows that vanadia addition on the catalysts affects the oxygenate content per carbon number of the Fischer-Tropsch product. The oxygenate content from catalysts with low vanadia loadings (0 and 1.1 ML catalysts) is very low about 2 mol-%. The oxygenate content then increases with increasing vanadia content in the catalysts. On the 24-hour analysis the C_5 and C_9 oxygenate fraction increases and reaches a maximum of 5 and 10 mol-% at respectively for the 1-ML catalyst. Beyond 1-monolayer V_2O_5 content, the molar content of oxygenates then drops to zero for the catalysts with higher vanadia loadings.

The effect of vanadia promotion on the formation of oxygenates is very pronounced in the catalyst in the higher hydrocarbon product fractions. The oxygenate content of the C_9 fraction has been chosen to demonstrate this. The 24 and 30 hours results indicates an increase in oxygenate content from around 10% for both C_5 and C_9 fraction to a maximum of about 23 and 30 mol-% respectively for the 1 ML and *2 ML catalysts. The oxygenate content from the *5 ML catalysts was low and similar to the contents obtained from the catalysts with low vanadia contents. These observations suggests that the vanadia content in the catalysts may improve the oxygenate formation in Fischer-Tropsch synthesis. The oxygenate formation is enhanced especially in high hydrocarbon numbers.

Chapter 4
Discussion

4 DISCUSSION

V_2O_5 is a known strong oxidation catalyst (Weckhuysen and Keller, 2003). A majority of the documented studies on vanadia (V_2O_5) as a catalysts has focussed mainly supporting V_2O_5 on metal oxide supports to improve activity and selectivity of redox reactions, oxidative dehydrogenation reactions, and deNO_x reactions (Eon et al., 1994; Miki et al., 1995; Amiridis et al., 1996; Lemonidou, 2000). Little has been published on promotion of Fischer-Tropsch catalysts by vanadium. Cobalt based Fischer-Tropsch catalyst promotion with manganese and/or vanadium has recently been patented by Shell where it is claimed that such promotion improves catalyst activity and C_{5+} selectivity in Fischer-Tropsch synthesis (Geerlings et al., 1997). An iron-based Fischer-Tropsch catalyst promoted with V_2O_5 and supported on silica [Fe-Cu-SiO_2-V_2O_5] was by mentioned Dry (1981). This catalyst was reported to show improved activity and wax selectivity in Fischer-Tropsch synthesis.

In this study, a systematic investigation of the effect of V_2O_5 promotion on a γ-Al_2O_3 supported cobalt-based Fischer-Tropsch catalyst was carried out. The effect of vanadia promotion was evaluated by relating the physical properties of the catalysts to their catalytic performance under typical industrial Fischer-Tropsch synthesis conditions. The physico-chemical properties of the vanadia promoted catalysts were characterised using Atomic Adsorption Spectroscopy (AAS), zeta-potential measurements, and BET measurements, X-ray Diffraction (XRD), Temperature Programmed Reduction (TPR), Transmission Electron Microscopy (TEM), and CO chemisorption. Table 4-1 summarises the physical and chemical properties of the catalysts obtained from the different characterisation procedures.

Table 4-1: Summery of the physico-chemical properties of supports/catalysts

Catalyst	**0 ML**	**0.1 ML**	**0.5 ML**	**1 ML**	***2 ML**	***5 ML**
PZC*	8.2	7.8	7.1	6.3	6	3.9
BET surface area ($m^2/g_{cat.}$)	153.8	155.6	150.5	152.0	150.6	151.5
BET average pore size (Å)	109.3	103.3	102.8	91.3	99.1	109.2
Cobalt content (wt-%)[a]	9.2	8.9	8.7	8.8	8.2	9.5
Dispersion (%)[b]	9.7	7.2	-	-	-	-
Active area ($m^2/g_{cat.}$)[b]	6.5	4.8	-	-	-	-
Co_3O_4 crystallite size (nm)[b]	10.3	13.9	-	-	-	-
Co_4O_4 crystallite size (nm)[c]	11.0	10.1	9.8	12.6	13.2	13.1
Co_3O_4 crystallite size (nm)[d]	11.2	10.9	10.5	9.8	10.2	10.4

*Estimated from zeta-potential plots for modified supports

[a] Co content measured by AAS

[b] Parameters estimated from CO chemisorption.

[c] Co_2O_3 crystallite size estimated from XRD

[d] Co_2O_3 crystallite size estimated from TEM

4.1 Characterisation of vanadia-modified supports and catalysts

Zeta potential measurements indicated the pH at the point of zero charge (PZC). At pH values below the PZC, an oxide support bears a net positive surface charge while the reverse is true for pH values above the PZC (Che et al., 1998). The interaction between of impregnated Co and support to some degree depends on the net surface charge of the support. If Co impregnation on support takes place at a pH above the PZC, the support, which bears a negative net surface charge, is expected to exhibit strong electrostatic attraction on the positively charged Co ions from its precursor. In a nutshell the PZC indicates whether the impregnated cobalt will be attracted or repelled by the support at any given impregnation pH.

The pH at PZC shifts from a high pH towards a lower pH with increased vanadia loading on the supports. Zeta potential measurements for the impregnating cobalt hydroxide colloid was measured in the pH range 7.3-7.85 and was found to be positive (~+30 mV). The pH values at PZC for the V_2O_5-modified supports ranged from 4.4 to ~8 (see Figure 3-1). The observed shift in PZC of the modified supports might influence the chemical properties of the final catalysts in as far as interaction between cobalt hydroxide and the surface support is concerned.

AAS results show that both supports and catalysts contained low vanadia contents than theoretical expectations beyond 1-monolayer vanadia loadings. The supports which were modified so as to contain 2 and 5 monolayer vanadia content, show PZC values below the pH (pH=6) at which ion exchange was carried out. That being the case it is to be expected that adsorption of the meta-vanadate ion (VO^{3-}) onto the supports would be enhanced in this pH range, because supports bear a positive net surface charge. The poor vanadia loadings on these two supports suggest that the positive net surface charge had little effect in attracting the VO^{3-} on to the already vanadia coated support surface. Eon et al. (1994) reported that they managed to load about a one-third of an equivalent V_2O_5 monolayer on γ–Al_2O_3 at pH=7 and about two-thirds at pH=2.5 when they percolated a NH_4VO_3 solution through a bed of γ-Al_2O_3. The amount of vanadia loading on γ-Al_2O_3 is strongly dependent on the pH of impregnating solution. There exists an ion-exchange equilibrium at a certain pH beyond which when a certain concentration of ions has been exchange, there would be no more uptake of exchanged ions beyond this point. It seems that this equilibrium is the catalysts under study was reached at 1-monolayer vanadia loading on γ-Al_2O_3.

Co impregnation on all the supports was effected at pH=7.8. The zeta potential profiles for pure γ-Al_2O_3 to 1-ML supports show PZC values above the Co impregnation pH. Interaction between the surface and Co^{2+} ions would be enhanced since the supports bear a net negative charge in this pH range.

The remainder of the vanadia promoted supports show PZC values below the Co impregnation pH (i.e. the net surface charge on the supports is positive). Under these circumstances interaction between support and Co^{2+} is expected to be minimal owing to the increase electrostatic repulsion arising from the predicted net positive surface charge at pH values above the PZC.

AAS results showed a constant Co content (~10 wt-%) in all six catalysts. This does not however imply that PZC does not affect the nature of the final catalyst. There are other factors affecting cobalt loading on supports other than the PZC. The nature of the support i.e. crystallinity and surface defects and surface hydroxyl groups which provides anchoring points for the active metal (Che et al., 1997). It would have been interesting to look at how shift in PZC affects Co dispersion and active metal surface area in the catalysts with varying vanadia loading. Because of the complex nature of CO adsorption shown by Co-V-Al system, only analysis for two catalysts were analysed, which could not shed light on how the vanadia content and hence the subsequent shift in PZC affected Co dispersion on the catalysts.

XRD profiles for the catalysts (see Figure 3-21) showed both Co_3O_4 and γ-Al_2O_3 diffraction peaks, which appeared, at almost similar diffraction angles. There were no fundamental differences between the diffraction patterns of the catalysts indicating that they have the same degree of crystallinity. Noted on the diffraction patterns of the catalysts was the absence of the highly crystalline V_2O_5 diffraction pattern, which might be indicative that the vanadia layer on the catalysts was either X-ray amorphous or existed in another V_xO_y phase. Catalysts with high vanadia content were expected to show XRD crystalline profiles like the one exhibited by pure V_2O_5. The absence of the crystalline V_2O_5 phase even from the catalysts, which were expected to contain high vanadia content, is consistent with AAS results, which reflects low vanadia loadings than theoretically predicted at high vanadia loadings. The absence of V_2O_5 peaks on the XRD patterns contradicts the observations made on TEM images. If the needles observed on TEM images for the

vanadia promoted catalysts reflect dissolved VO_x phases, then it have been shown on the XRD patterns, unless if these were X-ray amorphous. From the TEM images is hard to see the vanadia phase on both supports and catalysts.

The zeta potential profiles for the *2 and *5-ML supports were also expected to mimic the pure V_2O_5 profile if complete coverage on the γ-Al_2O_3 was achieved. This was not observed probably because vanadia loading beyond 1-monolayer coverage was not successful either because of ion exchange equilibrium limitations during the multi-step ion exchange procedure employed when trying to load more vanadia on the already modified supports.

The average cobalt crystallite size on the catalysts was estimated from TEM data, XRD line broadening analysis and CO chemisorption analysis. The estimated Co_3O_4 average crystallite ranged from 10-15 nm with no systematic order, which could be linked to the vanadia loading on the catalysts. The surprising result was the estimated crystallite size from CO chemisorption data. The average crystallite size estimated using this method was expected to be slightly smaller than those obtained from TEM and XRD analysis because chemisorption experiments were performed on reduced cobalt. Reduced cobalt crystallites are supposed to be at least 20% smaller than cobalt oxide crystallites.

CO chemisorption analysis was very complex. The modified supports and catalysts adsorbed appreciable amounts of CO and could not be modelled by the basic Langmuir isotherm adsorption model. The dual site Langmuir adsorption model fitted the data well for the unpromoted catalyst with low and vanadia content (0-ML and 0.1-ML catalysts). The fact that the dual site Langmuir adsorption model fit the data well indicates that there are at least two CO adsorption sites in this catalyst system. The modified supports showed more CO uptake compared to the corresponding catalysts; making the task of establishing CO uptake attributed only to Co adsorption very

difficult, hence crystal size analysis was only carried out for the base case and 0.1-ML catalysts.

The BET surface area for the catalysts was not affected by vanadia loading. The initially pore volume decreased with increasing vanadia loading and subsequently increased beyond 1-monolayer vanadia coverage. The decrease is attributed to pore narrowing caused by the successive accumulation of vanadia on the support pores. The observed slight increase in pore volume of the catalysts with more than 1-monolayer vanadia coverage might have been caused by some pores being blocked by the impregnated cobalt phase.

The TPR profiles vanadia promoted catalysts show a third low temperature reduction peak appears after the initial two Co_3O_4 low temperature reduction peaks. It appears that the presence of cobalt in the catalysts enhances the reduction of vanadia phase. Both catalysts and vanadia promoted supports show reducible phases. The peak intensity of reduction peaks of the modified supports remains more or less the same after 1-monolayer vanadia coverage indicating that the catalysts contained same amount of reducible vanadia species; further confirming that beyond that more than 1 monolayer vanadia loading was not successful. The quantitative H_2/Co ratios for the vanadia promoted catalysts are higher than the theoretically predicted value of 1.33. This seems to suggest that there is a vanadia phase reduction besides Co_3O_4, which contributes towards the total H_2 consumption during reduction in the catalyst system under study.

In general, vanadia loading on the catalysts does not influence the physical properties on the catalysts. The only significant influence of vanadia loading is observed on the support surface charge variation as a result of increasing vanadia content on the supports, which might have profound effects on product selectivity and overall catalyst performance during Fischer-Tropsch synthesis.

4.2 Effect of vanadia loading on Fischer-Tropsch Synthesis.

The vanadia unpromoted catalyst was used as a basis of comparing the effect of vanadia promotion of Co/Al_2O_3 Fischer-Tropsch catalysts. In preparing the catalysts great effort was made to archive the same amount of cobalt in all the catalysts. During Fischer-Tropsch synthesis, the same amount of each catalyst was used; all catalysts were pre-treated and run under similar reaction conditions.

4.3 Influence of vanadia promotion on catalyst activity

The base case catalysts Co/Al_2O_3 showed an high initial activity while the vanadia promoted catalysts showed a decline in initial activity with increasing vanadia loading. The unpromoted catalysts also show high deactivation rates as towards steady state, which was obtained after 24 hrs for all the catalysts. The deactivation rates in the initial stages of the Fischer-Tropsch synthesis for the vanadia promoted catalysts are relatively lower than the base case catalysts. One possible reason why this might occur is that the vanadia in the promoted catalysts might be spreading and covering some of the Co active sites the Fischer-Tropsch reaction, thus lowering the CO conversion rates.

4.4 Influence of vanadia promotion on chain growth probability

Anderson-Schulz-Flory (ASF) plots plotted from hydrocarbon analysis data for all catalysts overlapped indicating that vanadia content in the catalysts did not affect the chain growth properties the cobalt catalysts. Chain growth probabilities estimated from the slopes of the ASF plots (TOS=24 hours) between C_3 and C_9 varied between 0.85-0.87 with no trend attributable to vanadia content and physico-chemical properties of the catalysts.

4.5 Influence of vanadia promotion on C_{5+} selectivity.

Figure 4-1 shows a plot of the C_{5+} selectivity against vanadia content in the six tested catalysts. Vanadia content in the catalysts does not seem to affect the C_{5+} selectivity, which is in line with the observed negligible changes on the chain growth probabilities, obtained from each of the synthesis runs. Slightly higher C_{5+} selectivity values were observed for vanadia promoted catalysts compared to base case catalysts. Also vanadia promoted catalysts showed decreased methane selectivities (see Figure 3-23), which is consistent with the increased C_{5+} selectivities for these catalysts at the same steady state conversions. However, these observations cannot be attributed to structural changes in the catalyst.

The decrease in pore diameter as a result of vanadia loading on catalyst appears not to have a significant effect on the secondary readsorption reactions of 1-olefins as predicted by the transport model proposed by Iglesia et al. (1995). According to the model by Iglesia (1995) pore narrowing would result in a increase in the structural parameter, χ, resulting in longer intrapellet residence times of 1-olefins in the pores, thus increasing the probability of 1-olefinf readsorption and a subsequent increase in C_{5+} selectivity. An increase in C_{5+} selectivity can be interpreted as an increase in the extent of readsorption of the small reactive products into the chain growth mechanism of the Fischer-Tropsch synthesis (van Steen et al., 1996; Schulz and Claeys (a), 1999).

The selectivity towards C_{5+} products in the Fischer Tropsch synthesis could not be correlated with the structural parameter which might be attributed to the small changes in structural parameter.

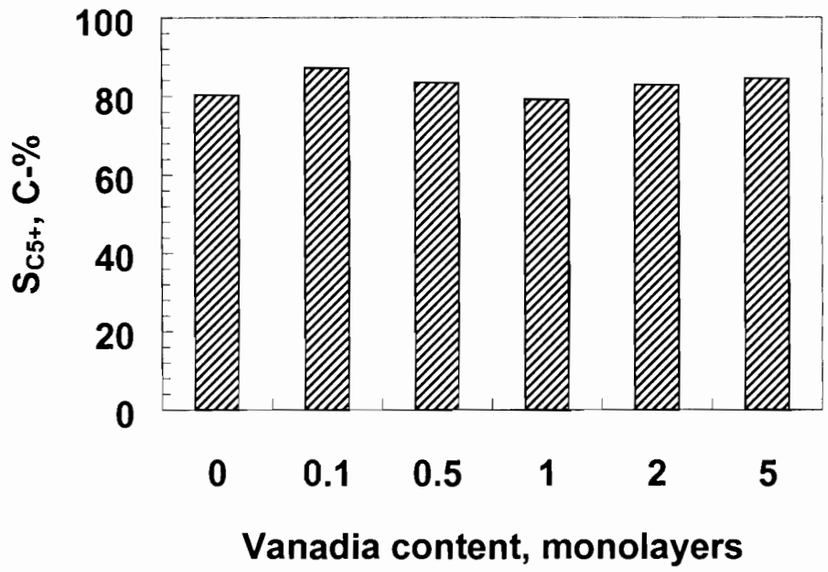

Figure 4-1 Effect of vanadia content in catalysts the C_{5+} selectivity in Fischer-Tropsch linear hydrocarbon product TOS=30 hrs. (m_{cat}~ 0.5g, T=220^{O}C, P=20 bar (abs), H_2:CO=2:1, WHSV=1.125 g_{CO}/g_{cat}.hr):

4.6 Influence of vanadia promotion on olefin content

Olefin content in the Fischer-Tropsch product can yield information about the extent to which primary formed olefins are hydrogenated. When intra pellet diffusional limitations of the olefins is large, i.e. high χ values, the olefin content is expected to decrease owing to enhanced secondary readsorption owing to increased intrapellet residence times. In this work the olefin content was observed to increase with vanadia content in the catalysts even though the catalysts structural parameters remained more or less constant.

The observed increase in olefin content in the vanadia promoted catalysts suggests that the vanadia in the catalysts suppress secondary hydrogenation reactions in Fischer-Tropsch synthesis. The nature of inhibition of secondary hydrogenation cannot be attributed to structural changes in the catalysts, but other factors in the Co-V-Al catalyst system. One possible explanation of the observed increase in olefin content in the vanadia promoted catalysts may be that the vanadia spreads and covers some the Co active sites. If this occurs

the number of site available for olefin readsorption will be less hence low secondary hydrogenation reactions. This would also result in loss of some of the overall activity in the Fischer-Tropsch synthesis.

4.7 Influence of vanadia on Double bond Isomerisation

1-Olefin content is an indicator of the degree of double bond isomerisation in the Fischer-Tropsch product. The degree of double bond isomerisation depends, among other factors, temperature and on the acidity of the catalyst. Acidic catalyst have been reported to enhance double bond isomerisation (Gates, 1992). The 1-olefin content in this work was observed to be high in the vanadia promoted catalysts (see Figure 3-28) implying that vanadia content in the catalyst suppresses double bond isomerisation of 1-olefins into internal olefins. The basic V_2O_3 phase was predicted as the thermodynamically stable oxide phase than the acidic V_2O_5 phase under Fischer-Tropsch synthesis conditions. It therefore follows that the observed low double bond isomerisation was a result of the dominant presence of the basic V_2O_3 phase, which suppressed isomerisation.

The observed increase in 1-olefin content is also directly linked to the observed increase in n-olefin content with increasing vanadia content in the catalysts. One expects that increase in n-olefin content should result in a corresponding increase of 1-olefin content in n-olefins. This is because the increase in n-olefin content in linear hydrocarbon products is indicative of less involvement of olefins in secondary reactions in the Fischer-Tropsch synthesis.

4.8 Influence of vanadia on Skeletal Isomerisation

The degree of branching in the Fischer-Tropsch synthesis was unaffected by vanadia content in the catalysts. Because of increasing acidic character on the catalyst imparted by vanadia promotion, it was expected that more branched products would be obtained from the vanadia promoted catalysts in the Fischer-Tropsch synthesis because acidic catalysts enhance the degree

of skeletal isomerisation. This was not the case in this work, because the content of branched hydrocarbons analysed in the C_5 fraction of the Fischer-Tropsch synthesis product (see Figure 3-24) remained low (~2 mol-%) irrespective of vanadia content in the catalysts. This is a further indicator of the presence of basic V_2O_3 in the catalysts during Fischer-Tropsch synthesis.

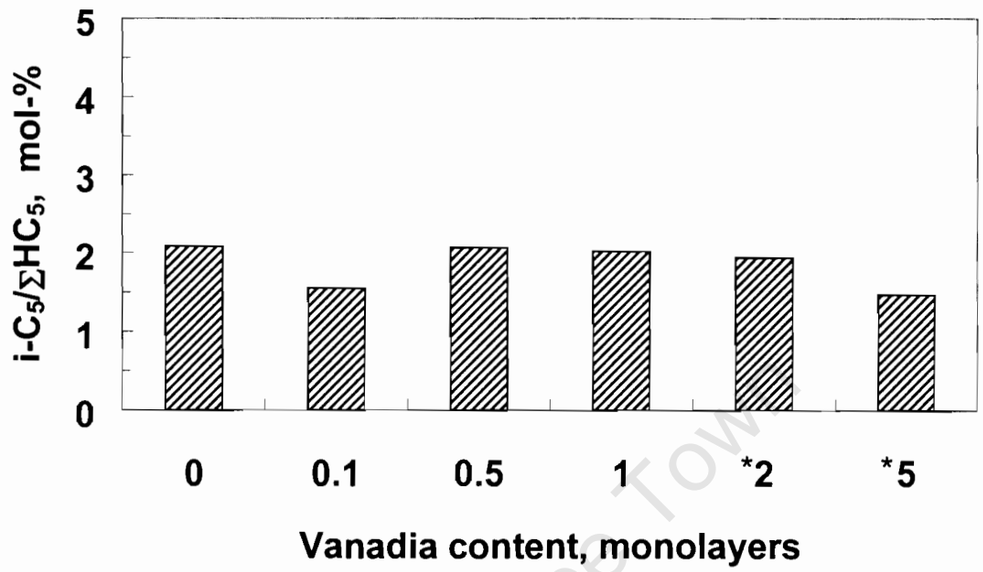

Figure 4-2: Effect of vanadia content in catalysts on chain branching in the C_5 hydrocarbon fraction. (m_{cat}~ 0.5g, T=220^{O}C, P=20 bar (abs), H_2:CO=2:1, WHSV=1.125 g_{CO}/g_{cat}.hr), TOS=30 hrs.

4.9 Influence of vanadia promotion on Oxygenate products

Vanadia promoted catalysts showed surprisingly high oxygenate content in the Fischer-Tropsch product. The oxygenate content (predominantly aldehydes and alcohols) increased with increasing vanadia loading from almost nothing for the base case catalyst to about 30 mol-% for the vanadia promoted catalysts in the C_9 fraction (see Figure 3-30). The observed increase in the oxygenate content with increasing vanadia content in the catalysts was also evident in the other carbon number fractions in the Fischer-Tropsch product.

The mechanistic route for oxygenate formation in Fischer-Tropsch synthesis is still a debatable subject (Schulz et al. (c), 1999). Its generally believed oxygenates are formed via CO insertion into growing surface alkyl species, through secondary olefin hydroformylation and the reaction of hydroxyl with alkylene species (Schulz et al. (c), 1999).

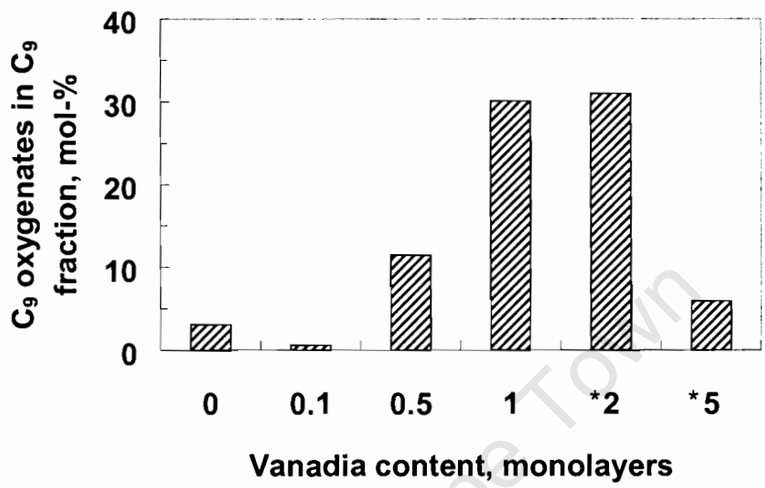

Figure 4-3: Effect of vanadia content in catalysts on the oxygenate content in C_9 fraction. (m_{cat}~ 0.5g, T=220^{O}C, P=20 bar (abs), H_2:CO=2:1, WHSV=1.125 g_{CO}/g_{cat}.hr), TOS=30hrs.

It appears that the inherent oxygenate formation in the Fischer-Tropsch synthesis is enhanced by the presence of vanadia in the catalysts. Oxidation of aromatic and aliphatic hydrocarbon catalysed by vanadia has been reported where oxidation of aliphatic hydrocarbon produces a large number of oxidation products (Mars and van Krevelen, 1954). In the Mars van Krevelen mechanism, V_2O_5 provides oxygen atoms for oxidising the hydrocarbon into oxygenate product and is reduced to a lower oxidation state. The reduced vanadium oxide is then re-oxidised by oxygen from gaseous phase oxygen.

Haber (1996) outlined possible surface reaction routes which hydrocarbons would undertake at an oxide surface. The hydrocarbon intermediate and the

resultant products depend mainly on the basic properties of the oxide catalytic surface. According to Haber (1996), if the oxide catalyst contains OH groups Bronstead acidic OH groups, their protons may form weak hydrogen bonds with the π-bond of the olefins. When the acid properties of the surface OH groups are strong enough, proton transfer from the surface to the olefin may take place resulting in the formation of a carbocation. This may start network of reactions proceeding by the carbocation mechanism, e.g. isomerisation, transalkylation, cracking, etc.

The π-bond of the olefin may also react with the transition metal if transition displays Lewis acid properties to form a surface π-complex. When the basicity of the surface oxide ions (O^{2-}) is strong enough, a nucleophilic attack on C-H bonds in the α position might occur; resulting in the abstraction of hydrogen. This leads to the formation of a surface OH group and an allylic species bonded to the transition metal either side-on as the so called π-allyl, or end-on as the α-allyl (Haber, 1996). The π-allyl and α-allyl species are in equilibrium at the surface. The π-allyl is an intermediate for the formation of dienes while α-allyl undergoes nucleophilic oxidation by another surface oxide to form in an aldehyde in case of an attack on primary carbon atom of the hydrocarbon molecule, or a ketone in case of a secondary one (Harber, 1996; Oyama 1996).

In this work it is difficult to envisage oxygenate formation via the Mars van Krevelen mechanism in the highly reducing medium of the Fischer-Tropsch synthesis, where gaseous oxygen is not available. Furthermore, basic V_2O_3 is the thermodynamically predicted stable phase under Fischer-Tropsch synthesis conditions, in conjunction with the evident absence of V_2O_5 phase in the catalysts as shown by TPR and XRD results completely oppose the notion that the oxygenates are formed via the Mars van Krevelen mechanism.

One might speculate that if the high content of oxygenates are formed via this mechanistic route, part of the surface oxygen species from the dissociative

CO chemisorption is used in re-oxidising the reduced vanadium oxide sites instead of total hydrogenation to water. This would be possible if the surface Co sites are in close proximity with the V_xO_y oxidising sites to facilitate the re-oxidation of the reduced sites by oxygen transfer from CoO to the reduced V_xO_y sites after the oxygenate is formed. If such a transfer is possible, the result would be the formation of metallic Co and a regenerated oxidising site.

Chapter 5
Conclusions

5 Conclusions

Modification of γ-Al_2O_3 beyond 1-monolayer vanadia loading appeared not successful by the ion exchange at the given conditions. This might be caused by ion exchange equilibrium limitations. Generally the physical properties e.g., surface area, pore volume, and average Co_3O_4 crystallite size of the modified supports and catalysts were unperturbed to appreciable extents by vanadia promotion. The chemical properties such as phases present in the support/catalyst systems and the reduction behaviour of the catalysts were affected by vanadia content. Vanadia in the catalyst had some influence on the catalyst performance in the Fischer-Tropsch synthesis. In brief, the overall effect of vanadia content in the Fischer-Tropsch synthesis can be summarised as follows:

- Vanadia promoted catalysts suppresses methane production in the Fischer-Tropsch synthesis.
- Vanadia promoted catalysts showed lower initial catalyst activity, but less deactivation during the initial phase in the Fischer-Tropsch synthesis.
- There was no clear effect of vanadia promotion on chain growth and selectivity towards C_{5+} hydrocarbon products.
- Vanadia promoted catalysts products with high olefin content probably because vanadia spread and covered some of the active sites; suppressing olefin secondary hydrogenation reactions.
- The observed high 1-olefin contents from vanadia promoted catalysts suggest that vanadia inhibits the extent of double bond isomerisation.
- The surprisingly high oxygenate contents obtained from vanadia promoted catalyst leads to the speculation that the extra oxygenates are formed via another mechanistic route other than the conventional mechanisms believed to occur in the Fischer-Tropsch synthesis.

The model proposed by Iglesia et al. (1995), for the prediction of C_{5+} and CH_4 selectivities was not useful in this work because the physical properties of the catalysts did not change with vanadia content, hence the structural parameter χ was not affected. The observed selectivity changes observed in this work can not be attributed to structural parameter χ.

Chapter 6
References

6 References

Adesina, A.A.
Hydrocarbon synthesis via Fischer-Tropsch reaction: travails and triumphs. Applied Catalysis A: General **138** (1996) 345-367.

Amiridis, M.D., Wachs, I.E., Deo, G., Jehng, J., and Kim D.
Reactivity of V_2O_5 catalysts for the selective catalytic reduction of NO by NH_3: Influence of vanadia loading, H_2O and SO_2
Journal of Catalysis **161**(1996) 247-253.

Arnoldy, P., and Moulijn J.A.
Temperature-programmed reduction of CoO/Al_2O_3 catalysts
Journal of Catalysis **93** (1985) 38-54.

Baes, F. B. Jr., and Mesmer, R.E.
In *"The Hydrolysis of Cations"*
John Wiley and Sons (1976) New York, pg. 197-209.

Basini, L., and Piosevan, L.
Reduction on synthesis gas costs by decrease of steam/carbon and oxygen/carbon ratios in the feedstock
Ind.Eng.Chem.Res.**37** (1998) 258-266.

Bergeret, G., and Gallezot, P.
Particle Size an Dispersion measurements
In "*Handbook of Heterogeneous Catalysis*"
(Ertl, G. Knozinger, H., and Weitkamp, J. Eds.), Wiley-VCH: Weinheim,(1997) Vol. 2

Brady, R.C., and Pettit, R.
On the mechanism of the Fischer-Tropsch reaction. The chain propagation step.
Journal of the American Chemical Society. **103**, (1981), 1287-1289.

Buonomo,F., Sanfilipppo,D., and Trifiro,F.
Dehydrogenation of alkenes.
In *"Handbook of Heterogeneous Catalysis"*
(Ertl, G. Knozinger, H., and Weitkamp, J. Eds.), Wiley-VCH: Weinheim, (1997) Vol. 5

Chary, K.V.R., Kishan, G., Kumar, C.P., and Sagar, G.V.
Structure and catalytic properties of vanadium oxide supported on alumina
Applied Catalysis A: General **246** (2003) 1-16.

Che, M., Clause, O., and Marcilly, C. H.
Supported catalysts
In *"Handbook of Heterogeneous Catalysis"*
(Ertl, G. Knozinger, H., and Weitkamp, J. Eds.), Wiley-VCH: Weinheim, (1997) Vol. **2**.

Clark, R.L.H.
In "*Comprehensive Inorganic Chemistry*"
Pergamon Press, Oxford, 1973,1st ed. pg. 494-435.

Corke, J.C.
GTL technologies focus on lowering costs
Oil & Gas Journal (1998), 71-77.

Cybulki, A., Edvinson, R., Irandoust, S., and Anderson, B.
Liquid-phase methanol synthesis: modelling a monolithic reactor
Chemical Engineering Science **48** (1993) 3463-3478.

Dawe, R.
In *"Modern Petroleum Technology"*
John Wiley & Sons, Chichester (2001), pg 376-381, vol. 1

Deo, G, and Wachs, I.E.
Predicting molecular structures of surface metal oxide species on oxide supports under ambient conditions.
Journal of Physical and Chemistry 1 A **95** (1991) 5889-5895.

Doesburg, E.B.M., and van Hooff, J.H.C.
Preparation of supports and Zeolites.
In "*Studies in Surface Science and Catalysis*"
(Moulijn, J.A., van Leeuwen, P.W.N.M., and van Santen, R.A. Eds.), Elsevier, Amsterdam, **79** (1993) 309-332

Dry, M.E.
The Fischer- Tropsch Process: 1950-2000
Catalysis Today **71** (2002), 227-241.

Dry, M.E.
High-quality diesel via the Fischer-Tropch process- a review.
Journal of Chemical Technology and Biotechnology **77** (2001) 43-50.

Dry, M.E.
The Fischer-Tropsch Process - Commercial aspects
Catalysis Today **6** (1990), 183-206.

Dry, M.E.
Catalytic aspects for the Fischer-Tropsch Synthesis
Journal of Molecular Catalysis A **17** (1982), 133-144.

Dry M.E.
In *"Catalysis Science and Technology"*
(Anderson, J.R., Bourdart, M. Eds.) Springler Verby:New York, vol.**1**1981

Eon, J.G, Olier, R, and Volta, J.C.
Oxidative dehydrogenation of propane on γ-Al_2O_3 supported vanadium oxides.
Journal of Catalysis **145** (1994) 318-326.

Feller, A., Claeys, M., and van Steen, E.
Cobalt cluster effects in zirconium promoted Co/SiO_2 Fischer-Tropsch catalysts
Journal of Catalysis **185** (1999) 120-130.

Fischer, F., and Tropsch, H.
Übe die Hesterllung synthetischer Ölgemische (Synthol) durch Aufbau ause kohlenoxyd und wassertoff
Bennstoff-Chemie 4 (1923), s.276

Fogler, H.S.
In *"Elements in Chemical Reaction Engineering."*
Prentice Hall PTR, 2nd Ed. New Jersey, (1992), pg. 434-447

Gallie, A., Nieto, J.L.M, Dejoz, M., and Vazquez, M.I.
The effect of potassium on the selective oxidation of *n*-butane over Al_2O_3 supported vanadia catalysts.
Catalysis Letters **13** (1995) 51-58.

Gates, B.C
In *"Catalytic Chemistry."*
John Wiley & Sons, Inc., 1st Ed., New York,.(1992) pg. 340-400.

Geerlings, J.J., Huisman, H.M, Lange, J.P., Oostenbeek, H, Ree, P.J.M, and Schadebhorst, D.B.
Catalyst and process for the preparation of hydrocarbons
PCT/EP96/02577P (1997), assigned to Shell

Geus, J.W., and van Veen, J.A.R.
Preparation of supported catalysts
In "*Studies in Surface Science and Catalysis.*"
(Moulijn, J.A., van Leeuwen, P.W.N.M., and van Santen, R.A. Eds.), Elsevier, Amsterdam, **79** (1993) 335-352

Gil-Llambias, F.J., Escudey, A.M., Fierro, J.L.G., and Agudo A.L.
Determination of the active surface area of vanadia by electrophoresis migration and XPS measurements.
Journal of Catalysis **95** (1985) 520-226.

Haber, J.
Selectivity in heterogeneous catalytic oxidation of hydrocarbons
In *"Heterogeneous Hydrocarbon Oxidation."*
(Warren, B.K and Oyama, S.T Eds.) ACS Symposium Series **638** (1996) 20-35.

Iglesia, E., Reyes, S.C., and Madon, R.J.
Transport-enhanced α-olefin readsorption pathways in Ru-catalyzed hydrocarbon synthesis.
Journal of Catalysis **129** (1991) 238-256.

Iglesia, E., Soled S.L, Baumgartner, J.E., and Reyes, S.C.
Synthesis and catalytic properties of eggshell cobalt catalysts for the Fischer-Tropsch Synthesis.
Jounal of Catalysis **153** (1995) 108-122.

Iglesia, E.
Design Synthesis, and use of cobalt-based Fischer-Tropsch synthesis catalysts.
Applied Catalysis A: General **161** (1997) 59-78.

Khader, M.M.
Surface acidity of V_2O_5 /Al_2O_3 catalysts: IR and TPD studies.
Journal of Molecular Catalysis A: Chemical **104** (1995) 87-94.

Knacke, O., Kubaschewski, O and Hesselmann, K.
In *"Thermochemical Properties of Inorganic Substances."*
Springer-Verlag: Berlin 2nd ed., 1991, Vol. 1.

Knottenbelt, C.
Mossgas "gas-to-liquids" diesel fuels- an environmentally friendly option.
Catalysis Today **71** (2002), 437-445.

Kogelbauer, A., Goodwin, J.G., and Oukaci, R.J.
Ruthenium promotion of Co/Al_2O_3 Fischer-Tropsch catalysts.
Journal of Catalysis **160** (1996) 125-133.

Krishna, R., Vlugt, T.J.H., and Smit, B.
Influence of isotherm inflection on diffusion in a silicalite.
Chemical Engineering Science **54** (1999) 1751-1757.

Lemonidou, A.A., Nalbandian, L., and Vasalos, I.A.
Oxidative dehydrogenation of propane over vanadium oxide base catalysts: Effect of support and alkali promoter
Catalysis Today **61** (2000) 333-341.

Le Page, J.L.
Preparation of solid catalysts: developing industrial catalyts
In "*Handbook of Heterogeneous Catalysis*"
(Ertl, G. Knozinger, H., and Weitkamp, J. Eds.), Wiley-VCH:Weinheim,(1997) Vol. 1.

Maitlis, P.M., Long, H.C., Turner, M.L., Fornasiero, P., Kaspar, J., and Graziani, M.
Vinylic initiation of the Fischer-Tropsch reaction over ruthenium on silica catalysts.
Journal of Catalysis **167**,172-179(1997).

Mars, P., and van Krevelen, D.W.
Oxidations carried out by means of vanadium oxide catalysts
Special Supplement to Chemical Engineering Science, **3** (1954) 41-58

Miki , J., Konoshi, Y., Tachibana, Y, and Shikada, T.
Selective oxidation of toluene to benzoic acid by modified vanadium oxides
Applied Catalysis A: General **137** (1996) 93-104.

Moulijn, J.A, Ponec. V.
Heterogeous Catalysis
In *"Studies in Surface Science and Catalysis"*
(Moulijn, J.A., van Leeuwen, P.W.N.M., and van Santen, R.A. Eds.), Elsevier, Amsterdam, **79** (1993) 159-194.

Mugalie, R. and Blaise, D.
Fischer-Tropsch synthesis process in the presence of a catalyst the metallic particles of which have a controlled size.
US 6,214,890 B1 (2001). Assigned to Institut Francais Du Petrole.

Muller, T.H
Sulphuric Acid and Sulphur Trioxide
In *"Kirk-Othmer's Encyclopaedia of Chemical Technology"*
Kroschwitz, J.I., and Grant, M.H., Eds., John Wiley & Sons: New York, 4th ed., **23** (1997)363-408.

Ndlovu, S.B., Phala, N.S., Hearshaw-Timme, Beagly, P., Moss, J.R., Claeys, M., and van Steen, E
Some Evidence refuting the alkenyl mechanism for chain growth in iron based Fischer-Tropsch synthesis
Catalysis Today **71** (2002), 343-349.

Oyama, S.T.
Factors affecting selectivity and catalytic partial oxidation and combustion reactions.
In "*Heterogeneous hydrocarbon oxidation.*"
Warren, B.K and Oyama, S.T Eds. ACS Symposium Series **638 (**1996) 2-19.

Patzlaff, J., Liu, Y., Graffmann, C., and Gaube, J.
Studies on product distributions of iron and cobalt Fischer-Tropsch synthesis
Applied Catalysis A: General **187** (1999) 109-119.

Pay, T.D., Patel, S. S.
Foreign Coal-Liquefaction-Technology Survey and Assessment – 1981 Oak Ridge National Lab.
http://www.fischer-tropsch.org/DOE/DOE_reports/13837_6/13837_6_toc.htm
(website accessed in 2003)

Perry's Chemical Engineers Handbook",
Perry, R.H, Green, D.W., and Maloney, J.O Eds. McGraw-Hill: New York 7th ed., (1997) 2-121.

Pichler. P., and Schulz H.
Neuere Erkenntnisse auf dem Gerbiet der Synthese von Kohlenwasserstsoffen aus CO und H_2
Chemie Ingenieur Technik **42** (1970) 1162-1174

Sabatier,P., and Sanderens, J.B.
Direct hydrogenation of oxides of carbon in the presence of various metals.
Journal of Chemical Society vol.82,II (1902) 137.

Sasol Facts
Sasol corporate communications (2001) 1-52.

Schulz, H., Claeys.M. (a)
Reactions of α-olefins of different chain length added durion Fischer-Tropsch synthasis on a cobalt catalyst in a slurry reactor.
Applied Catalysis A: General **186** (1999) 71-90.

Schulz, H. and Claeys, M. (b)
Kinetic modelling of Fischer-Tropsch product distributions
Applied Catalysis A: General **186** (1999) 90-107.

Schulz, H., Schaub, G., Claeys, M, and Riedel, T. (c)
Transient initial kinetic regimes of Fischer-Tropsch synthesis
Applied Catalysis A: General **186** (1999) 215-227

Schulz, H., Nie, Z., and Ousmanov, F.,
Construction of the Fischer-Tropsch regime with cobalt catalysts
Catalysis Today **71** (2002), 351-360.

Schuth, F., and Under, K.
Preparation of solid catalysts: precipitation and poprecipitation.
In "*Handbook of Heterogeneous Catalysis*"
(Ertl, G. Knozinger, H., and Weitkamp, J., Eds.), Wiley-VCH: Weinheim (1997) Vol. 1

Sie, S.T.
Process development and scale up: IV Case history of the development of a Fischer-Tropsch Synthesis process.
Review Chemical Engineering **14** (1998) 109-157.

Smith, J.M.
In "*Chemical Engineering Kinetics.*"
McGraw Hill, Inc., New York 3rd ed. (1981).

Storch, H. H, Columbic, M.S., and Anderson, R.B.
"*The Fischer-Tropsch and Related Synthesis.*"
John Wiley & Sons, Inc., New York (1951).

Vada, S., Chen, B., and Goodwin.Jr, G.
Isotopic transient study of La promotion of Co/Al_2O_3 for CO hydrogenation
Journal of Catalysis **153** (1995) 224-231.

van Barneveld, W.A.A., and Ponec, V.
Reactions of CH_XCl_{4-X} with hydrogen: Relation to the Fischer-Tropsch synthesis of hydrocarbons.
Journal of Catalysis **88** (1983) 382-387

Van Berge, P.J, Barradas, S., van de Loosdrecht, J., and Visagie, J.L.
Advances in the cobalt-catalysed Fischer-Tropsch.
DGMK conference:Synthesis gas chemistry (2000); Dresden, Germany (September 2002).

Van Berge, P.J and Everson, R.C.
Cobalt as an alternative Fischer-Tropsch catalyst to iron for the production of middle distillates .
In "*Studies in Surface Science and Catalysis*,"
(De Pontes, M., Espinoza, R.L., Nicolides, C.P., Scholz, J.H, and Scurrell, M.S. Eds.), Natural Gas Conversion IV. **107** (1997) 207-212

Van der Laan, G.P.
PHD Thesis (University of Gronigen, 1999)

Vannice, M.A.
The catalytic synthesis of hydrocarbons from H_2/CO mixtures over group VIII metals-V. The catalytic behaviour of silica supported metals
Journal of Catalysis **50** (1977) 228-236.

Vannice, M.A.
The catalytic synthesis of hydrocarbons from H_2/CO mixtures over group VIII metals- I. The specific activities and product distributions of supported metals
Journal of Catalysis **34** (1975) 449-461.

van Steen, E. Sewell, G.S., Makhote, A.R. Micklethwaite,C.,Maistein, H., de Lange, M., and O'Conner, C.T.
TRP Study on the Preparation of Impregnated Co/SiO_2 Catalysts.
Journal of catalysis **162** (1996) 220-229

Weckhuysen, B.M., and Keller, D.E
Chemistry, spectroscopy and the role of supported vanadium oxides in heterogeneous catalysis.
Catalysis Today **78** (2003) 25-46.

Woolery, M.
Vanadium Compounds
In *"Kirk-Othmer's Encyclopaedia of Chemical Technology"*
(Kroschwitz, J.I., and Grant, M.H., Eds.), John Wiley & Sons: New York, 4^{th} ed., **24** (1997) 782-811.

Xu, L., Bao, S., O'brian, R.J., Raje, A., and Davis, B.H.
Don't rule out iron catalysts for Fischer-Tropsch synthesis.
Chemtech January Issue (1998) 47-53.

Yakobson, D.L.
Rentech, Inc, "GasTech 2000 conference."
http://www.rentechinc.com/GasTech2000.pdf. *(Website accessed in 2002)*

Zheng., C.,Apeloig.,Y.,and Hoffmann,R.
Bonding and coupling of C_1 fragments on metal surfaces.
Journal of American Chemical Society **110** (1988) 749-774.

Chapter 7
Appendices

7 Appendices

Appendix: CO Chemisorption analysis, Langmuir model-fitting

The CO chemisorption data (pressure and volume) was fitted into the single-site and dual-site Langmuir isotherms to establish CO 1-monolayer surface volume coverage v_m. The value of v_m was used to estimate the catalyst active crystallite size, surface area and metal dispersion. The single site Langmuir isotherm model for the adsorption of CO can be stated as follows (Smith, 1981):

$$\theta = \frac{K \cdot P_{CO}}{1 + K \cdot P_{CO}} = \frac{v}{v_m}$$

Where θ is the fractional surface coverage, K is the equilibrium adsorption constant, P_{CO} is the adsorbed pressure of CO, v the volume of CO adsorbed at P_{CO} and v_m is the saturation volume at 1 monolayer surface coverage. After linearising equation 2.3 a plot $1/v$ as a function of $1/P_{CO}$ should yield a straight line with the slope equal to 1/K and an intercept corresponding to $1/ v_m$. When two different active sites are competing for adsorption of the same gas the dual-site Langmuir (DSL) model is used to fit volume pressure data from chemisorption experiments. The dual-site Langmuir model can be stated as (Krishna et al., 1998):

$$\theta = \frac{\theta_1 \cdot K_1 \cdot P_{CO}}{1 + K_1 \cdot P_{CO}} + \frac{\theta_2 \cdot K_2 \cdot P_{CO}}{1 + K_2 \cdot P_{CO}} = \frac{v}{v_m}$$

Where θ_1 and θ_2 are fractional coverages in site 1 and site 2 respectively; K_1 and K_2 are the equilibrium adsorption constants on site 1 and 2. P_{CO}, θ and v_m are as defined in the single site model. The model parameters for the dual site Langmuir isotherm model were calculated by CO chemisorption data regression in Polymath non-linear regression fitting model. The program uses the Levenberg-Marquardt (LM) algorithm for finding the parameter values. For converged results, the graphical and statistical information provided was used for assessing the quality of the fit. Once the saturation volume at 1-monolayer

surface coverage *(v_m)* had been established, active metal surface area and metal dispersion were then evaluated using following formulae:

Specific metal surface area (A):

$$A = \left(\frac{v_m}{22414}\right) \times N_A \times n \times \frac{1}{m} \times a_m \times \frac{100}{wt} \qquad (m^2.g^{-1} \text{ metal})$$

Where: v_m –1 monolayer gas volume coverage (cm^3, STP)

N_A- Avogadros number (6.022×10^{23} mol^{-1})

n- Chemisorption stoichiometry (assumed =1 for Co).

m- mass of sample (g).

a_m- metal surface area for 1 Co metal atom (6.58E-20 m^2)

wt- % metal loading.

Metal dispersion (D):

$$D = \frac{\left(\frac{v_m \times n}{22414 \times m}\right)}{\left(\frac{wt}{100 \times M}\right)}$$

Where M ($g.mol^{-1}$) is the Atomic mass of the active metal

Crystallite diameter (d_{VA}):

$$d_{VA} = \frac{6}{S_p \cdot \rho_{CO}} \quad (m)$$

ρ_{Co}- density for cobalt (8.9 $g.cm^{-3}$)

(Bergeret and Gallezot, 1997).

Appendix: TRP calibration and data analysis

To convert the conductivity signal obtained from the TPR apparatus into holes on H_2 consumed during the reduction program, NiO was used as a standard to calibrate the apparatus. About 0.05 g (0.4 mmols) of NiO was loaded into the quartz reactor of the TPR set-up and was reduced under 5.6-vol% H_2-Ar mixture flowing at 50ml.min^{-1} (NTP). The reduction was carried out at a ramping rate of 10^{O}C.min^{-1} up to 260^{O}C. Figure 2-2 shows the TPR profile for the reduction of NiO. The reduction of NiO is governed by the following chemical equation:

$$NiO(s) + H_2(g) \longrightarrow Ni(s) + H_2O(g)$$

The time - conductivity profile with arbitrary units (a.u) was integrated using Trapezoidal rule to obtain the area under the curve. The area under the curve is proportional to the amount of H_2 consumed during NiO reduction since every mole of H_2 removes one oxygen atom when NiO is reduced completely. A sample calculation will be done based on NiO calibration curve and V_2O_5 TPR experiment to demonstrate both the instrument calibration and H_2 consumption evaluation procedures in a typical TPR experiment. The experimental data for NiO calibration and the V_2O_5 TPR experiment are depicted in Figure 2-2.

By the Trapezoidal rule the area under the curve is given by:

$$Area = \sum (0.5) \times (S_{n+1} + S_n) \times (t_{n+1} + t_n)$$

Where S_i and t_i are TCD signal values and time at time i.

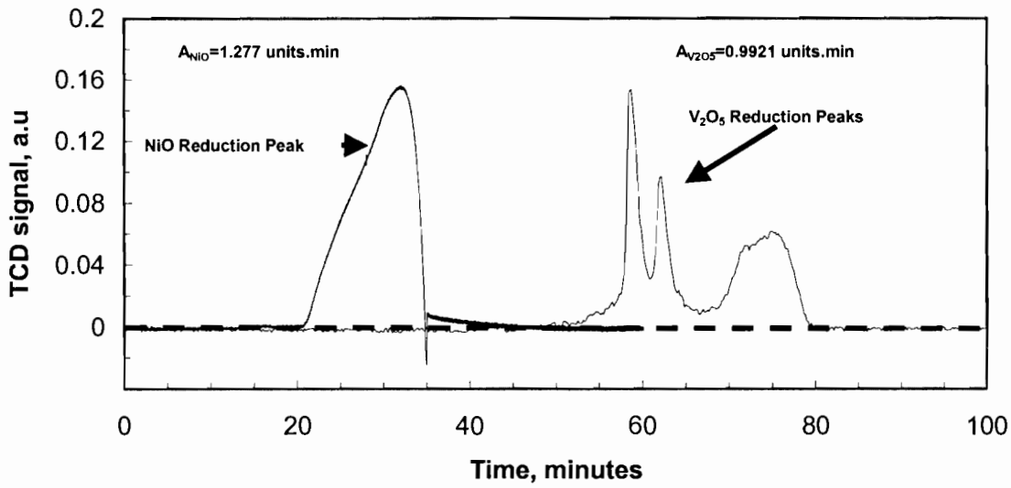

Figure AI-1: TPR conductivity-time profile for NiO and V_2O_5 under 50ml.min^{-1} of 5.6% H_2-Ar mixture at a ramping rate of 10^{O}C.min^{-1}. M_{NiO} =~0.031 g (0.415 mmols), M_{V2O5}=~0.0305g (0.168 mmols).

The amount of hydrogen consumption by the different catalysts and supports during the TPR experiments is given by:

$$C_{H_2} = \left(\frac{A_{Cat}}{A_{NiO}} \right) \times \left(C_{NiO} \right)$$

Where C_{H2} is the hydrogen consumed per experimental run in milli-moles, A_{H2} and A_{NiO}, are areas under TPR conductivity-time profiles for the analysed catalyst/support and NiO, respectively. C_{NiO} (0.4150mmols) is the number of moles of oxygen atoms consumed in the standard (calibration) sample of NiO.

The amount of H_2 consumed in the reduction of V_2O_5 will therefore be:

=(0.992/1.277)*(0.415) mmols

=~0.332 mmols H_2

H_2 consumption per mole V_2O_5: 0.332/(0.0305/188.88)/1000

=1.92 mol/mol

Appendix: Calibration of mass flow controllers

Mass flow controllers were calibrated by measuring the correct flow using a bubble meter. The measured true flows were subsequently correlated to the set point setting on the flow meter to obtain calibration curved for each gas supply line. Figure AII-1 to AII-3 depicts calibration curves for H_2, CO and N_2/cyclohexane supply lines.

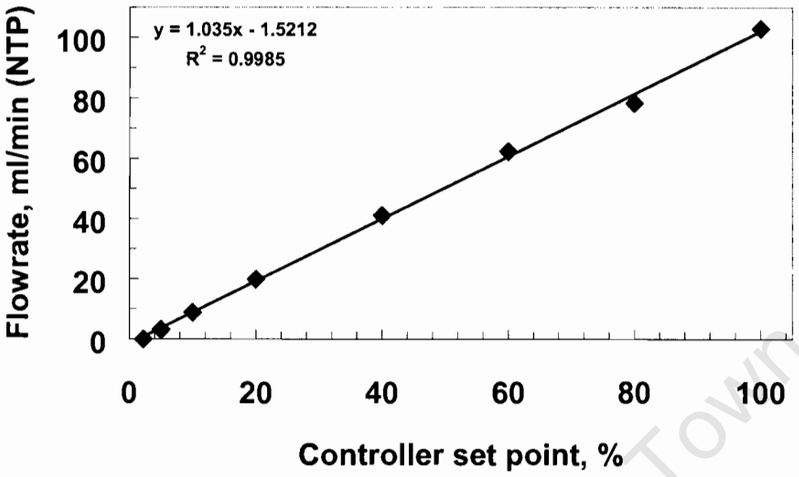

Figure AII-1: Calibration curve for the H_2 mass flow controller

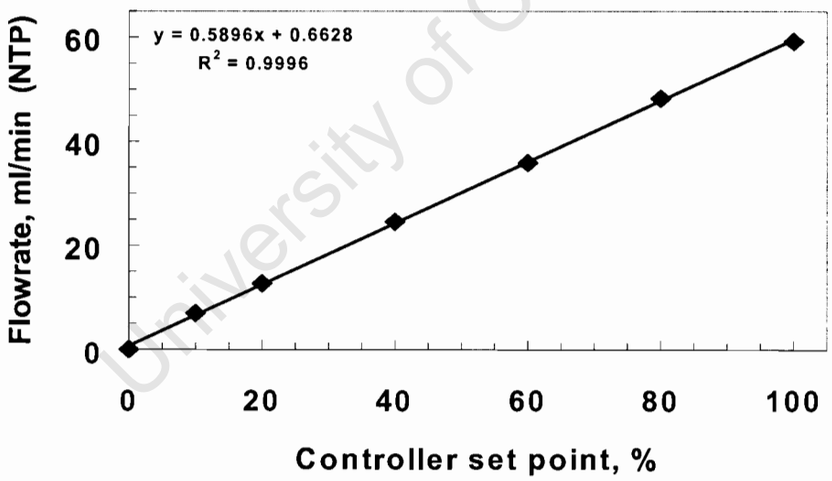

Figure AII-2: Calibration curve for the CO mass flow controller

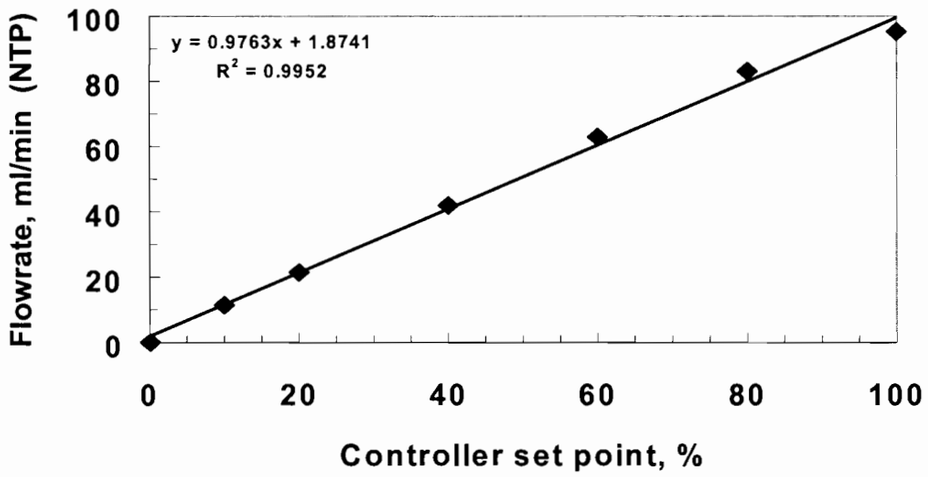

Figure AII-3: Calibration curve for the N_2/cyclohexane mass flow controller

Appendix: Time on stream TCD data for Fischer-Tropsch synthesis

Time on stream TCD data 0 ML Catalysts									
TOS	TCD AREAS						CO Conversion.	CH_4 Yield	CH_4 Selectivity
[Hrs]	H_2	N_2	CO	CH_4	H_2/N_2	CO/N_2	x_{co}, C-%	Y_{CH4}	S_{CH4}, C-%
0.3	3.932E+04	255682	0	9810	0.013	0.000	100.0	1.2	1.2
0.5	1.856E+05	257831	9871	21502	0.060	0.040	95.7	2.6	2.7
0.7	3.262E+05	323546	17132	28047	0.083	0.055	94.1	2.7	2.9
0.8	4.413E+05	338659	20259	28690	0.108	0.062	93.3	2.6	2.8
1.1	7.383E+05	253577	31762	42965	0.241	0.129	86.0	5.3	6.2
1.2	7.774E+05	255209	33641	42774	0.252	0.136	85.3	5.2	6.1
1.4	8.141E+05	253528	36760	44722	0.266	0.150	83.8	5.5	6.6
1.6	8.602E+05	252565	37827	45765	0.282	0.155	83.3	5.7	6.8
1.7	7.278E+05	404728	46295	36586	0.149	0.118	87.3	2.8	3.2
1.9	8.877E+05	277312	50554	46859	0.265	0.188	79.7	5.3	6.6
2.3	9.874E+05	251590	45137	53937	0.325	0.185	80.0	6.7	8.4
2.4	1.102E+06	251294	51795	56080	0.363	0.213	77.0	7.0	9.1
2.6	1.169E+06	252363	53560	55277	0.383	0.219	76.4	6.8	9.0
3.1	1.398E+06	276501	73251	58179	0.418	0.273	70.5	6.6	9.3
3.2	1.361E+06	273555	71140	53753	0.411	0.268	71.0	6.1	8.7
3.7	1.629E+06	274201	84336	58053	0.491	0.317	65.7	6.6	10.1
4.2	1.870E+06	276092	93412	57185	0.560	0.349	62.3	6.5	10.4
4.4	1.597E+06	260268	70003	47768	0.507	0.278	70.0	5.7	8.2
4.6	1.823E+06	280588	90620	50011	0.537	0.333	64.0	5.6	8.7
4.7	1.587E+06	273738	80237	44161	0.479	0.302	67.3	5.0	7.5
5.6	1.949E+06	269672	98283	49277	0.598	0.376	59.4	5.7	9.6
5.7	2.064E+06	267402	101417	52531	0.638	0.391	57.7	6.1	10.6
6.0	2.252E+06	273009	108759	54940	0.682	0.411	55.6	6.3	11.3
6.2	2.305E+06	273282	116306	52977	0.698	0.439	52.6	6.1	11.5
7.9	2.347E+05	270498	113804	53813	0.072	0.434	53.1	6.2	11.7
8.1	2.208E+06	269193	106089	50086	0.678	0.407	56.1	5.8	10.4
8.3	2.277E+06	263630	107697	49294	0.714	0.422	54.5	5.8	10.7
9.5	2.473E+06	274619	119030	54845	0.745	0.447	51.7	6.2	12.1
9.7	2.407E+06	275464	114700	52398	0.723	0.430	53.6	5.9	11.1
10.0	2.456E+06	276157	117208	52843	0.736	0.438	52.7	6.0	11.4
10.3	2.293E+06	276676	106230	49336	0.685	0.396	57.2	5.6	9.7
28.3	2.675E+06	270620	124830	49127	0.817	0.476	48.6	5.7	11.7
28.5	2.661E+06	271772	125714	48996	0.810	0.477	48.5	5.6	11.6
28.8	2.722E+06	271654	127264	48621	0.829	0.483	47.8	5.6	11.7
29.0	2.702E+06	271198	124093	47221	0.824	0.472	49.0	5.4	11.1
31.3	2.732E+06	268716	126389	48824	0.841	0.485	47.6	5.7	11.9
31.4	2.782E+06	266326	128245	50979	0.864	0.497	46.4	6.0	12.9
31.6	2.739E+06	266133	127438	48558	0.851	0.494	46.7	5.7	12.2
51.0	2.869E+06	267223	132877	47406	0.888	0.513	44.6	5.5	12.4
51.1	2.879E+06	268245	133604	46832	0.887	0.514	44.5	5.5	12.3
51.5	2.848E+06	269770	132117	47152	0.873	0.505	45.4	5.5	12.0
71.4	6.606E+06	643115	315449	115331	0.849	0.506	45.4	5.6	12.4
71.8	6.580E+06	646810	318328	113891	0.841	0.508	45.2	5.5	12.2

Time on stream TCD data 0.1 ML Catalysts									
TOS	TCD AREAS						CO Conversion	CH_4 Yield	CH_4 Selectivity
[Hrs]	H_2	N_2	CO	CH_4	H_2/N_2	CO/N_2	x_{co}, C-%	Y_{CH4}	S_{CH4}, C-%
0.3	1.219E+04	261557	0	4445	0.004	0.000	100.0	0.6	0.6
0.6	1.251E+05	244235	2952	18291	0.512	0.012	98.6	2.5	2.5
0.8	2.527E+05	237454	6587	26117	1.064	0.028	96.7	3.7	3.8
1.0	3.626E+05	240113	11302	28110	1.510	0.047	94.4	3.9	4.1
1.3	4.715E+05	245178	15108	30684	1.923	0.062	92.7	4.2	4.5
2.4	6.839E+05	239199	22364	34635	2.859	0.093	88.9	4.8	5.4
2.5	5.897E+05	240617	19466	30581	2.451	0.081	90.4	4.2	4.7
2.7	6.205E+05	240192	20127	31664	2.583	0.084	90.1	4.4	4.9
2.8	6.300E+05	240496	20170	33644	2.620	0.084	90.1	4.6	5.2
3.0	6.476E+05	240364	20413	34474	2.694	0.085	90.0	4.8	5.3
3.8	6.748E+05	241267	24119	31842	2.797	0.100	88.2	4.4	5.0
4.0	7.765E+05	248496	37374	35636	3.125	0.150	82.2	4.8	5.8
4.2	9.101E+05	267306	31161	37200	3.405	0.117	86.2	4.6	5.4
4.3	9.533E+05	248288	33860	38440	3.840	0.136	83.9	5.1	6.1
4.5	9.518E+05	251268	34062	38253	3.788	0.136	84.0	5.1	6.0
4.7	6.853E+05	248674	33471	40148	2.756	0.135	84.1	5.4	6.4
4.8	8.750E+05	231499	31004	34007	3.780	0.134	84.2	4.9	5.8
5.0	9.340E+05	251021	43780	36152	3.721	0.174	79.4	4.8	6.0
5.2	9.689E+05	241522	35031	37756	4.011	0.145	82.8	5.2	6.3
8.0	1.137E+06	250715	54107	35956	4.536	0.216	74.5	4.8	6.4
8.2	1.158E+05	283517	41055	35874	0.408	0.145	82.9	4.2	5.1
8.3	1.297E+06	261627	46286	38732	4.957	0.177	79.1	4.9	6.2
8.5	1.248E+06	255558	41055	38714	4.883	0.161	81.0	5.0	6.2
8.8	1.185E+06	254599	42727	37062	4.656	0.168	80.1	4.8	6.0
8.9	9.877E+05	240868	36038	31304	4.101	0.150	82.3	4.3	5.2
9.0	1.017E+06	254578	48399	31431	3.996	0.190	77.5	4.1	5.3
9.3	1.115E+06	277248	52287	34658	4.023	0.189	77.7	4.2	5.3
11.9	1.360E+06	240700	61742	38688	5.651	0.257	69.7	5.3	7.7
12.1	1.287E+06	270610	58463	36546	4.756	0.216	74.4	4.5	6.0
12.3	1.328E+06	300131	61198	38833	4.423	0.204	75.9	4.3	5.7
12.4	1.293E+06	264932	59170	37344	4.879	0.223	73.6	4.7	6.4
12.5	1.271E+06	246104	57607	36543	5.163	0.234	72.3	4.9	6.8
12.7	1.093E+06	251811	51681	30654	4.340	0.205	75.7	4.0	5.3
16.7	1.355E+06	243000	61447	34014	5.578	0.253	70.1	4.6	6.6
16.8	1.386E+06	231608	63657	34853	5.985	0.275	67.5	5.0	7.4
17.0	1.395E+06	244044	62623	33798	5.716	0.257	69.6	4.6	6.6
21.0	1.470E+06	235778	54600	35148	6.234	0.232	72.6	4.9	6.8
21.1	1.320E+06	236474	51235	32559	5.581	0.217	74.4	4.6	6.1
21.3	1.471E+06	246248	67134	34326	5.972	0.273	67.8	4.6	6.8
21.7	1.480E+06	250232	66585	35585	5.914	0.266	68.5	4.7	6.9
24.0	1.491E+06	239711	56156	34736	6.219	0.234	72.3	4.8	6.7
24.1	1.507E+06	253763	69212	34781	5.938	0.273	67.7	4.6	6.7
29.7	1.564E+06	246818	69570	34427	6.335	0.282	66.7	4.6	6.9
29.9	1.565E+06	247577	72013	33940	6.321	0.291	65.6	4.6	6.9
30.0	1.577E+06	241245	72068	33771	6.536	0.299	64.7	4.6	7.2

Time on stream TCD data 0.5 ML Catalysts									
TOS	TCD AREAS						CO Conversion.	CH_4 Yield	CH_4 Selectivity
[Hrs]	H_2	N_2	CO	CH_4	H_2/N_2	CO/N_2	$x_{co,}$ C-%	Y_{CH4}	$S_{CH4,}$ C-%
0.3	6.826E+05	203682	26026	30431	0.277	0.132	85.1	4.9	5.7
0.5	9.925E+05	232368	42518	33891	0.353	0.189	78.7	4.8	6.1
0.7	1.131E+06	225249	48258	35565	0.415	0.221	75.0	5.2	6.9
0.8	1.175E+06	229279	48572	34901	0.424	0.219	75.3	5.0	6.6
1.0	1.185E+06	245280	51229	37296	0.399	0.216	75.7	5.0	6.6
1.3	1.222E+06	230815	52498	37567	0.438	0.235	73.5	5.3	7.2
1.5	1.250E+06	234285	53218	38070	0.441	0.234	73.5	5.3	7.2
1.8	1.248E+06	219862	42409	37795	0.470	0.199	77.5	5.6	7.3
2.0	1.278E+06	219393	44846	34276	0.482	0.211	76.2	5.1	6.7
2.2	1.295E+06	230459	54848	37707	0.465	0.246	72.3	5.4	7.4
2.3	1.219E+06	231656	51342	33943	0.435	0.229	74.2	4.8	6.5
2.5	1.238E+06	221226	42442	37494	0.463	0.198	77.6	5.5	7.1
3.0	1.248E+06	221269	42791	38516	0.466	0.200	77.5	5.7	7.3
4.0	1.273E+06	230019	43455	38708	0.458	0.195	78.0	5.5	7.1
4.4	1.342E+06	297864	56948	39074	0.373	0.197	77.7	4.3	5.5
4.6	1.384E+06	255091	58261	38364	0.449	0.236	73.4	4.9	6.7
6.5	1.452E+06	234963	62264	37936	0.511	0.273	69.1	5.3	7.6
6.6	1.243E+06	243615	54898	32150	0.422	0.233	73.7	4.3	5.9
7.0	1.456E+06	247814	61881	38357	0.486	0.258	70.9	5.1	7.1
7.3	1.463E+06	267452	64053	43702	0.452	0.247	72.1	5.3	7.4
7.4	1.215E+06	243927	52761	31987	0.412	0.223	74.8	4.3	5.7
7.5	1.361E+06	243776	59374	35292	0.462	0.251	71.6	4.7	6.6
12.4	1.502E+06	220133	54391	34953	0.564	0.255	71.2	5.2	7.3
12.8	1.606E+06	237430	68661	34596	0.560	0.298	66.3	4.8	7.2
13.0	1.596E+06	230594	68668	36121	0.573	0.307	65.3	5.1	7.8
13.3	1.589E+06	235330	67302	34466	0.558	0.295	66.7	4.8	7.2
13.4	1.598E+06	234094	67788	36276	0.565	0.299	66.3	5.1	7.6
13.6	1.608E+06	235346	69542	32431	0.565	0.305	65.6	4.5	6.9
20.0	1.779E+06	227421	73659	36858	0.647	0.334	62.3	5.3	8.5
20.2	1.774E+05	215935	65456	35412	0.068	0.313	64.7	5.4	8.3
22.5	1.778E+06	226877	73446	34554	0.648	0.334	62.3	5.0	8.0
23.0	1.796E+06	227240	76698	36909	0.653	0.348	60.7	5.3	8.8
23.8	1.776E+06	228220	74256	34944	0.644	0.336	62.1	5.0	8.1
24.0	1.787E+06	229443	76655	35381	0.644	0.345	61.1	5.0	8.3
24.2	1.794E+06	230023	74590	34575	0.645	0.335	62.2	4.9	7.9
24.3	1.794E+06	230023	74590	34575	0.645	0.335	62.2	4.9	7.9
29.7	1.820E+06	231830	78659	33810	0.649	0.350	60.5	4.8	7.9
29.8	1.813E+06	230747	75671	34660	0.650	0.338	61.8	4.9	8.0
30.0	1.833E+06	230147	76406	34283	0.659	0.343	61.3	4.9	7.9
36.0	1.892E+06	229963	77136	36321	0.681	0.346	60.9	5.2	8.5
36.2	1.914E+06	250258	78001	36894	0.633	0.322	63.7	4.8	7.6
36.3	1.965E+06	231016	78563	37125	0.703	0.351	60.4	5.3	8.7

Time on stream TCD data 1 ML Catalysts									
TOS	TCD AREAS						CO Conversion.	CH_4 Yield	CH_4 Selectivity
[Hrs]	H_2	N_2	CO	CH_4	H_2/N_2	CO/N_2	$x_{co,}$ C-%	Y_{CH4}	$S_{CH4,}$ C-%
0.3	1.361E+06	255503	64189	32164	0.440	0.259	70.7	4.1	5.8
0.5	1.818E+06	254276	74859	31950	0.591	0.304	65.7	4.1	6.3
0.7	1.952E+06	255131	80709	32802	0.633	0.326	63.1	4.2	6.7
0.8	1.979E+06	256632	82172	32931	0.638	0.330	62.7	4.2	6.7
1.0	2.090E+06	264964	89321	35026	0.652	0.348	60.7	4.3	7.1
1.2	2.055E+06	254743	83821	34380	0.667	0.340	61.7	4.4	7.2
1.3	2.080E+06	255146	86200	33906	0.674	0.349	60.6	4.3	7.2
1.5	2.076E+06	252464	87200	34959	0.680	0.356	59.8	4.5	7.6
1.8	2.049E+06	252575	85514	34371	0.671	0.349	60.6	4.4	7.3
2.0	2.094E+06	254298	88039	33866	0.681	0.357	59.7	4.4	7.3
2.2	2.055E+06	251405	86153	33662	0.676	0.354	60.1	4.4	7.3
2.3	2.081E+06	260480	85659	33272	0.661	0.339	61.7	4.2	6.8
2.5	2.075E+06	248919	86663	33347	0.689	0.359	59.4	4.4	7.4
2.9	2.111E+06	250188	88502	35190	0.698	0.365	58.8	4.6	7.8
3.0	2.075E+06	254910	87106	33241	0.673	0.353	60.2	4.3	7.1
3.3	2.050E+06	257082	85400	33499	0.660	0.343	61.3	4.3	6.9
3.5	2.124E+06	257306	90308	33914	0.683	0.362	59.1	4.3	7.3
3.8	2.137E+06	255579	96914	40586	0.691	0.391	55.8	5.2	9.3
4.0	2.175E+06	250159	96596	35426	0.719	0.398	55.0	4.6	8.4
4.2	2.283E+06	219260	93516	36957	0.861	0.440	50.3	5.5	11.0
7.7	2.775E+06	247795	115072	39606	0.926	0.479	45.9	5.2	11.4
7.8	2.731E+06	260928	114274	39292	0.866	0.452	49.0	4.9	10.1
8.0	2.699E+06	261157	113072	38976	0.855	0.447	49.6	4.9	9.8
14.0	2.725E+06	270495	111684	37764	0.833	0.426	51.9	4.6	8.8
14.2	2.756E+06	274162	113140	37132	0.831	0.426	51.9	4.4	8.5
14.3	2.828E+06	252928	116757	37530	0.925	0.476	46.2	4.9	10.5
23.5	2.912E+06	245195	119038	39322	0.982	0.501	43.4	5.2	12.1
23.7	2.927E+06	249336	120419	37196	0.971	0.498	43.7	4.9	11.2
24.0	2.810E+06	284297	119714	35930	0.817	0.434	50.9	4.1	8.1
24.1	2.929E+06	251669	119406	38407	0.963	0.490	44.7	5.0	11.2
29.8	2.935E+06	247094	122241	37547	0.982	0.510	42.4	5.0	11.7
30.0	2.982E+06	244756	122783	35688	1.008	0.518	41.6	4.8	11.5
30.3	2.989E+06	252841	123453	36905	0.978	0.504	43.1	4.8	11.1
36.5	2.789E+06	236200	105599	39278	0.976	0.461	47.9	5.4	11.3
36.9	2.750E+06	236207	111879	35893	0.963	0.489	44.8	5.0	11.1
37.3	2.770E+06	229972	113358	35893	0.996	0.509	42.6	5.1	12.0
37.5	2.791E+06	215683	117182	35348	1.070	0.561	36.7	5.4	14.6
38.3	2.755E+05	233610	114005	35005	0.098	0.504	43.2	4.9	11.4
42.2	2.866E+06	242600	117862	35507	0.977	0.501	43.4	4.8	11.0
42.5	3.045E+06	229915	125445	36844	1.095	0.563	36.4	5.2	14.4
43.0	2.999E+06	244406	124126	37965	1.015	0.524	40.8	5.1	12.4

Time on stream TCD data 2 ML Catalysts									
TOS	TCD AREAS						CO Conversion.	CH_4 Yield	CH_4 Selectivity
[Hrs]	H_2	N_2	CO	CH_4	H_2/N_2	CO/N_2	x_{co}, C-%	Y_{CH4}	S_{CH4}, C-%
0.3	1.900E+06	252278	83836	31491	0.623	0.343	62.1	4.0	6.4
0.5	2.382E+06	252633	93767	31122	0.780	0.383	57.7	3.9	6.8
0.7	2.515E+06	251884	99585	32018	0.826	0.408	54.9	4.1	7.4
0.8	2.487E+06	250058	100729	30033	0.822	0.416	54.0	3.8	7.1
1.0	2.615E+06	253322	100953	31833	0.854	0.411	54.5	4.0	7.4
1.2	2.612E+06	253393	102021	31200	0.852	0.415	54.1	3.9	7.3
1.3	2.464E+06	281559	99981	29689	0.724	0.366	59.5	3.4	5.7
1.5	2.644E+06	252638	104511	31911	0.866	0.427	52.8	4.0	7.7
1.7	2.637E+05	251778	104468	30913	0.087	0.428	52.7	3.9	7.5
2.0	2.718E+06	252359	107132	30702	0.891	0.438	51.6	3.9	7.6
2.2	2.677E+06	253135	107644	30035	0.874	0.439	51.5	3.8	7.4
2.5	2.671E+06	251541	110044	28935	0.878	0.451	50.1	3.7	7.4
2.7	2.714E+06	254346	108410	30444	0.882	0.440	51.4	3.8	7.5
2.8	2.730E+06	254211	109499	30825	0.888	0.444	50.9	3.9	7.6
3.0	2.692E+06	255713	108817	31153	0.871	0.439	51.5	3.9	7.6
3.2	2.690E+06	255125	106750	30496	0.872	0.432	52.3	3.8	7.3
3.8	2.692E+06	254702	108191	30218	0.874	0.438	51.5	3.8	7.4
4.0	2.690E+06	254607	108503	30326	0.874	0.440	51.4	3.8	7.4
4.5	2.646E+06	256428	105306	29514	0.853	0.424	53.2	3.7	6.9
4.7	2.720E+06	256581	108425	30015	0.877	0.436	51.8	3.7	7.2
4.8	2.714E+06	255913	110222	30358	0.877	0.444	50.9	3.8	7.5
5.0	2.708E+06	256628	104831	32833	0.873	0.421	53.4	4.1	7.7
8.0	3.088E+06	257143	124501	34473	0.993	0.500	44.8	4.3	9.6
8.2	3.088E+06	257143	124501	34743	0.993	0.500	44.8	4.3	9.7
8.3	3.112E+06	256649	126204	35478	1.003	0.507	43.9	4.4	10.1
8.5	3.114E+06	255766	126277	35438	1.007	0.509	43.7	4.4	10.2
8.7	3.097E+06	256494	127538	35856	0.998	0.513	43.3	4.5	10.3
8.8	3.114E+06	257254	124122	34981	1.001	0.498	45.0	4.4	9.7
9.0	3.134E+06	257501	126650	35929	1.007	0.507	43.9	4.5	10.2
9.2	3.116E+06	256121	124670	34155	1.006	0.502	44.5	4.3	9.6
20.2	3.119E+06	236620	126530	29244	1.090	0.552	39.0	4.0	10.1
20.3	3.126E+06	237384	127087	29407	1.089	0.552	38.9	4.0	10.2
20.5	3.121E+06	237945	126763	28792	1.085	0.550	39.2	3.9	9.9
29.8	3.156E+06	240968	127212	28546	1.083	0.545	39.8	3.8	9.5
30.0	3.135E+06	235178	126967	27297	1.102	0.557	38.4	3.7	9.7
30.2	3.153E+06	236987	126967	28794	1.100	0.553	38.9	3.9	10.0
30.3	3.130E+06	236871	127478	27451	1.093	0.555	38.6	3.7	9.6
30.5	3.147E+06	239963	127496	28442	1.085	0.548	39.4	3.8	9.6
35.7	3.405E+06	241689	138407	28622	1.165	0.591	34.7	3.8	10.9
35.8	3.415E+06	240051	137350	29007	1.176	0.590	34.7	3.9	11.1
36.0	3.389E+06	239736	136749	29296	1.169	0.589	34.9	3.9	11.2
36.2	3.388E+06	239402	138472	28711	1.170	0.597	34.0	3.8	11.3
36.3	3.386E+06	238260	137457	27650	1.175	0.595	34.2	3.7	10.9
47.4	3.366E+06	232762	137220	27213	1.196	0.608	32.7	3.7	11.4
47.6	3.430E+06	232660	138506	27987	1.219	0.614	32.1	3.9	12.0
48.0	3.393E+06	234268	137141	27724	1.198	0.604	33.2	3.8	11.4

Time on stream TCD data 5 ML Catalysts									
TOS	TCD AREAS						CO Conversion.	CH_4 Yield	CH_4 Selectivity
[Hrs]	H_2	N_2	CO	CH_4	H_2/N_2	CO/N_2	x_{co}, C-%	Y_{CH4}	S_{CH4}, C-%
0.3	1.938E+06	178543	82798	25916	0.898	0.478	45.9	4.8	10.3
0.5	2.466E+06	190458	95351	23006	1.071	0.517	41.6	4.0	9.5
0.7	2.490E+06	233247	98597	21687	0.883	0.436	50.7	3.0	6.0
0.8	2.513E+06	237032	99736	34901	0.877	0.434	50.9	4.8	9.5
1.0	2.566E+06	272653	102748	21221	0.778	0.389	56.1	2.5	4.5
1.2	2.549E+06	239737	100768	23199	0.879	0.434	51.0	3.2	6.2
2.5	2.535E+06	249100	103171	21972	0.842	0.427	51.7	2.9	5.6
2.7	2.473E+06	229633	99723	23891	0.891	0.448	49.4	3.4	6.9
3.0	2.562E+06	230403	104433	23416	0.920	0.468	47.2	3.3	7.1
3.2	2.566E+06	229104	101653	24729	0.926	0.458	48.3	3.5	7.3
3.3	2.535E+06	230854	102067	22954	0.908	0.456	48.4	3.3	6.7
4.0	2.505E+06	232163	98752	23138	0.892	0.439	50.4	3.3	6.5
4.4	2.456E+06	235009	98224	22436	0.864	0.431	51.3	3.1	6.1
6.7	2.432E+06	233762	96865	23308	0.860	0.428	51.7	3.3	6.3
7.0	2.476E+06	235412	98080	25279	0.870	0.430	51.4	3.5	6.8
7.2	2.374E+06	244110	95823	25311	0.804	0.405	54.2	3.4	6.3
8.4	2.455E+06	240469	99828	25733	0.844	0.428	51.6	3.5	6.8
17.5	2.192E+06	239120	87055	22809	0.758	0.376	57.6	3.1	5.4
17.7	2.372E+06	236675	97080	25826	0.829	0.423	52.2	3.6	6.8
17.8	2.394E+06	236499	97270	25932	0.837	0.424	52.0	3.6	6.9
18.0	2.383E+06	235001	96031	25376	0.839	0.422	52.4	3.5	6.7
18.2	2.384E+06	236288	96315	26690	0.834	0.421	52.5	3.7	7.0
23.5	2.408E+06	225701	97013	27860	0.882	0.443	49.9	4.0	8.1
23.8	2.405E+06	225292	96705	27783	0.883	0.443	50.0	4.0	8.1
24.0	2.404E+06	227890	95513	25868	0.872	0.432	51.1	3.7	7.3
29.5	2.303E+06	242126	94454	28054	0.787	0.403	54.5	3.8	7.0
29.7	2.361E+06	240690	95235	28348	0.811	0.408	53.9	3.9	7.2
29.9	2.393E+06	240264	97663	28053	0.824	0.419	52.6	3.8	7.3
30.0	2.429E+06	235197	97651	27760	0.854	0.428	51.6	3.9	7.5
30.2	2.404E+06	241136	98650	27447	0.824	0.422	52.3	3.7	7.1
30.3	2.418E+06	240997	97367	27761	0.830	0.417	52.9	3.8	7.1
30.5	2.428E+06	242640	100398	27115	0.828	0.427	51.8	3.7	7.1
35.7	3.000E+06	237142	123776	36839	1.046	0.539	39.1	5.1	13.0
35.8	3.090E+06	235366	125858	36915	1.086	0.552	37.7	5.1	13.6
36.2	3.090E+06	236852	128185	36485	1.079	0.558	36.9	5.0	13.7
36.3	3.072E+06	233568	126055	36547	1.088	0.557	37.1	5.1	13.8
45.7	3.024E+06	242199	125567	40625	1.033	0.535	39.6	5.5	13.9
45.8	3.004E+06	239345	127120	38977	1.038	0.548	38.1	5.3	14.0
46.0	3.002E+06	233459	122253	38725	1.064	0.540	38.9	5.4	13.9
46.2	3.040E+06	240747	128712	38149	1.044	0.552	37.7	5.2	13.8

Appendix: Fischer-Tropch synthesis FID data

0 MLCatalyst TOS 24 hours										
Carbon N°	FID Corrected Areas					ASF	Molar Contents, mol %			
NC	A_{Tot}	Paraffin	1-Olefin	n-Olefin	Ald+Alc	$\log(A_i/A_{Tot.})$	$X_{n\text{-}Olef}$	$X_{1\text{-}Olef}$	$X_{Oxyg.}$	$X_{Brach.}$
1	12208788.0	12208788.0	-	-	nd	1.83	0.0	-	-	-
2	690924.5	516886.0	174038.5	174038.5	nd	0.59	25.2	-	-	-
3	811842.0	466924.0	344918.0	344918.0	nd	0.66	42.5	-	-	-
4	762910.3	496332.0	223659.3	266578.3	nd	0.63	34.9	83.9	-	-
5	609508.8	430379.6	146002.6	179129.2	14164.8	0.53	29.4	81.5	22.2	2.3
6	508191.2	389514.8	90045.2	118676.3	23189.9	0.45	23.4	75.9	15.3	4.5
7	424715.9	347603.1	53742.1	77112.7	17941.3	0.38	18.2	69.7	15.0	4.1
8	362230.4	309071.3	31041.0	53159.1	16013.4	0.31	14.7	58.4	18.7	4.4
9	302551.8	268626.4	17921.4	33925.3	14037.5	0.23	11.2	52.8	30.7	4.5
10	256836.9	234201.3	13628.3	22635.6	12277.4	0.16	8.8	60.2	50.1	4.4
11	207335.7	204696.2	5152.5	2639.5	7567.6	0.11	1.3		61.4	3.4
12	192846.2	190047.2	1113.6	2799.0	5379.0	0.06	1.5		45.2	2.7
13	167568.7	164861.1	1088.0	2707.6		0.01	1.6			
14	122485.9	120191.1	1484.6	2294.8		-0.04	1.9			
15	80344.7	78474.8	950.1	1869.9		-0.09	2.3			

0.1 MLCatalyst TOS 24 hours										
Carbon N°	FID Corrected Areas					ASF	Molar Contents, mol %			
NC	A_{Tot}	Paraffin	1-Olefin	n-Olefin	Ald+Alc	$\log(A_i/A_{Tot.})$	$X_{n\text{-}Olef}$	$X_{1\text{-}Olef}$	$X_{Oxyg.}$	$X_{Brach.}$
1	12761832.0	12761832.0	-	-	nd	1.81	-	-	-	-
2	729379.5	524603.0	204776.5	204776.5	nd	0.57	28.1	-	-	-
3	817185.7	460084.7	357101.0	357101.0	nd	0.62	43.7	-	-	-
4	785271.0	481617.8	240037.8	303653.3	nd	0.60	38.7	79.0	-	-
5	657058.8	444189.2	164582.0	212869.6	nd	0.52	32.4	77.3	0.0	1.7
6	574623.8	421326.7	104248.2	153297.2	29856.0	0.46	26.7	68.0	5.1	1.5
7	504846.9	396429.7	65423.4	108417.1	26869.4	0.41	21.5	60.3	5.2	1.5
8	444716.1	370290.6	37735.4	74425.5	23553.0	0.35	16.7	50.7	5.1	4.0
9	392951.2	337840.2	21821.0	55111.0	23901.4	0.30	14.0	39.6	5.8	2.1
10	346051.2	309691.4	12833.1	36359.8	16255.9	0.24	10.5	35.3	4.5	2.2
11	287392.5	281614.0	4114.5	5778.5	10613.2	0.11	2.0		3.5	4.0
12	245001.5	239004.5	2149.9	5997.0	7990.7	-0.02	2.4		3.1	4.8
13	200110.7	194835.7	2481.6	5275.0		-0.15	2.6			6.7
14	157483.3	155431.9	371.3	2051.4		-0.28	1.3			
15	131748.2	128409.9	581.8	3338.3		-0.42	2.5			

0.5 MLCatalyst TOS 24 hours										
Carbon N°	FID Corrected Areas					ASF	Molar Contents, mol %			
NC	A_{Tot}	Paraffin	1-Olefin	n-Olefin	Ald+Alc	$\log(A_i/A_{Tot.})$	$X_{n\text{-}Olef}$	$X_{1\text{-}Olef}$	$X_{Oxyg.}$	$X_{Brach.}$
1	12442048.0	12442048.0	-	-	nd	1.80	-	-	-	-
2	935477.5	538246.5	397231.0	397231.0	nd	0.68	42.5	0.0	-	-
3	921562.7	424672.0	496890.7	496890.7	nd	0.67	53.9	0.0	-	-
4	835602.5	443299.0	324984.0	392303.5	nd	0.63	46.9	82.8	-	-
5	684271.4	406875.4	228193.6	277396.0	13085.2	0.54	40.5	82.3	1.9	1.5
6	590284.5	391228.8	148132.2	199055.7	36286.7	0.48	33.7	74.4	6.0	1.2
7	512071.7	373147.7	92112.9	138924.0	36533.1	0.42	27.1	66.3	6.9	1.5
8	453839.9	356401.0	55741.5	97438.9	32992.4	0.37	21.5	57.2	6.9	3.6
9	406506.9	333397.9	33119.6	73109.0	27730.9	0.32	18.0	45.3	6.7	0.9
10	357196.6	307338.4	19488.5	49858.2	17829.1	0.26	14.0	39.1	4.8	2.3
11	272600.4	263876.1	9969.4	8724.3	13411.8	0.15	3.2		4.7	1.8
12	200273.2	189752.0	5326.9	10521.2	8837.7	0.03	5.3		4.2	4.9
13	129176.4	124734.3	1722.2	4442.1	5933.4	-0.08	3.4		4.4	3.8
14	89213.8	87454.2	273.7	1759.6	4716.2	-0.20	2.0		5.0	
15	78219.8	73120.9	80.0	5098.9	3222.0	-0.31	6.5		3.895	

nd-not detected

1 MLCatalyst TOS 24 hours										
Carbon N°	FID Corrected Areas					ASF	Molar Contents, mol %			
NC	A_{Tot}	Paraffin	1-Olefin	n-Olefin	Ald+Alc	$\log(A_i/A_{Tot.})$	$X_{n\text{-}Olef}$	$X_{1\text{-}Olef}$	$X_{Oxyg.}$	$X_{Brach.}$
1	13373880.0	13373880.0	-	-	nd	1.84	-	-	-	-
2	834980.0	448593.5	386386.5	386386.5	nd	0.64	46.3	-	-	-
3	740988.7	387905.0	353083.7	353083.7	nd	0.59	47.7	-	-	-
4	674017.0	391984.5	240521.0	282032.5	nd	0.55	41.8	85.3	-	-
5	548794.6	345253.4	173188.2	203541.2	24113.1	0.46	37.1	85.1	4.2	1.8
6	454243.8	312877.8	114296.5	141366.0	42243.1	0.37	31.1	80.9	8.7	1.6
7	374329.1	280360.9	70361.3	93968.3	39290.9	0.29	25.1	74.9	9.8	1.6
8	313805.1	251754.8	42116.1	62050.4	38272.7	0.21	19.8	67.9	11.1	3.4
9	264919.6	222819.1	24853.6	42100.4	33241.6	0.14	15.9	59.0	11.5	2.8
10	221338.2	195916.5	15149.5	25421.7	28952.1	0.06	11.5	59.6	11.7	4.5
11	165356.1	162612.7	8952.9	2743.4	28268.3	-0.07	1.7		14.6	4.9
12	146085.5	138467.1	5651.8	7618.4	25002.7	-0.21	5.2		14.7	6.9
13	123853.6	121517.1	973.9	2336.5	22650.3	-0.34	1.9		15.9	4.8
14	126734.4	125639.8	0.0	1094.6		-0.48	0.9			
15	165821.7	161131.2	445.1	4690.5		-0.62	2.8			

2 MLCatalyst TOS 24 hours										
Carbon N°	FID Corrected Areas					ASF	Molar Contents, mol %			
NC	A_{Tot}	Paraffin	1-Olefin	n-Olefin	Ald+Alc	$\log(A_i/A_{Tot.})$	$X_{n\text{-}Olef}$	$X_{1\text{-}Olef}$	$X_{Oxyg.}$	$X_{Brach.}$
1	18373968.0	18373968.0	0.0	-	-	1.82	-	-	-	-
2	1391230.0	890446.0	500784.0	500784.0	-	0.70	36.0	-	-	-
3	1277374.3	836957.3	440417.0	440417.0	-	0.66	34.5	-	-	-
4	1193446.0	835207.3	268063.8	358238.8	-	0.63	30.0	74.8	-	-
5	1006082.4	765490.8	172994.8	240591.6	4285.2	0.55	23.9	71.9	0.4	2.0
6	867963.3	699987.7	106041.7	167975.7	30135.2	0.49	19.4	63.1	3.4	1.8
7	751778.1	638415.6	64328.9	113362.6	28834.0	0.43	15.1	56.7	3.7	1.7
8	677971.4	596990.4	37583.9	80981.0	32460.3	0.38	11.9	46.4	4.6	3.4
9	583310.0	524001.1	21612.2	59308.9	16894.6	0.32	10.2	36.4	2.8	2.7
10	512593.2	473532.5	13533.8	39060.7	13983.3	0.26	7.6	34.6	2.6	2.9
11	414127.0	409743.5	9036.2	4383.5	6920.2	0.13	1.1		1.6	3.6
12	327947.9	319339.8	6247.9	8608.2	5417.4	0.00	2.6		1.6	4.7
13	235157.1	229113.6	4905.5	6043.5	3565.0	-0.14	2.6		1.5	4.1
14	166980.9	163060.6	3165.5	3920.4		-0.27	2.3			
15	134652.3	128896.8	1972.7	5755.5		-0.40	4.3			

5 MLCatalyst TOS 24 hours										
Carbon N°	FID Corrected Areas					ASF	Molar Contents, mol %			
NC	A_{Tot}	Paraffin	1-Olefin	n-Olefin	Ald+Alc	$\log(A_i/A_{Tot.})$	$X_{n\text{-}Olef}$	$X_{1\text{-}Olef}$	$X_{Oxyg.}$	$X_{Brach.}$
1	8252765.0	8252765.0	-	-	nd	1.82	-	-	-	-
2	673845.0	350549.5	323295.5	323295.5	nd	0.73	48.0	-	-	-
3	606509.3	213223.0	393286.3	393286.3	nd	0.69	64.8	-	-	-
4	522709.5	224791.0	265517.5	297918.5	nd	0.62	57.0	89.1	-	-
5	418631.0	204497.8	192315.8	214133.2	1863.5	0.53	51.2	89.8	0.4	1.5
6	354093.2	198634.7	132767.0	155458.5	17786.5	0.45	43.9	85.4	5.0	1.1
7	302116.0	192625.1	86683.3	109490.9	20973.4	0.38	36.2	79.2	6.8	1.1
8	263505.1	186123.3	55548.4	77381.9	19232.4	0.33	29.4	71.8	7.0	3.3
9	232875.9	177983.0	34397.4	54892.9	13291.8	0.27	23.6	62.7	5.6	1.5
10	210166.0	170706.5	21470.5	39459.5	7465.6	0.23	18.8	54.4	3.5	2.6
11	159925.0	152882.6	11984.2	7042.4	11411.4	0.11	4.4		6.8	2.8
12	135113.3	125048.3	5730.9	10065.0	2609.5	0.00	7.4		1.9	4.4
13	92021.2	86548.2	3094.3	5472.9	1913.8	-0.12	5.9		2.0	1.8
14	61665.4	59047.7	1356.1	2617.7	2997.8	-0.24	4.2			
15	49042.7	43454.7	599.5	5588.0		-0.35	11.4			

nd-not detected

0 ML Catalyst TOS 30 hours										
Carbon N°	FID Corrected Areas					ASF	Molar Contents, mol %			
NC	A_{Tot}	Paraffin	1-Olefin	n-Olefin	Ald+Alc	$\log(A_i/A_{Tot})$	$X_{n\text{-}Olef}$	$X_{1\text{-}Olef}$	$X_{Oxyg.}$	$X_{Brach.}$
1	29021904.0	29021904.0	-	-	nd	1.78	-	-	-	-
2	1546841.5	1085314.5	461527.0	461527.0	nd	0.50	29.8	-	-	-
3	2717259.7	1936721.0	780538.7	780538.7	nd	0.75	28.7	-	-	-
4	2279831.8	1628655.3	467681.8	651176.5	nd	0.67	28.6	71.8	-	-
5	1857816.6	1460646.4	300867.8	397170.2	15891.0	0.58	21.4	75.8	0.8	2.1
6	1575923.0	1296607.0	186063.3	279316.0	37837.7	0.51	17.7	66.6	2.3	1.9
7	1314874.7	1134491.0	109361.9	180383.7	26550.7	0.43	13.7	60.6	2.0	2.0
8	1103410.0	986632.4	62122.8	116777.6	32044.1	0.36	10.6	53.2	2.8	4.2
9	924014.6	844077.9	35006.1	79936.7	29852.3	0.28	8.7	43.8	3.1	3.3
10	774951.5	726373.6	19443.8	48577.9	23758.7	0.20	6.3	40.0	3.0	3.0
11	634822.6	629366.1	11906.0	5456.5	19063.9	0.15	0.9		2.9	3.4
12	570830.8	557784.3	9251.7	13046.5	16583.7	0.11	2.3		2.8	3.2
13	503018.4	499712.2	896.0	3306.2	7967.8	0.06	0.7		1.5	2.9
14	454078.6	451507.2	717.9	2571.4		0.01	0.6			
15	422552.9	418641.3	0.0	3911.7		-0.04	0.9			

0.1 ML Catalyst TOS 30 hours										
Carbon N°	FID Corrected Areas					ASF	Molar Contents, mol %			
NC	A_{Tot}	Paraffin	1-Olefin	n-Olefin	Ald+Alc	$\log(A_i/A_{Tot})$	$X_{n\text{-}Olef}$	$X_{1\text{-}Olef}$	$X_{Oxyg.}$	$X_{Brach.}$
1	22070896.0	22070896.0	-	-	nd	1.77	-	-	-	-
2	1263208.0	789517.0	473691.0	473691.0	nd	0.52	37.5	-	-	-
3	2417250.7	1536933.3	880317.3	880317.3	nd	0.81	36.4	-	-	-
4	1877511.0	1133490.5	622105.5	744020.5	nd	0.70	39.6	83.6	-	-
5	1621029.8	1062808.4	456033.0	558221.4	38370.3	0.63	34.4	81.7	2.3	1.5
6	1433869.8	1034881.7	290151.3	398988.2	77347.1	0.58	27.8	72.7	5.2	1.4
7	1237882.0	967674.6	175282.3	270207.4	32795.3	0.51	21.8	64.9	2.6	0.8
8	1800207.9	1611083.0	95963.1	189124.9	13212.6	0.68	10.5	50.7	0.7	1.3
9	1964196.1	1811275.6	50587.7	152920.6	12265.2	0.71	7.8	33.1	0.6	3.3
10	1004928.6	940399.4	22421.2	64529.2	11701.1	0.42	6.4	34.7	1.1	2.5
11	529393.0	520262.7	3986.1	9130.3	9519.8	0.29	1.7		1.8	3.1
12	198920.0	189870.9	5817.3	9049.1	8368.3	0.16	4.5		4.0	3.8
13	146063.8	137774.2	6103.7	8289.7	7410.6	0.03	5.7		4.8	3.9
14	101993.1	97481.6	3481.4	4511.5	3500.2	-0.10	4.4		3.2	
15	81310.5	77364.4	2654.4	3946.1	4425.8	-0.24	4.9			

0.5 ML Catalyst TOS 30 hours										
Carbon N°	FID Corrected Areas					ASF	Molar Contents, mol %			
NC	A_{Tot}	Paraffin	1-Olefin	n-Olefin	Ald+Alc	$\log(A_i/A_{Tot})$	$X_{n\text{-}Olef}$	$X_{1\text{-}Olef}$	$X_{Oxyg.}$	$X_{Brach.}$
1	13427624.0	13427624.0	0.0	0.0	nd	1.72	-	-	-	-
2	2973640.0	801201.5	2172438.5	2172438.5	nd	1.07	73.1	-	-	-
3	1344208.3	880297.7	463910.7	463910.7	nd	0.72	34.5	-	-	-
4	1119931.3	519801.5	508641.8	600129.8	nd	0.64	53.6	84.8	-	-
5	838810.8	470094.8	325094.8	368716.0	57006.9	0.52	44.0	88.2	6.5	2.1
6	747146.5	438051.0	266713.7	309095.5	62961.1	0.47	41.4	86.3	8.0	1.7
7	610353.3	397619.6	175424.1	212733.7	52680.9	0.38	34.9	82.5	8.0	3.7
8	478406.0	342423.6	105416.5	135982.4	52211.8	0.27	28.4	77.5	9.9	3.9
9	417262.3	331481.3	54273.8	85781.0	52334.1	0.21	20.6	63.3	11.4	4.1
10	239221.0	197339.6	26692.4	41881.4	68850.1	-0.03	17.5	63.7	23.9	4.9
11	198533.5	190766.7	12216.1	7766.8	84933.1	-0.14	3.9		33.7	2.9
12	286373.0	266858.2	12124.0	19514.8	90652.6	-0.26	6.8		27.2	2.5
13	417094.3	403551.3	3578.7	13543.0	100957.8	-0.37	3.2		22.1	2.0
14	566013.2	564349.9	1435.9	1663.4	88277.4	-0.49	0.3		15.0	
15	766475.5	764851.2	1473.1	1624.3		-0.60	0.2			

nd-not detected

1 MLCatalyst TOS 30 hours										
Carbon N°	FID Corrected Areas					ASF	Molar Contents, mol %			
NC	A_{Tot}	Paraffin	1-Olefin	n-Olefin	Ald+Alc	$\log(A_i/A_{Tot.})$	$X_{n\text{-}Olef}$	$X_{1\text{-}Olef}$	$X_{Oxyg.}$	$X_{Brach.}$
1	8323827.0	8323827.0	-	-	nd	1.73	-	-	-	-
2	538190.5	281460.0	256730.5	256730.5	nd	0.54	47.7	-	-	-
3	884386.3	448081.3	436305.0	436305.0	nd	0.76	49.3	-	-	-
4	750667.3	436729.3	261773.0	313938.0	nd	0.69	41.8	83.4	-	-
5	604712.6	391533.4	193729.2	213179.2	135032.1	0.59	35.3	90.9	18.6	2.0
6	514701.5	357415.5	126865.2	157286.0	124523.8	0.52	30.6	80.7	19.2	8.5
7	422280.1	321569.9	76980.4	100710.3	127497.3	0.44	23.8	76.4	24.3	2.2
8	355494.4	286598.6	46327.5	68895.8	119526.5	0.36	19.4	67.2	25.8	4.6
9	296645.1	247141.1	28433.8	49504.0	115426.2	0.29	16.7	57.4	30.1	1.9
10	247331.5	216957.1	16544.0	30374.4	101735.7	0.21	12.3	54.5	30.9	7.9
11	225729.8	214162.4	952.5	11567.5	105060.6	0.07	5.1		33.4	6.8
12	246901.0	234156.7	9797.2	12744.3	63880.9	-0.06	5.2		20.3	3.4
13	353591.2	291109.7	59570.5	62481.5	27328.2	-0.20	17.7		7.2	2.8
14	419085.1	368007.6	47654.0	51077.6		-0.34	12.2			
15	527511.2	478307.2	44290.9	49204.0		-0.47	9.3			

2 MLCatalyst TOS 30 hours										
Carbon N°	FID Corrected Areas					ASF	Molar Contents, mol %			
NC	A_{Tot}	Paraffin	1-Olefin	n-Olefin	Ald+Alc	$\log(A_i/A_{Tot.})$	$X_{n\text{-}Olef}$	$X_{1\text{-}Olef}$	$X_{Oxyg.}$	$X_{Brach.}$
1	6668288.0	6668288.0	-	-	nd	1.77	0.0	-	-	-
2	435567.0	222485.0	213082.0	213082.0	nd	0.59	48.9	-	-	-
3	756790.0	346010.7	410779.3	410779.3	nd	0.83	54.3	-	-	-
4	576776.5	315756.8	241051.8	261019.8	nd	0.71	45.3	92.4	-	-
5	487225.6	284538.8	177559.6	202686.8	140046.8	0.64	41.6	87.6	22.9	1.9
6	389816.3	254448.8	121719.3	135367.5	113359.7	0.54	34.7	89.9	22.4	9.2
7	325422.0	229075.0	77467.6	96347.0	105758.0	0.46	29.6	80.4	25.2	4.4
8	274769.0	206627.6	47815.3	68141.4	104337.0	0.39	24.8	70.2	28.4	5.8
9	220667.7	176541.3	28465.6	44126.3	96125.4	0.29	20.0	64.5	31.0	8.2
10	176296.6	147423.0	16386.9	28873.6	99447.9	0.20	16.4	56.8	37.1	12.8
11	130735.6	125278.2	9558.5	5457.5	95291.9	0.06	4.2	45.1	42.8	13.2
12	131741.5	121463.6	6517.9	10277.9	86113.8	-0.07	7.8		39.8	14.9
13	138860.5	134876.5	616.4	3984.1	82758.9	-0.20	2.9		42.8	2.4
14	170768.6	166659.3	1438.4	4109.3	79974.5	-0.34	2.4		36.6	
15	227280.7	224151.9	2654.4	3128.8	59280.4	-0.47	1.4		21.8	

5 MLCatalyst TOS 30 hours										
Carbon N°	FID Corrected Areas					ASF	Molar Contents, mol %			
NC	A_{Tot}	Paraffin	1-Olefin	n-Olefin	Ald+Alc	$\log(A_i/A_{Tot.})$	$X_{n\text{-}Olef}$	$X_{1\text{-}Olef}$	$X_{Oxyg.}$	$X_{Brach.}$
1	9199546.0	9199546.0	-	-	nd	1.75	0.0	-	-	-
2	668143.5	340176.5	327967.0	327967.0	nd	0.61	49.1	-	-	-
3	1500480.3	389038.3	1111442.0	1111442.0	nd	0.96	74.1	-	-	-
4	1033071.5	447972.0	521482.0	585099.5	nd	0.80	56.6	89.1	-	-
5	811161.2	403774.2	365139.8	407387.0	9151.9	0.69	50.2	89.6	1.1	1.5
6	679538.0	389923.5	245661.3	289614.5	37380.1	0.62	42.6	84.8	5.5	0.0
7	572369.1	372420.9	158773.1	199948.3	33688.3	0.54	34.9	79.4	5.8	1.1
8	484681.6	350771.3	96131.8	133910.4	29385.1	0.47	27.6	71.8	6.0	0.0
9	399653.6	312180.4	55024.6	87473.1	24369.5	0.39	21.9	62.9	5.9	1.5
10	314578.7	260704.8	29748.8	53873.9	17892.9	0.28	17.1	55.2	5.4	4.7
11	209805.0	207965.5	1014.1	1839.5	7275.0	0.17	0.9	55.1	3.3	3.6
12	171224.1	156793.1	9066.3	14431.0	6198.4	0.05	8.4		3.5	4.5
13	121410.2	116768.4	825.8	4641.8		-0.07	3.8		0.0	4.3
14	92657.5	87785.9	2385.1	4871.6		-0.18	5.3		0.0	
15	73212.1	70050.7	699.1	3161.4		-0.30	4.3		0	

nd-not detected

Appendix: AAS results

Theoretical vanadium (V) content theoretically determined (V_2O_5/Al_2O_3) mass ratio and experimentally determined (V_2O_5/Al_2O_3) mass ratio in the six catalysts under study.

V_2O_5 coverage	$(V)_{Theory}$ wt-%	$(V_2O_5/Al_2O_3)_{Theory}$ g/g	$(V_2O_5/Al_2O_3)_{AAS}$ g/g
0 ML	0	0	0
0.1 ML	1	0.02	0.04
0.5 ML	5	0.09	0.15
1 ML	5	0.18	0.12
***2 ML**	15	0.37	0.18
***5 ML**	27	0.93	0.17

*-Catalysts showing V_2O_5/Al_2O_3) mass ratios below theoretical predictions.

ML- V_2O_5 monolayers on g-Al_2O_3 surface.

Note: All catalysts contained 10 wt-% Co.

Appendix: AAS results

Theoretical vanadium (V) content theoretically determined (V_2O_5/Al_2O_3) mass ratio and experimentally determined (V_2O_5/Al_2O_3) mass ratio in the six catalysts under study.

V_2O_5 coverage	$(V)_{Theory}$ wt-%	$(V_2O_5/Al_2O_3)_{Theory}$ g/g	$(V_2O_5/Al_2O_3)_{AAS}$ g/g
0 ML	0	0	0
0.1 ML	1	0.02	0.04
0.5 ML	5	0.09	0.15
1 ML	9	0.18	0.12
*2 ML	15	0.37	0.18
*5 ML	27	0.93	0.17

*-Catalysts showing V_2O_5/Al_2O_3) mass ratios below theoretical predictions.

ML- V_2O_5 monolayers on g-Al_2O_3 surface.

Note: All catalysts contained 10 wt-% Co.